Characterization of arsenic occurrence, mobility and retardation in sandstone and dolomite aquifers of the Fox River Valley, Wisconsin

by:

Katie L. Thornburg

A thesis submitted in partial fulfillment of the

requirements for the degree of

Masters of Science

(Geology and Geophysics)

at the

UNIVERSITY OF WISCONSIN – MADISON

2003

Abstract

Elevated groundwater arsenic levels are found in the Fox River Valley in eastern Wisconsin. The aim of this study is to determine arsenic speciation and mobility at near neutral pH representative of the Fox River Valley groundwater. Core and hand samples of the Sinnipee Group Dolomite and the St. Peters Sandstone, which make up the regional aquifer, were studied to characterize mineralogical occurrence of arsenic and to assess the kinetics of arsenic release and retardation within the rocks. All grain fractions were characterized mineralogically by optical microscopy of thin-sections, powder X-Ray diffraction, Raman spectroscopy, and Electron Microprobe analysis. The samples contain dolomite, quartz, marcasite, pyrite, arsenic bearing marcasite/pyrite, and goethite. Chemical characterization was done on whole rock sample by Electron Microprobe analysis and acid digestion of sulfide, quartz, and dolomite fractions followed by Inductively Coupled Plasma-Atomic Emission Spectrometry. The digested samples are enriched in magnesium, silicon, arsenic, iron, sulfur, potassium, nickel, and to lesser degrees, lead. Quartz, dolomite, and sulfide fractions from both the sandstones and dolomites were reaction for 3 weeks under both nitrogen and oxygen atmospheres. Inductively Coupled Plasma-Optical Emission Spectrometry (ICP-OES) was used to determine total dissolved arsenic (As_T), As (III) and As (V) concentrations. Arsenic was detected in solutions reacting with the denser PM/PMG fraction, but not with the lighter quartz and dolomite fractions. Arsenic mobility of a known arsenopyrite sample from Mexico was also measured for comparison with the Fox River Valley arsenic bearing pyrites. The As_T, As (III), As (V), Fe_T and S_T concentrations verses time profiles for the arsenopyrite was similar to the arsenic bearing pyrites with concentrations increasing for

the first 1 hour, followed by an initial rapid decline over the next 1-3 hours, and slower decreasing concentrations over several weeks. Results indicate arsenic was released through oxidative dissolution of arsenic bearing pyrite and marcasite, with subsequent goethite formation. The arsenic is taken up as a sorbed phase on the goethite as indicated by sequential extractions and Raman Spectroscopy of reacted sulfide fractions. Arsenic is released as As (III) and persists as such in solution for 120 hours because the oxidation rate is extremely slow. In for Fox River Valley, WI, arsenic is released into the groundwater through the introduction of dissolved oxygen through pumping and arsenic will continue to be a problem as long as dissolved oxygen is supplied.

Acknowledgements

This research was funded by the Wisconsin Department of Natural Resources, the University of Wisconsin-Madison Department of Geology and Geophysics, and a research grant # 135-0829 A344832 from the Wisconsin Alumni Research Foundation.

Special thanks to Professor Toni Simo for serving on my G&E committee, to Madeline Gotkowitz for providing samples used in this research and for interesting and helpful discussions concerning arsenic occurrence in the Fox River Valley. Several people provided advice and counsel through the duration of the project, including Dr. Martin Shafer, Dr. George Helz at the University of Maryland-College Park, Katya Delak, and Jeffrey Brownson. Also thank you to Professor Robert Hammers and Sarah Baker at the UW-Madison Chemistry Department for their help with Raman Spectroscopy. Thanks to Tara Root for the discussions and for the generous sharing of methods she developed for arsenic analysis with me. I would like to thank my advisor, Professor Nita Sahai, for her advice, encouragement, and support. And last, but not least, thank you to my husband, Justin Stariha, and my family, Les, Pam, and Jennifer Thornburg for all of their patience, unfailing support, and encouragement.

Table of Contents

List of Tables

List of Figures

List of Appendices

CHAPTER I - INTRODUCTION

1.1 MOTIVATION

Arsenic is a naturally occurring element that is found in the earth's crust on average in concentrations of 2 ppm (Cullen and Reimer, 1989). Arsenic contamination of groundwater has recently become a major environmental concern on the local, national and international levels. This is because, effective January 2006, the drinking water limit of arsenic will be reduced from 50 to 10 $\mu g\ L^{-1}$ by the Environmental Protection Agency, with the same recommendation made by the World Health Organization. Elevated arsenic levels in the body can be toxic to humans and animals and causes several chronic conditions, including hyperkeratosis of the hands, legs and feet, gastro-intestinal track and liver problems, diabetes, skin tumors and cancer (Ryu et al., 2002; Cullen and Reimer, 1989). Doses of 50-340 mg are lethal to humans (Julloit et al., 1999).

While arsenic contamination alone is of great concern, its toxic effects are magnified by the presence other elements such as antimony, manganese, nickel, and chromium, that commonly occur in the same natural settings (Rawls, 2002). Arsenic in ground and surface water frequently has anthropogenic sources such as the use of arsenic containing pesticides, disposal of fly ash and mine drainage, but can also be released naturally through mineral dissolution and geothermal discharge (Goldberg, 2002). While arsenic contamination of drinking water is largely due to anthropogenic sources, many people suffer from overexposure to naturally occurring arsenic, most notably peoples of Bangladesh and Taiwan (Rawls, 2002; Nickson et al., 2000; Chen et al., 1994).

Most remediation efforts are aimed at removing arsenic from contaminated drinking water by adsorption at various natural and synthetic substrate surfaces (Farquhar et al., 2002; Goldberg, 2002; de Vitre et al., 2001; Lin and Puls, 2001; Han and Fyfe, 2000; Jain et al., 1999; Lombi et al., 1999; Carrillo and Drever, 1998; Myneni et al. 1998; Raven et al., 1998; Sun and Doner, 1998; Fendorf et al., 1997; Manning and Goldberg, 1997; Bowell, 1994). The processes responsible for releasing arsenic into groundwater have been examined in fewer studies, for example by studying arsenic leaching rates from sandstone samples (Kim et al., 2000). A comparison of the adsorption and solution experiments studies show that there exists in the literature a variety of interpretations of arsenic mobility related to sulfide oxidation and ferric reduction. It would, therefore, be useful to study the entire process of arsenic release and retardation in natural aquifer materials.

High concentrations of arsenic, up to 15,000 ppm, have been measured in drinking water wells in the Fox River Valley, which is located between Lake Winnebago in Winnebago County and Green Bay in Brown County, Eastern Wisconsin (Figure 1.1). Nearly a quarter of the wells in Outagamie and Winnebago counties exceed 10 $\mu g\ L^{-1}$ and 4% of the wells exceed 50 $\mu g\ L^{-1}$ (Schreiber et al., 2000). Research done by the Wisconsin Department of Natural Resources (WDNR) in the early late 1980's and early 1990's suggested that the predominant source of the high levels of arsenic is the contact between the St. Peter Sandstone and the Sinnipee Group. This prompted the WDNR to extend an advisory area with a 5 mile radius around either side of the St. Peters Sandstone subcrops in Outagamie and Winnebago Counties (Simo et al., 1997).

Figure 1.1. Schematic of the counties of the Fox River Valley (yellow), Wisconsin, with elevated arsenic concentrations in drinking water, namely Winnebago, Outagamie, and Brown County from southwest to northeast. Samples for this study were taken from Leonard quarry (sandstone sample LE7 and pyrite nodule Le25c) and a core (sandstone K1 and dolostone K2) from a field 4000 ft southeast of the quarry in Winnebago County (Created with ArcView using GIS data).

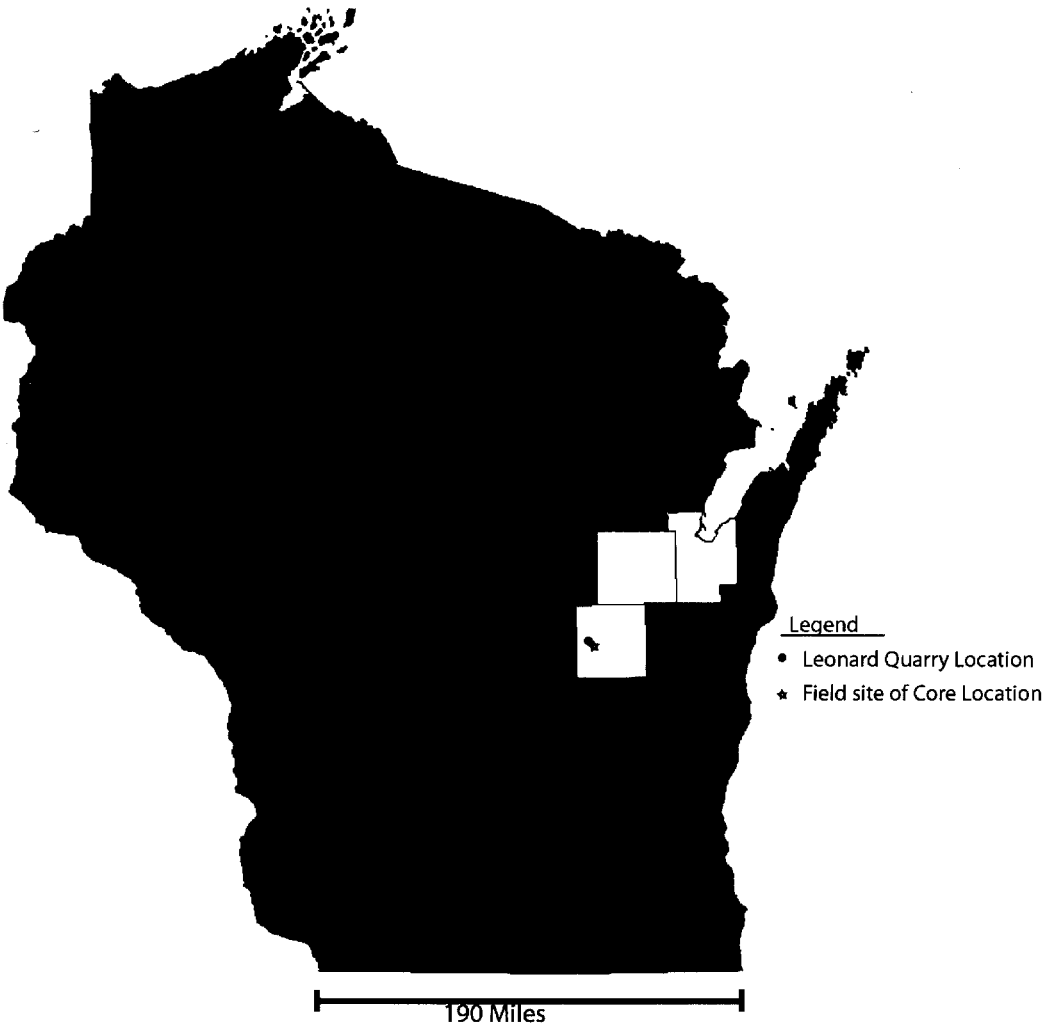

Figure 1.1. Schematic of the counties of the Fox River Valley (yellow), Wisconsin, with elevated arsenic concentrations in drinking water, namely Winnebago, Outagamie, and Brown County from southwest to northeast. Samples for this study were taken from Leonard quarry (sandstone sample LE7 and pyrite nodule Le25c) and a core (sandstone K1 and dolostone K2) from a field 4000 ft southeast of the quarry in Winnebago County (Created with ArcView using GIS data).

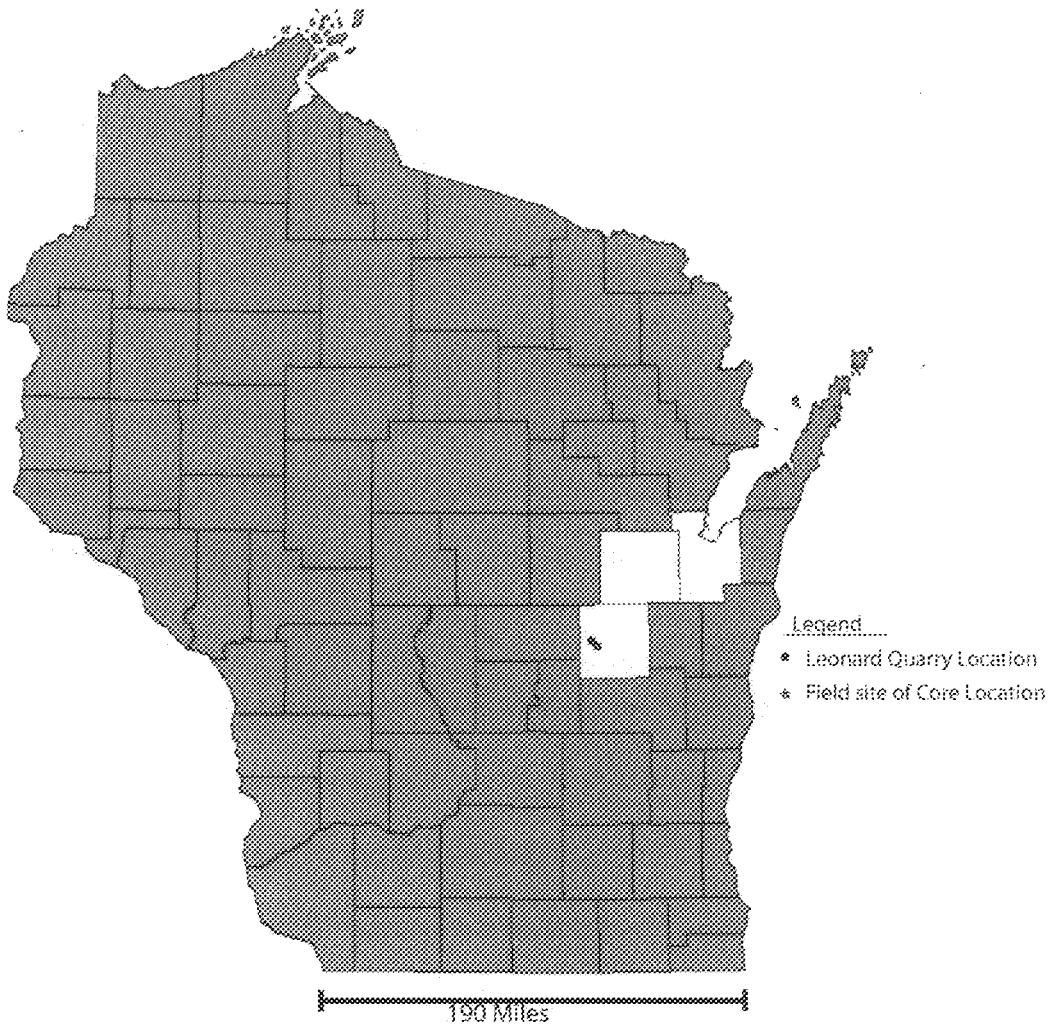

Pumping in drinking water wells is one possible process by which arsenic is released. Pumping causes fluctuations in well water levels which results in oxidative dissolution of a thin arsenic-rich pyrite horizon (Simo et al., 1997). The pyrite horizon occurs stratigraphically between the aquifer of the St. Peters sandstone and the overlying Sinnipee Group dolomite aquitard, but this horizon is not present in all localities that have arsenic contamination (Figure 1.2; Schreiber et al., 2000). It appears, therefore, that there are other sources for the arsenic or that arsenic is mobile in the subsurface. Some of the more likely alternative sources include arsenic-rich disseminated pyrite nodules in the sandstone, arsenic sorbed onto goethite (FeOOH) in the sandstone, and arsenic bearing pyrite veins in the dolostone. In order to better constrain the arsenic release rates and conditions, experiments at groundwater pH values ~7 are required. Further mineralogical analysis is also necessary to understand the release and uptake of arsenic within aquifer materials.

1.2 OBJECTIVES

The purpose of the present study purpose is to examine the mobility of arsenic released from sulfides in the sandstone and dolostone that makes up the aquifer in the Fox River Valley, Wisconsin. The broad aim of the study will be approached by focusing on the following questions:

1. What is the mineralogy of the St. Peter Sandstone and the Sinnipee Group Dolomite?
2. Which phases are enriched in arsenic?
3. Which phases are responsible for arsenic release?
4. Does bulk mineralogy change with reaction with solution?
5. What mechanisms are involved in arsenic release?
6. What is the mobile arsenic oxidation state and what is its fate?

Figure 1.2. General stratigraphic relationships of the Fox River Valley (not to scale). The As-rich sulfide mineral zone is located between the St. Peter Sandstone and the Sinnipee Group (modified from Schreiber et al., 2000).

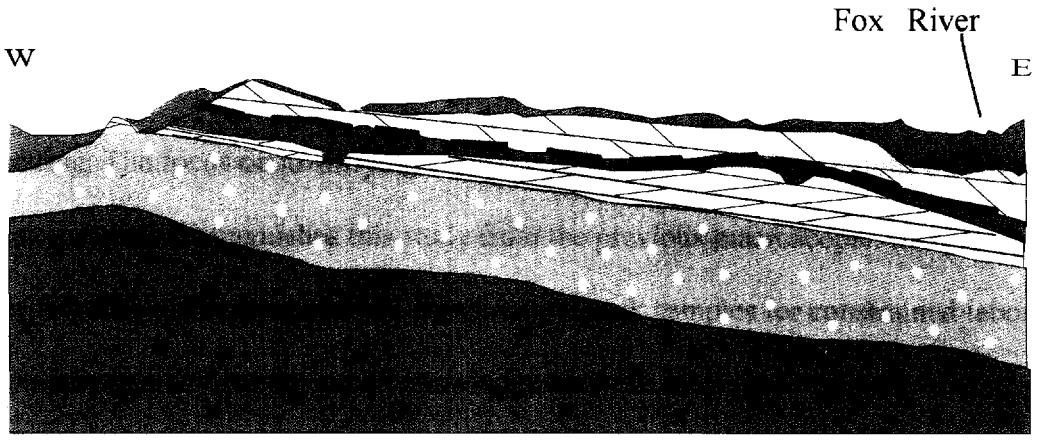

LEGEND

- Quaternary
- Sinnipee Group Dolomite
- St. Peter Sandstone
- Prairie du Chien Dolostone
- Cambrian Sandstone
- Precambrian
- Sulfide mineralization horizon

Figure 1.2. General stratigraphic relationships of the Fox River Valley (not to scale). The As-rich sulfide mineral zone is located between the St. Peter Sandstone and the Sinnipee Group (modified from Schreiber et al., 2000).

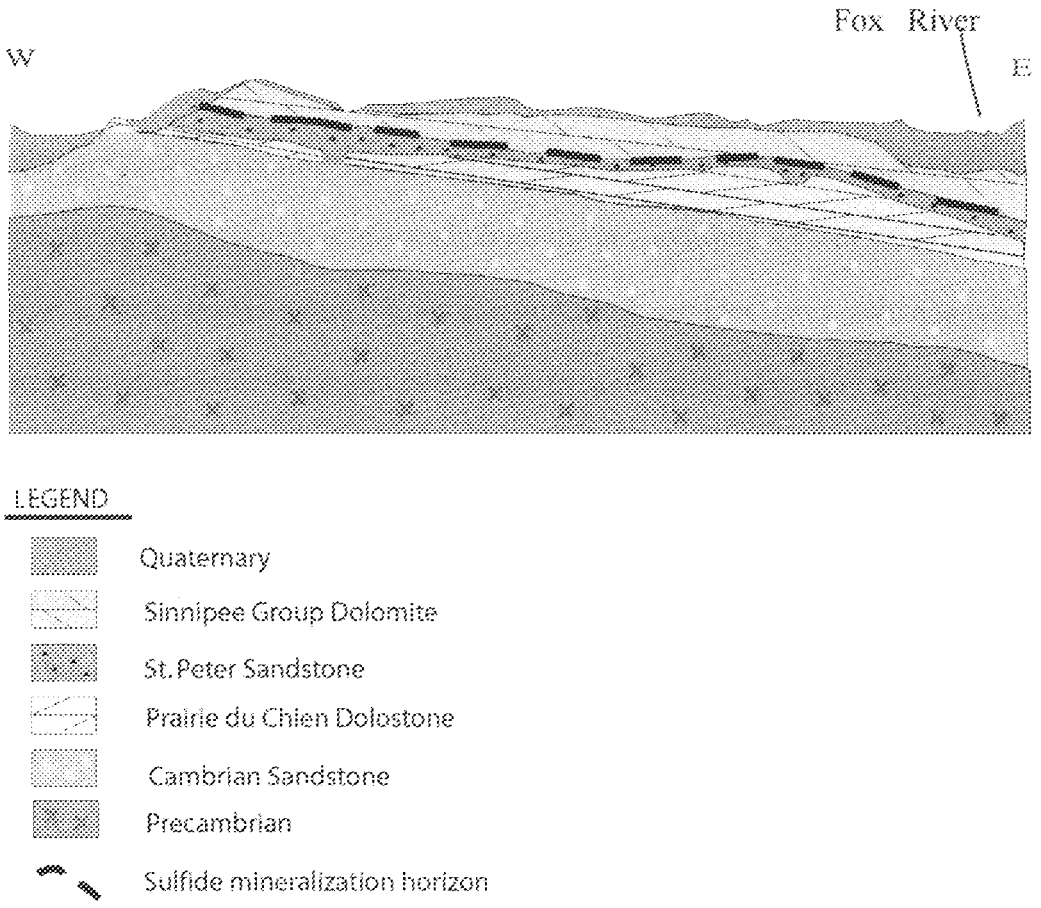

1.3 APPROACH

The questions posed above will be addressed by determining the mineralogy and chemical composition of rock samples from the Sinnipee Group Dolomite and the St. Peter Sandstone by identifying the reactions involved in arsenic release and re-uptake. A combination of laboratory sampling and extraction techniques, X-Ray diffraction, Electron Microscopy, Raman Spectroscopy and ICP-OES will be used to characterize the mineralogy, occurrence of arsenic associated with different mineral phases, and re-formation of arsenic bearing minerals after reaction with solution buffered at neutral pH. The results of these analyses will be used to develop a geochemical hypothesis for arsenic kinetics in a laboratory setting. The focus on identifying chemical species involved in reactions on the molecular to micron scale distinguishes this study from the previous macroscopic, field-scale work done in Wisconsin. Furthermore, the use of natural rock samples for constrained laboratory experiments bridges the gap in knowledge between ideal laboratory studies on synthetic mineral samples and completely unconstrained field studies. The application of this knowledge to the natural groundwater system in the Fox River Valley should contribute toward developing a plan for dealing with the arsenic contaminated drinking water.

1.4 BACKGROUND

1.4.1 Geology

The geologic setting has been well characterized (Schreiber et al., 2000; Simo et al., 1996). In this region of Wisconsin, Precambrian bedrock is overlain by Cambrian sandstones, which are in turn overlain by the Ordovician Prairie du Chien Group, the St. Peter Sandstone and the Sinnipee Group. The lithologies of these different groups vary widely. The Prairie du Chien Group (~12 m thick) is a dolomitized oolitic limestone with alternating beds of pure to

sandy dolostones (6.1 m thick), argillaceous to non-argillaceous sandstone beds (up to 2.1 m thick) and fissile clay beds (0.6 m thick). The Early Ordovician Prairie du Chien Group is unconformably overlain by the Middle Ordovician St. Peter Sandstone and the Middle Ordovician Sinnipee Group. This unconformity is interpreted to be paleokarstic topography filled by the St. Peter Sandstone, a porous, fine to medium grained, moderately well sorted, siliciclastic sandstone with minor shales and dolomitic sandstones, which varies from 35m to regionally pinching out against Prairie du Chien Group highs (Simo et al., 1996).

Overlying this package is the Late Ordovician Platteville Formation of the Sinnipee Group. It is 11-15m thick, and in many locations directly overlies the Prairie du Chien Group as the St. Peters disappears on karstic highs. The Platteville Formation consists of light gray, massive, dolostones to argillaceous dolostones that contain quartz grains. The zone of iron sulfide mineralization, referred to as the sulfide cement horizon (SCH) (Simo et al., 1996), occurs at the top of the St. Peter Sandstone and extends to the base of the Sinnipee Group. This iron sulfide horizon is believed to be the major source of arsenic in the region.

1.4.2 PREVIOUS WORK IN WISCONSIN

Previous work in the Fox River Valley indicates that 18% of private water-supply wells exceed the 10 $\mu g\ L^{-1}$ guideline of the World Health Organization (Burkel and Stoll, 1999). In response to these findings, units of the Ancell and Sinnipee Group have been stratigraphically characterized, along with the hydrostratigraphy, and identification of a Sulfide Cement Horizon (SCH) immediately below the base of the Sinnipee Group (Simo et al., 1996). Further work was conducted to investigate the mineralogy of the SCH and the geochemical groundwater characteristics (Schreiber et al., 2000; Simo et al., 1997). Results indicated that the major mineralogy of the SCH is pyrite and marcasite. Arsenic was initially

thought to occur along the outside edges of the pyrite and marcasite grain boundaries and have been observed on iron oxyhydroxides.

The highest arsenic concentrations within the Fox River valley appear to be associated with wells where the water table is near or intersecting the SCH and in areas of groundwater recharge. This observation and inadvertent introduction of oxygen into a sample in a groundwater experiment with low pH and dissolved oxygen (DO) suggests that DO is very important to the release of arsenic by acting as the dominant oxidant. Preliminary work suggests the source of the dissolved oxygen is the borehole acting as a conduit for oxygen/SCH interaction. This conduit system and regional pumping causing fluctuating water levels at the SCH interaction are the main explanations for the mobilization of arsenic within the aquifer (Schreiber et al., 2000).

1.5 ARSENIC GEOCHEMISTRY

Arsenic Stability

The main geochemical reactions involving arsenic are precipitation-dissolution and oxidation-reduction of oxides and sulfides, adsorption-desorption, and biochemical methylation. The chemical speciation of arsenic greatly affects is mobility, bioavailability, and toxicity (Ryu et al., 2002; Cullen and Reimer, 1989). Arsenic may occur in 4 oxidation states: (-III), (0), (+III), (+V), but As (+III) and As (+V) are the most common inorganic forms in natural waters (Juillot et al., 1999). The As (III) oxidation state is ~60 times more toxic than As (V). Increasing the level of methylation decreases arsenic toxicity (Jain and Ali, 2000; Yan et al., 2000; Panstar-Kallio and Manninen, 1997; Cullen and Reimer, 1989). Therefore, it is important to know arsenic speciation and phase diagrams.

Table 1.1. Arsenite and arsenate acid dissociation constants (from Wagman et al., 1982).

Arsenite	pK_a	Arsenate	pK_a
H_3AsO_3	9.22	H_3AsO_4	2.2
$H_2AsO_3^-$	12.13	$H_2AsO_4^-$	6.97
$HAsO_3^{2-}$	13.4	$HAsO_4^{2-}$	11.53

The As (V) species is stable at oxygenated conditions only and exists as H_3AsO_4, $H_2AsO_4^-$, and $HAsO_4^{2-}$ (Table 1.1). Therefore, As (V) should be the only detectable species in arsenic contaminated oxygenated waters. Arsenic (III)/Arsenic (V) ratios should then be easily predicted thermodynamically, but the predicted ratios are rarely observed (Cullen et al., 1989). Studies have shown that As (III), in the form of H_3AsO_3, $H_2AsO_3^-$, and $HAsO_3^{2-}$ (Table 1.1), is metastable in surface and deep ocean waters (Figure 1.3; Sun and Doner, 1998; Cullen and Reimer, 1989; Sadiq et al., 1983) and often found as a significant portion of total arsenic. The reason for this discrepancy is that arsenic redox kinetics are extremely slow, on the order of days to weeks (Ryu et al., 2002; Yan et al., 2000; Cherry et al., 1979). For example, a 1:1 (50 $\mu g\ L^{-1}$) arsenite:arsenate solution remained unchanged in deoxygenated buffer solutions at pH 2-10 under reducing and oxidizing conditions, for up to 3 weeks (Cherry et al., 1979). Redox agents such as high concentrations of oxidizers O_2 and Fe^{3+} and the reducer H_2S, are able to speed up the redox reactions at low pH values over the period of 10's of hours (Cullen and Reimer, 1989; Cherry et al., 1979).

Several arsenic sulfides exist under variable thermodynamically conditions. Under low Eh and pH ≤ 7 conditions, sulfide minerals such as As_2S_3 (orpiment) and AsS (realgar) will precipitate. When conditions are neutral or alkaline, arsenopyrite (AsFeS) and the more soluble thioarsenite (AsS_3^{3-}) become the dominant precipitates (Cullen and Reimer, 1989).

Under reducing conditions, arsenic is incorporated into sulfides, which are generated from sulfate. Sulfate can combine with Fe (II) to form iron sulfides such as troilite (FeS). Usually several monosulfide phases are first created (Rochette et al., 2000). In the presence of excess sulfide, these minerals are unstable and burial of these minerals will ultimately

Figure 1.3. Eh-pH diagram for the As-H_2O system at 25°C. Total dissolved arsenic species is set at $10^{-6.167}$ mol L^{-1}.

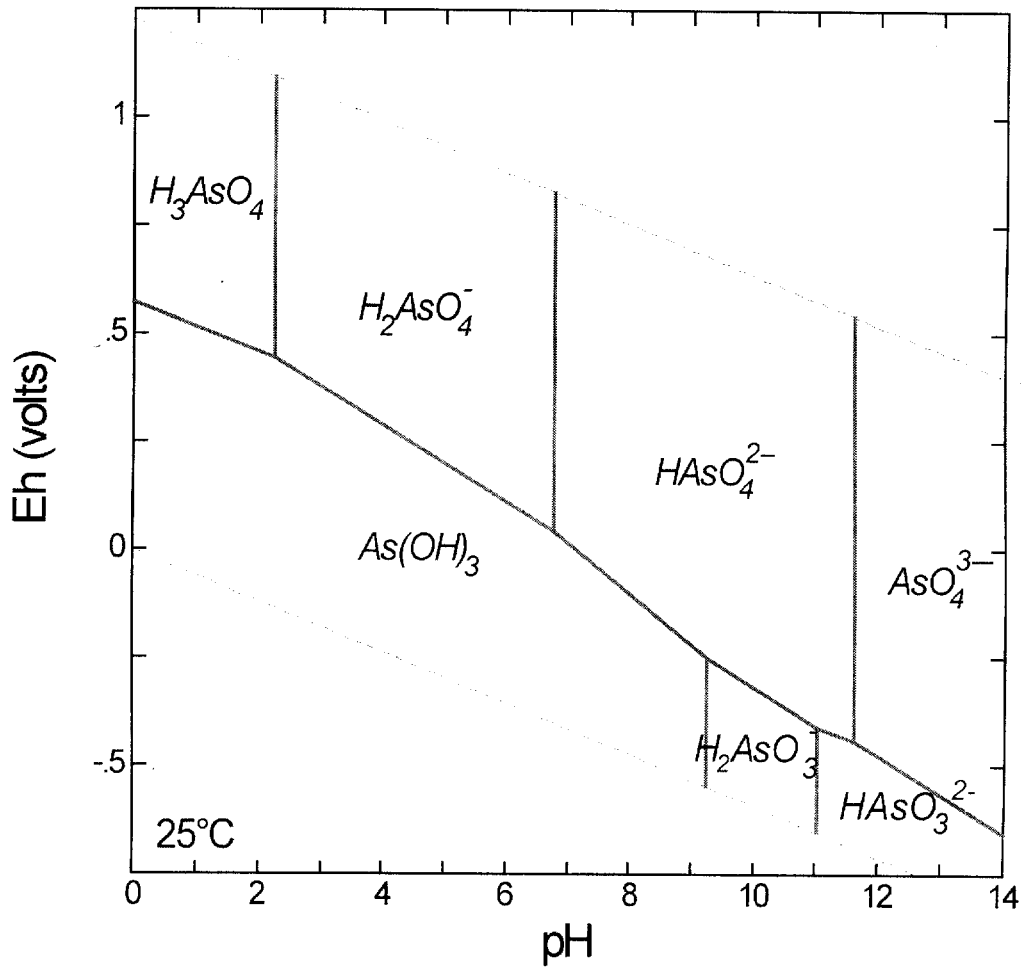

form pyrite (FeS_2). It is under the accompanying reducing conditions that arsenic can be incorporated into the mineral structure as a solid solution component in pyrite or as a precipitate forming arsenopyrite, AsFeS (Ryu et al., 2002) where arsenic substitutes for the sulfur ion in a mixed oxidation state, thus removing the contaminant from solution.

Arsenic release and reprecipitation

Arsenic toxicity is of less concern when bound in a solid phase, but once the ion is released into ground and surface waters it becomes dangerous because it is easily taken up by amino acids in organisms. There are two main types of reactions responsible for arsenic release from the bound phases: oxidative dissolution of sulfides such as arsenopyrite and pyrite (Eqns. 1.1 & 1.2) and reductive dissolution of oxides such as goethite (Eqn. 1.3) (Ryu et al., 2002; Julliot et al., 1999).

$$AsFeS + 11/2\ H_2O + 9/4\ O_2 \leftrightarrow H_2AsO_4^- + SO_4^{2-} + FeOOH + 8H^+ + 5e^- \quad (1.1)$$

$$2FeS_2 + 7O_2 + 6H_2O \leftrightarrow 2FeOOH + 4SO_4^{2-} + 10H^+ + 2e- \quad (1.2)$$

$$4FeOOH + CH_2O + 7H_2CO_3 \leftrightarrow 4Fe^{2+} + 8HCO_3^- + 6\ H_20 \quad (1.3)$$

where CH_2O represents organic matter, the reductant

The oxidative dissolution of sulfide (Eqns. 1.1-1.2) is often the source of arsenic contamination of ground water in mining districts from leaching of tailing piles (Tempel et al., 2000; Juillot et al., 1999; Armienta et al., 1997) and can also occur in areas of naturally occurring arsenic bearing pyrite minerals (Schreiber et al., 2000), such as in the Fox River Valley.

The other main route of arsenic release into natural waters is through reductive dissolution of ferric oxides releasing sorbed arsenic (Eqn. 1.3). Deuel and Swoboda (1972) reported an increase of total soluable arsenic under reducing conditions in laboratory experiments, interpreted as arsenic released from the reduction and mobilization of arsenic associated with ferric oxyhydroxides (McCreadie et al., 2000; Nickson et al., 2000).

Thermodynamics of Arsenic Adsorption

In efforts to identify materials for efficiently removing the contaminant from drinking water arsenic adsorption on ferrihydrite, goethite, and aluminum oxides has been studied extensively. Systems containing Fe (III) are very important because this ion is capable of controlling the fate of arsenic in the environment. In oxygenated waters, at near-neutral pH, Fe (III) is bound up in a solid phase as an iron oxide or iron oxyhydroxide. At neutral pH the dominant form of As (III) is H_3AsO_3 ($pKa_1 = 9.22$, see Table 1.1) whereas As (V) is present mainly as H_2AsO^{4-} and $HAsO_4^{2-}$. Also, at neutral pH, the iron oxide surfaces are positively charged (Point of Zero Charge ~ 9). Therefore, the greater electrostatic attraction between the As (V) anions and the positively charged oxide mineral surface causes it to be more efficiently removed. (Ryu et al., 2002; Lin and Puls, 2001; Han and Fyfe, 2000; Juillot et al., 1999; Lombi et al., 1999; Raven et al., 1998; Manning and Goldberg, 1997; Bowell, 1994; Ferguson and Gavis, 1972). Hence, arsenate is much less mobile than arsenite. In the case of clays, the amount of arsenite adsorption is greater than arsenate with decreasing solution pH, but at pH 5 neither predominates, likely due to the dissolution of clay minerals at this pH (Goldberg, 2002).

Results of batch adsorption studies, Fourier-Transform Infrared Spectroscopy (FTIR), and Extended X-ray Absorption Fine Structure Spectroscopy (EXAFS) have been combined

to identify the probable complexes arsenic forms when sorbing to iron hydroxides. Results of these studies show that As (III) and As (V) form inner-sphere surface complexes on goethite at surface coverages in thee mM arsenic concentration range. Variable inner-sphere surface complexes have been identified depending on the degree of surface loading. At low arsenate surface coverages (As_T = 1mM AsO_4^{3-}) the most distant As-Fe atoms at 3.59 Å were interpreted as linear arrangements with corner sharing arsenic tetrahedral- iron octahedral. This results in a monodentate As (V) surface complex at a >FeOH surface site that is singly coordinated to a central Fe atom. The most common distance observed for all surface coverages was 3.24 Å which is an intermediate between edge and corner sharing polyhedra, representing a bidentate-binuclear complex where the corner-sharing octahedra-tetrahedra do not result in a linear arrangement. The shortest As-Fe (2.85 Å) distances were interpreted to result from edge sharing tetrahedral and octahedral indicative of bidentate-mononuclear complexes. (Farquhar et al., 2002; Goldberg, 2002; Sun and Doner, 1998; Fendorf et al., 1997)

Kinetics of Arsenic Adsorption

Numerous studies illustrate that at relatively high arsenic concentrations and higher pH values arsenite adsorbs on iron oxides more strongly than arsenate, whereas arsenate adsorption dominates at lower As concentrations and lower pH conditions. Within their respective optimal conditions almost complete adsorption is achieved for both ions within the first couple of hours (Jain and Coeppert, 2000; Raven et al., 1998; Manning and Goldberg, 1997). Despite faster adsorption kinetics, As (III) is rarely observed in sediments and iron oxyhydroxide coatings because (de Vitre et al., 2001) adsorbed arsenite converts to arsenate over a period of ~20 days (Sun and Doner, 1998; Manning and Goldberg, 1997).

CHAPTER 2 – METHODS

The samples used in this study were taken from Leonard quarry and a core near Algoma Township, Winnebago County, WI. A summary description is provided in Table 2.1 and in Appendix A. An arsenopyrite hand sample from Mexico was obtained from the UW-Madison Geology Museum and is also included in Table 2.1 and Appendix A. All specimens referenced in this thesis are in the collections of the Department of Geology and Geophysics, University of Wisconsin-Madison, under file number UW1950.

2.1 Mineralogical Characterization

Microscope Analysis

Hand and core samples (Table 2.1; Appendix A) were cut into thin sections and examined using Nikon Labophot-Pol microscopes. Twenty watt lamps were used with 10x magnification under plane and polarized light to identify the major minerals present and any sedimentary features that could not be resolved at a larger scale. Mineral phases were identified based on their interference color and angles of extinction.

Grain Fractions Separation

Each sample was separated into clean quartz (Le7, K1), or dolomite (K2), and pyrite/marcasite (PM) fractions (Le7, Le25c, K2), for further mineralogical and chemical characterization. The only exception to this was the sandstone core, K1, which contained a high concentration of goethite coated quartz grains that could not to be separated from the sulfide fraction, denoted by PMG. The samples were crushed with a hammer to ~1mm (Figure 2.1) followed by density separation. This method involved placing one funnel above another and attaching a ½" polypropylene tubing hanging off the upper funnel. The tube

Table 2.1. Description of hand samples (HS) and core samples (CS).

Sample	Location	Description
Le7	Leonard Quarry, HS	Goethite coated quartz in sharp contact with an iron sulfide nodule that contains mixed sulfide (marcasite and pyrite) cement between grains. (UW1950/1.1 & UW1950/1.2)
Le25c	Leonard Quarry, HS	Pyrite/marcasite nodule from the St. Peter Sandstone. Rounded fine quartz grains in a pyrite cement. Goethite occurs at sulfide grain boundaries. (UW1950/2.1)
K1	Algoma Township, CS	Fine quartz grains with goethite coatings. Contains small pyrite/marcasite nodules within the sand matrix, often rimmed by goethite. (UW1950/3.1 & UW1950/3.2)
K2	Algoma Township, CS	Dolomite and quartz grains with veins of pyrite/marcasite filling in pores. Accessory goethite occurrence at sulfide/dolomite boundaries. (UW1950/4.1 & UW1950/4.2)
AsFeS	Mexico	3 x 3 x 5 cm^3 gray, pure arsenic sulfide sample rimmed by white quartz. (UW1950/5.1)

Figure 2.1. Samples were first physically crushed prior to physical separation of the mineral phases.

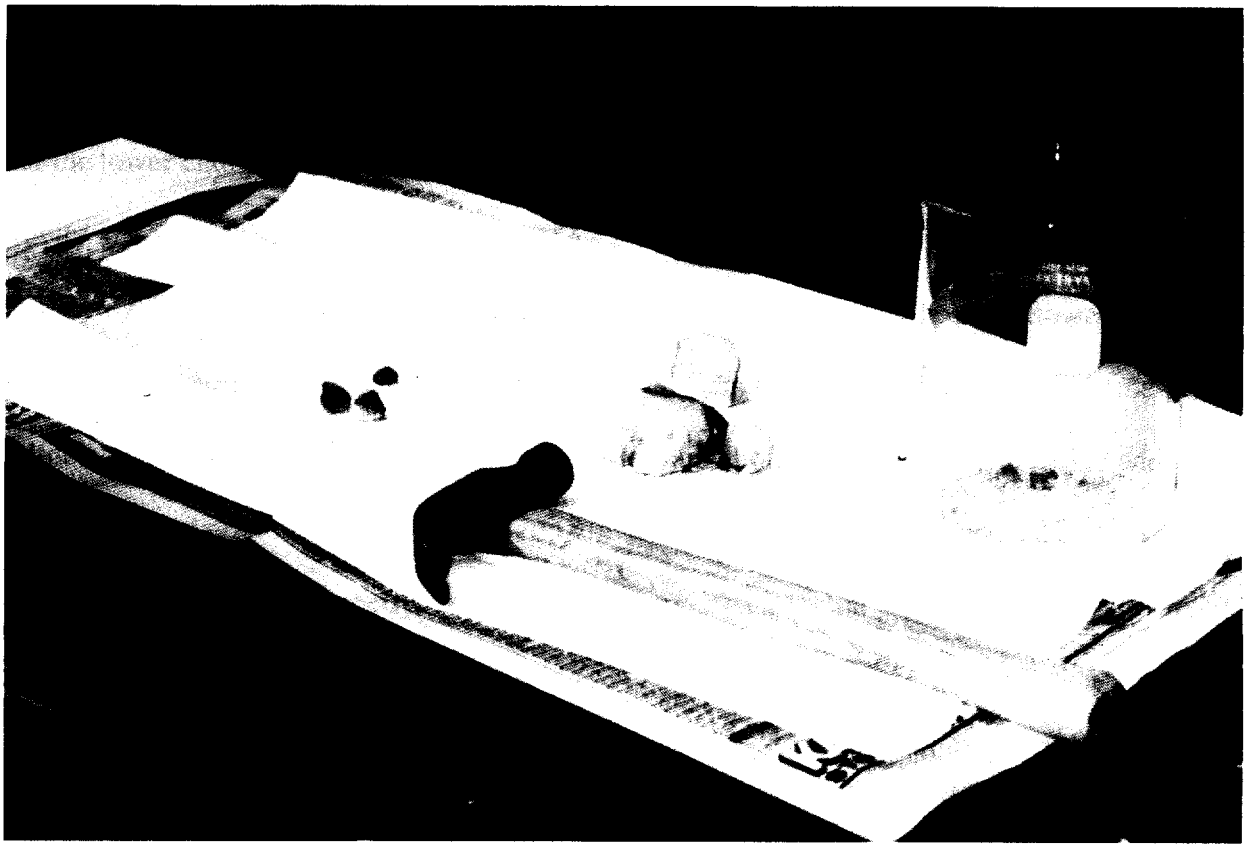

Figure 2.1. Samples were first physically crushed prior to physical separation of the mineral phases.

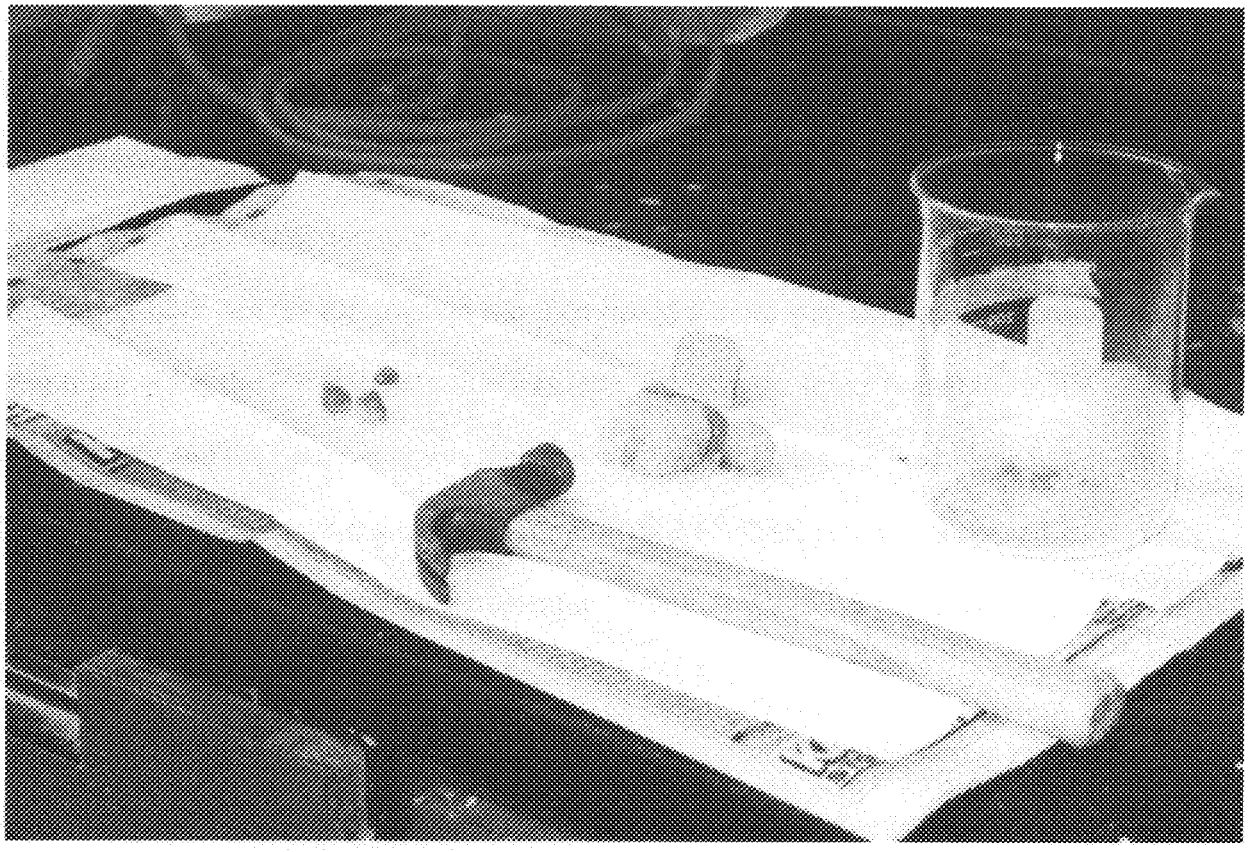

hung directly above the lower funnel that had a clamp at the bottom of the tubing to control flow (Figure 2.2). The lower funnel drained the density separation fluid into the flask below it. Methylene iodide (Geoliquids, Inc.), which has a specific gravity of 2.65, was poured into the upper funnel and 150g of sediment was poured into the methylene iodide, stirred, and allowed to density separate for 2 hours, with occasional stirring to keep the sediment covered in methylene iodide. After 2 hours, a clamp was added half way up the polypropylene tubing and the lower clamp was opened to release the high-density PM/PMG phases (specific gravity 4.3-5) into the underlying funnel. The methylene iodide was allowed to drain into the underlying flask and the PM fraction was then rinsed 3 times with acetone and allowed to dry over night. After the PM/PMG fraction was removed from the lower funnel the methylene iodide slurry and the filter paper was replaced, the clamp holding the methylene iodide and less dense quartz/dolomite fraction (specific gravity 2.65, 2.86) slurry was opened and allowed to drain into the underlying funnel for 1 hour, after which it was rinsed 3 times with acetone and allowed to dry over night also.

After drying, the separated fractions were crushed using a hand mortar and pestle, sieved to the 150 μm size fraction, and retained for further mineralogical and chemical characterization and for leaching experiments. The 150 μm size was chosen because it represents a very fine grain size and this size fraction was used in previous studies (Carrillo and Drever, 1998). This size fraction may be slightly smaller than sediments in the Fox River Valley, so sediments in this study may be more reactive than the natural system because of more surface area for reaction.

Figure 2.2. Apparatus for density sorting of grains.

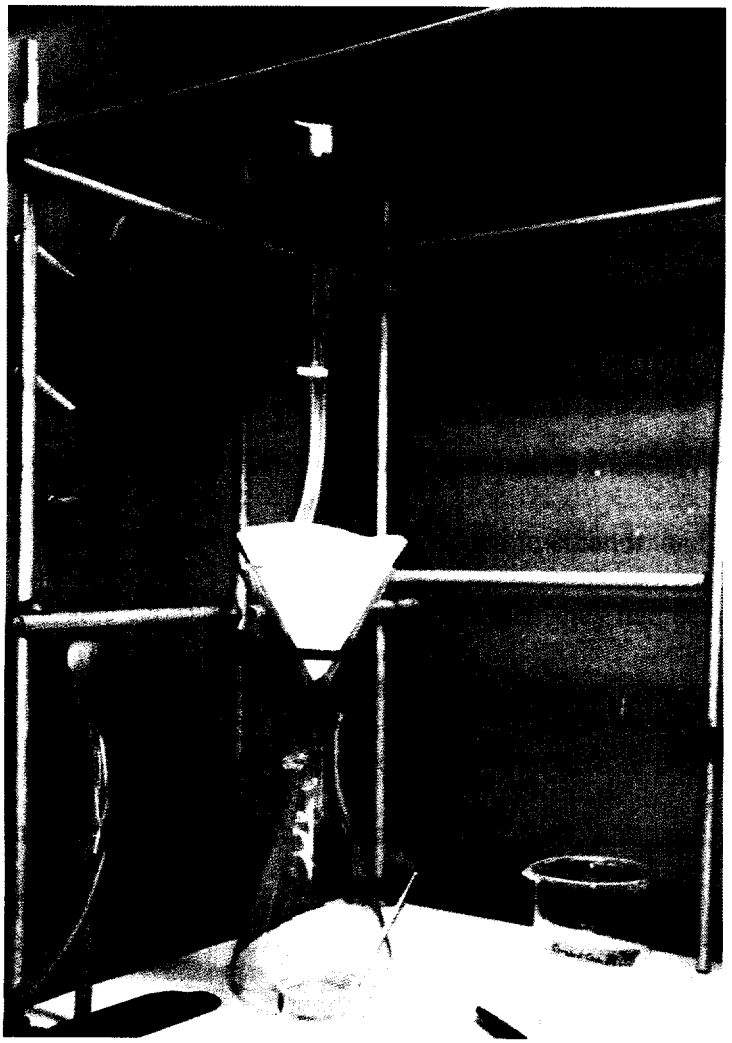

Figure 2.2. Apparatus for density sorting of grains.

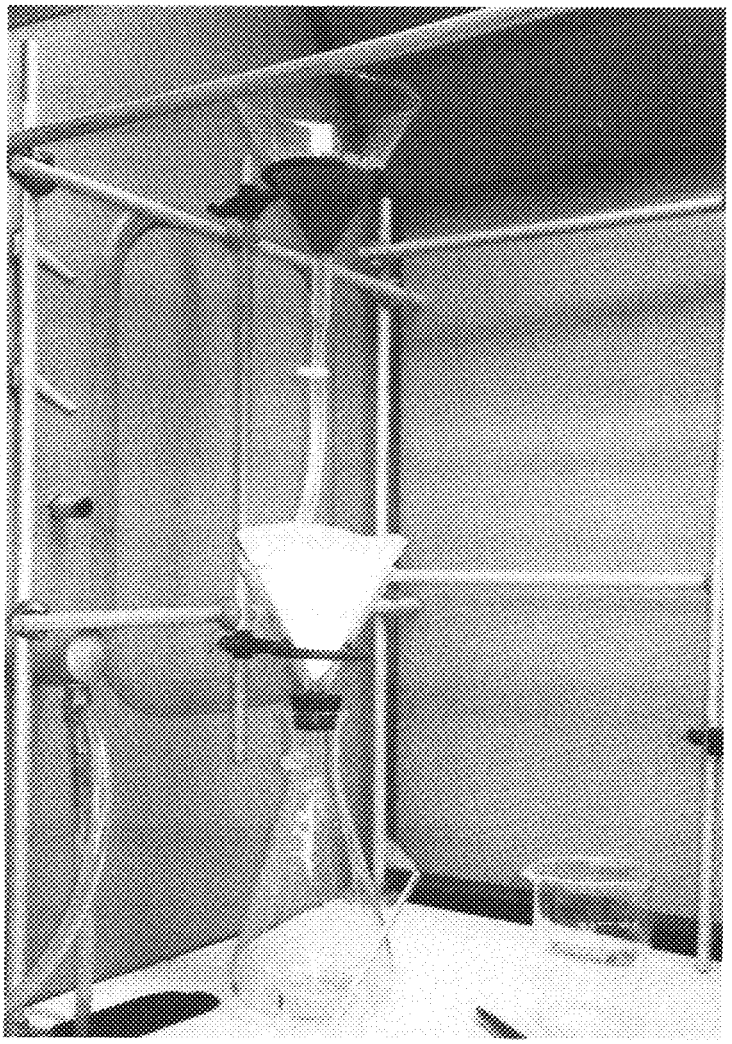

BET Specific Surface Area

The specific surface area was determined before reaction by a 3 point Krypton isotherm, Porous Materials, Inc., for all the PM fractions of Le25c and K2, the PMG for K1 and for the arsenopyrite sample from Mexico.

X-Ray Diffraction Analysis

X-Ray analysis was conducted on mineral fractions using a CuK alpha radiation Scintag PADV X-Ray Diffractometer at the Department of Geology, UW-Madison. The diffractometer was set to 35 keV and 40 millivolts with slit widths of 0.5, 1, 2, and 3 mm. Scans were run for 2 ½ hours with a 0.02° 2θ step size and a count rate of 4 seconds producing a scan between 16 and 60° 2θ. Samples for sulfide fractions from hand sample Le25c, K1and K2 were crushed to a powder, suspended in ethanol, and dried on a glass slide for analysis. These same samples were also analyzed after they had been reacted in aqueous solution for 3 weeks and were prepared by dropping the reacted powders, still wet from reaction, onto a glass slide. They were allowed to dry in oxygen or nitrogen, depending upon the atmosphere under which they had been reacted.

2.2 Chemical Characterization

Acid Digestion

In order to determine the mineral phases where arsenic was the most concentrated, separated mineralogical fractions of iron sulfide, quartz and dolomite were sent to ALS Chemex, Inc. for acid digestion using HF-HNO_3-$HClO_4$-HCl acid and ICP-AES elemental analysis.

Electron Microprobe Analysis

Arsenic bearing phases were chemically mapped using a Cameca SX50/51 (SN 485) Electron Microprobe (EMP) at the Department of Geology and Geophysics, UW-Madison. The EMP was operated with a beam current of 25 kilovolts and a beam size set at 0. Detection limit for arsenic is 0.065 weight percent. Both Backscattered Electron (BSE) images and X-Ray maps were made using Energy Dispersive Spectroscopy (EDS) in areas of elevated arsenic concentrations, as previously determined through backscattered images. Thin sections of core and hand samples were probed and traverses were made over contacts between arsenic bearing iron sulfide and iron oxide grains and the adjacent quartz/ dolomite matrix. This was done to determine arsenic concentrations associated with each mineral phase, to image grains with high arsenic concentrations, and to probe for any zoning that may be present. When elemental analysis contained lead the analysis was rejected because there is a strong interference with lead and arsenic peaks and the true elemental weight percentage of arsenic in the sample cannot to be determined.

Raman Spectroscopy

The Raman spectrometer consisted of a high-throughput f/1.8 spectrograph from Kaiser Optical Systems with fixed resolution of ~2 cm^{-1} and a charge coupled device (CCD) detector cooled by liquid nitrogen from Photometrics. Data were collected and analyzed on a computer with the Measurement and Analysis Photometerics Software (MAPS) program. Each sample was illuminated with an Ar laser operated at 514 nm and ~10mW power (McGuire et al., 2001). Acquisition times were approximately 2 minutes and the acquisition region extended from 100 to 2500 cm^{-1}. Only the range from 550 to 100 cm^{-1} is reported, because it contains the diagnostic Raman peaks.

2.3 Aqueous Reaction Methods

The separated and sieved mineral fractions were washed in ethanol (Fisher, Inc.) to remove any organics clinging to the grain surfaces (McGuire and Hamers, 2002). The separated sediment fractions were placed in Erlenmeyer flasks along with 30 mls of 100% ethyl alcohol and sonicated for 30 minutes. The ethyl alcohol was decanted and the sediment was allowed to dry by draining any extra liquid through filter paper. The sediment was then transferred to a beaker. The results from aqueous reaction are for samples Le25c, K1, and K2. There was not sufficient sample for the sulfide fraction of Le7 to conduct the experiment.

Subsequently, 1.5 grams was placed in 60 ml acid washed Low Density Polyethylene (LDPE) bottles, one for each sampling time. A 1 L solution of 0.01 M CsCl and pH 7.2 Tris-HCl buffer (Ultra Pure Grade, Sigma Aldrich, Inc.) was made using deionized water (Barnstead, 18MΩ) to simulate Fox River Valley groundwater pH conditions. Twenty milliliters of the buffer solution was added to each 60 ml bottle for the reaction with solution. Aqueous samples were collected at 10, 20, 30, 40, 50 minutes and 1, 2, 4, 6, 8, 10, 12, 24, 48, 72, 120, 168, 336, and 504 hours. Samples were allowed to react open to the atmosphere and under a N_2 atmosphere in a glove box. For experiments conducted in the glove box, the deionized water was aspirated for 1 hour to remove dissolved contaminants and N_2 was bubbled through the solution until the time of use. Dissolved oxygen was measured using Chemets (Chemetrics, Inc.) to ensure that the solution contained less than $\log f_{O2} = -1.605$ for samples run under N_2, which are generally the groundwater conditions of the Fox River Valley (Schreiber et al., 2003).

After reaction, dissolved oxygen was measured at each sampling time and 15 mls of solution were passed through a 0.45 μm filter (VDW International) into an acid washed polypropylene test tube. Preliminary tests showed no difference in arsenic concentrations when the 0.45 μm was compared to 0.2 μm filters. After filtration, 7 mls were removed and promptly passed through a speciation cartridge (MetalSoft, Inc.) that removed As (V), and allowed As (III) to be retained for analysis (Meng et al., 2002). The samples were then acidified by adding 2% Optima grade HNO_3^- (Optima Pure Grade Fisher Scientific) to each test tube for preservation of the samples. The samples were stored in a dark refrigerator at 4°C until analysis time.

ICP-OES Analysis

The concentrations of arsenic and other major species (Al, Fe, Mn, S, Si, Mg, K, Na, Ca) were determined by Inductively Coupled Plasma-Optical Emission Spectrum (ICP-OES) (Perkin Elmer Instruments, model Optima 4300 DV) within 2-7 days of sampling, with the exception of the K1 and LE7 quartz aqueous solution fractions. These samples were analyzed at 14 days due to instrument downtime. An autosampler was used to inject sample into a cyclonic nebulizer under the operating conditions listed in Appendix B, which were optimized for arsenic detection with multiple-elements conditions. Multiple wavelengths (Appendix C) of elements were analyzed by the ICP-OES in triplicate and the element concentrations were reported as the average of these three analyses. In the case of As, the 193.69 λ arsenic wavelength consistently did not report arsenic, so it was not incorporated into the final reported arsenic concentrations. Analyses were run using quality control, including a blank and known concentrations sample spikes. Working standards were prepared fresh the day before ICP-OES analysis. ICP re-calibration was done at regular

intervals, after 10-15 samples. Detection limit for arsenic from calibration calculations was 1 $\mu g\ L^{-1}$. Error estimates for arsenic concentrations were calculated by recording the standard deviations and were found to be ~1.2 $\mu g\ L^{-1}$.

2.4 Extraction

After ~120 hours of aqueous reaction, when dissolved arsenic was no longer detected, solution was decanted and the remaining PM/PMG sediment was extracted to determine arsenic concentrations associated with iron oxides (LaForce et al., 2002; Chao and Zhu, 1983: Tessier; 1979). The extraction was conducted to re-dissolve iron oxides by reducing ferric iron. This releases any arsenic held in or on the oxide. The oxide extraction was performed by preparing a solution of 75 mls of 18 MΩhm deionized water, 25 mls of glacial acetic acid, and 6.949 grams of hydroxylamine hydrochloride (Fisher Scientific, Inc.). Twenty milliliters of this 1M hydroxylamine hydrochloride/25% acetic acid solution was added to 5 grams sediment and vigorously shaken. The samples were placed in a boiling water bath for 6 hours, centrifuged for 20 minutes at 12000g, the supernant decanted and filtered through a 0.45 μm filter. The solution was then acidified to pH < 2 and analyzed with ICP-OES. In both extractions, samples were run in triplicate and a blank solution was used for quality control.

Geochemical Modeling

Equilibrium speciation and mineral stability calculations were done using Geochemists Workbench (3.1) (Bethke, 1998) which uses thermodynamic data from Johnston et al., (1991), Delany and Lundeen, (1990), Helgeson et al., (1978).

CHAPTER 3-RESULTS

3.1 Mineralogical Results

Optical Microscope Analysis

Core sample K1 of the St. Peter Sandstone was characterized as well-rounded, well-sorted, loosely cemented, fine to medium grained quartz arenite. Pores between the sand grains were filled with iron sulfide, creating sulfidic veins and nodules (¼ cm to 4 cm). A thin band, ¼ - ½ cm wide, of orange goethite commonly borders the arenite/sulfide contact. Sample Le25c is entirely an iron sulfide nodule, 3 x 5 x 4 cm^3, which occurred in the St. Peter Sandstone, and contained goethite and elemental sulfur on its exposed surfaces (Figure 3.1). Under 10x magnification, quartz grains are commonly fractured. In some areas of the fracture zones, PM grains encroach upon the quartz giving the grain edges a 'chewed' texture (Figure 3.2).

Core sample K2 (Figure 3.3) of the Sinnipee Group is a dark gray, argillaceous dolostone containing minor amounts of very fine grained sand. Iron sulfide in this unit occurs very differently from the St. Peter Sandstone. The sulfide mineralization appears as very thin (0.5 mm wide), undulatory sulfide layers that rarely contain oxidized zones of goethite between the dolomite/sulfide contact (Figure 3.4).

Previous work indicated that the iron sulfide consisted of both pyrite and marcasite (Schreiber et al., 2000). The present optical microscope analysis confirmed the co-presence of pyrite with marcasite, a polymorph of FeS_2. Determination of marcasite from pyrite was optically based on the stronger yellow appearance of marcasite, along with its characteristic strong white to yellowish birefringence and strong anisotropy, compared to the lack of

Figure 3.1. (a) Example of pyrite/marcasite nodule, Le25c, occurring in the quartz arenite. The orange-red and white are goethite and elemental sulfur, respectively. (b) Core sample K1 quartz arenite with 2 cm PM (nodule) showing oxidation to goethite at the edges. (UW1950/...2.1, 4.1)

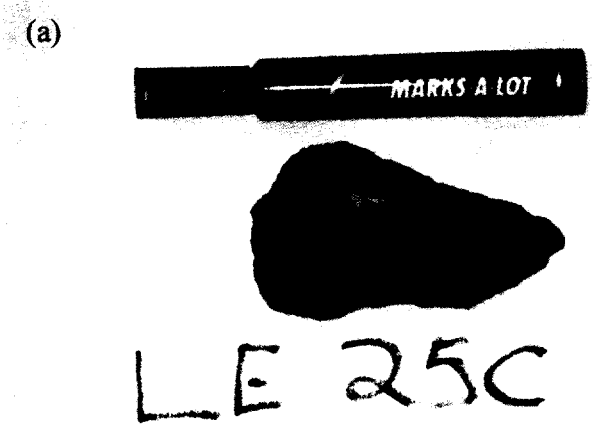

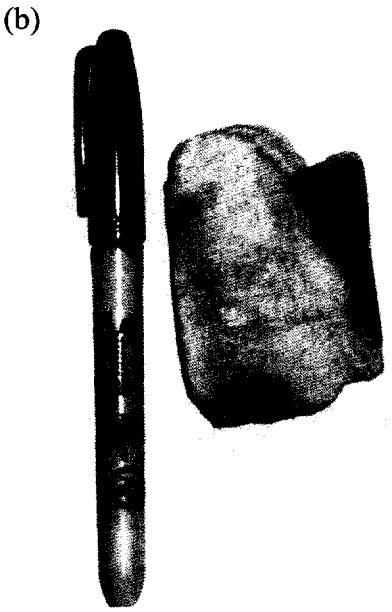

Figure 3.1. (a) Example of pyrite/marcasite nodule, Le25c, occurring in the quartz arenite. The orange-red and white are goethite and elemental sulfur, respectively. (b) Core sample K1 quartz arenite with 2 cm PM (nodule) showing oxidation to goethite at the edges. (UW1950/...2.1, 4.1)

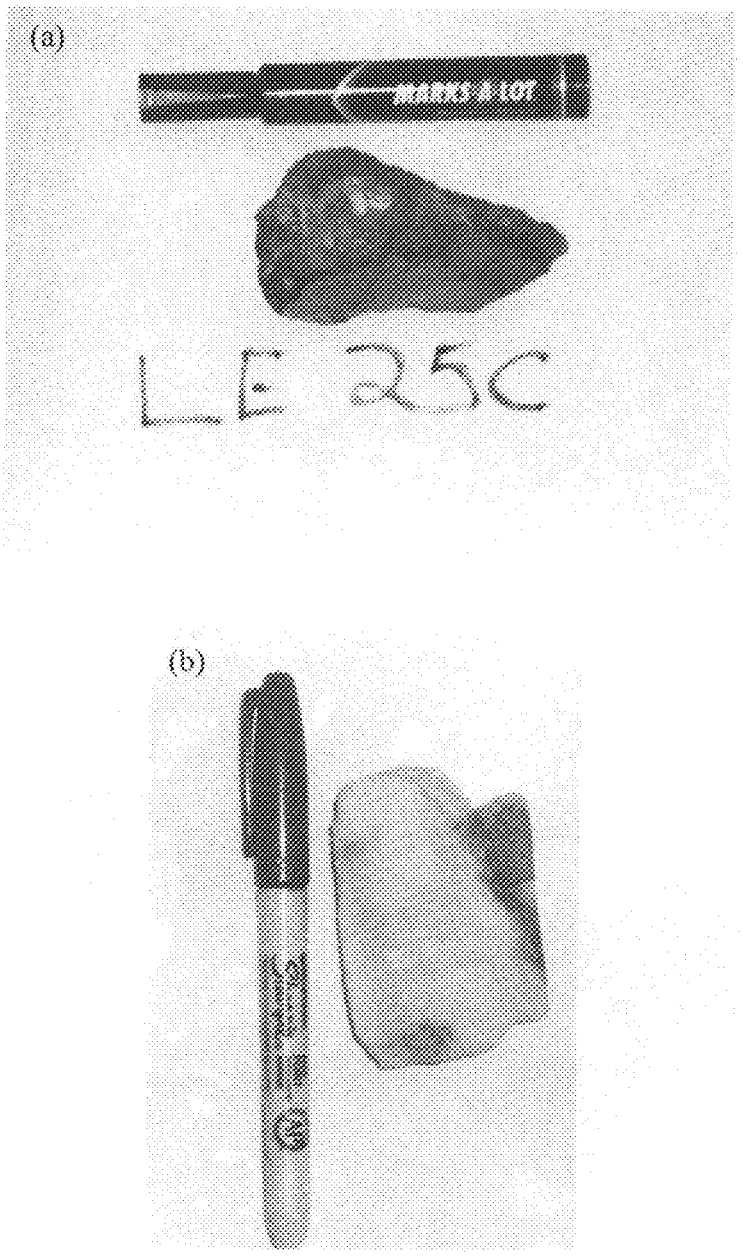

Figure 3.2 Photomicrographs of PM thin sections (a) K1 and (b) Le25c. Field of view is 2mm. Light grains are quartz, massive black areas are PM cement, and small dark black multi-granular regions are goethite. (UW1950/...3.5, 2.4)

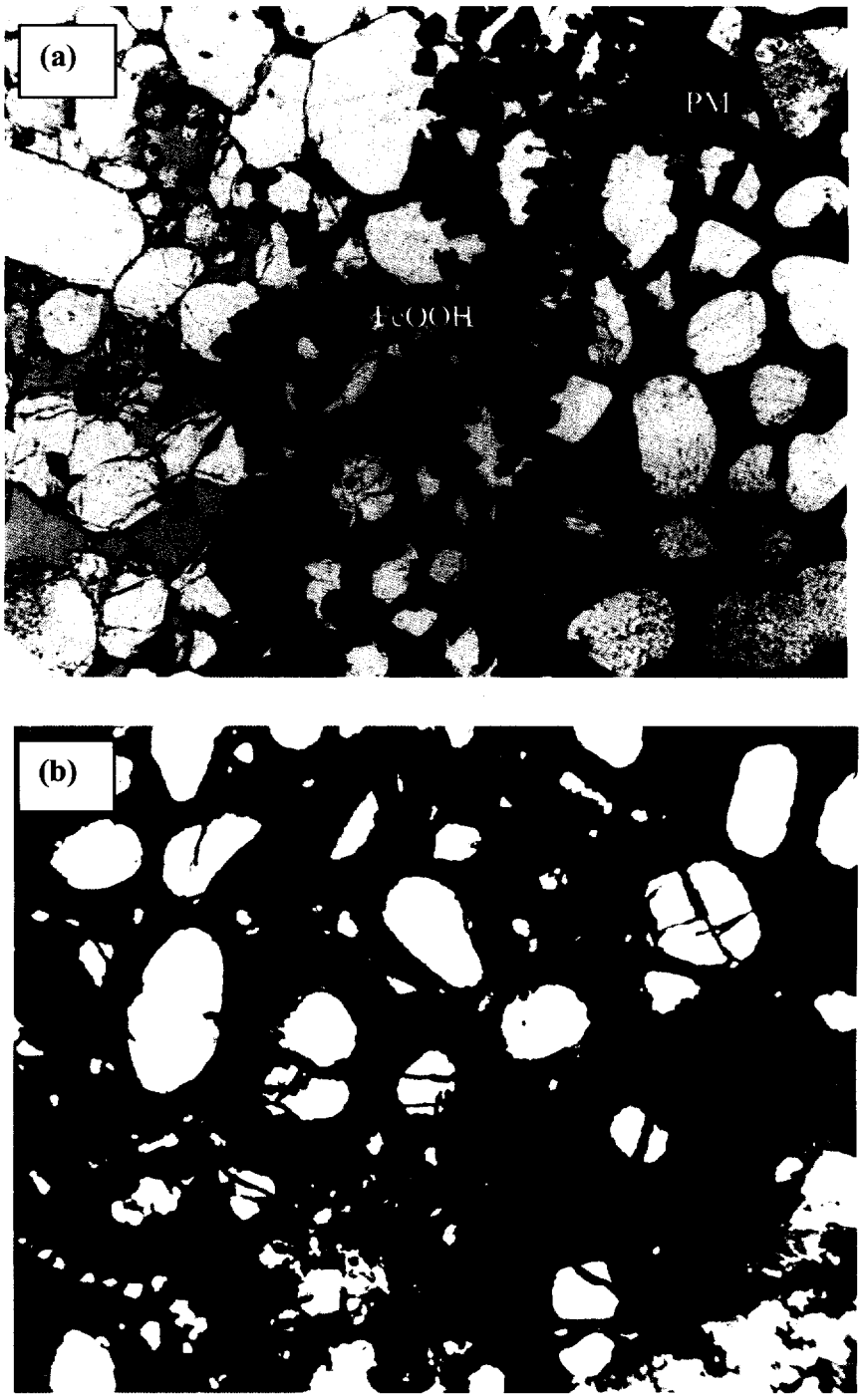

Figure 3.2 Photomicrographs of PM thin sections (a) K1 and (b) Le25c. Field of view is 2mm. Light grains are quartz, massive black areas are PM cement, and small dark black multi-granular regions are goethite. (UW1950/...3.5, 2.4)

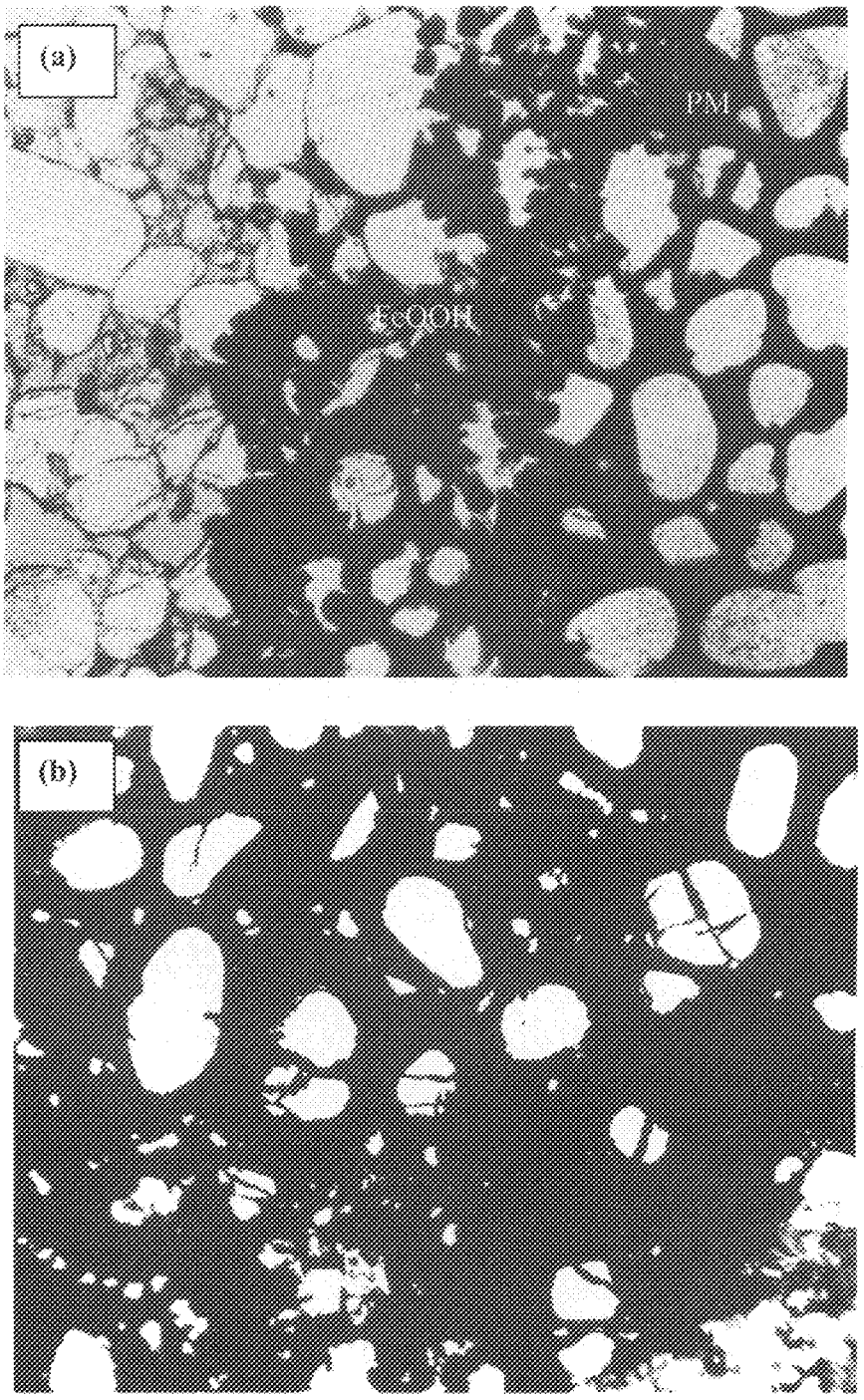

Figure 3.3. Dolostone core sample K2. Pyrite and marcasite occur as thin (0.5 mm), undulatory veins. (UW1950/4.1)

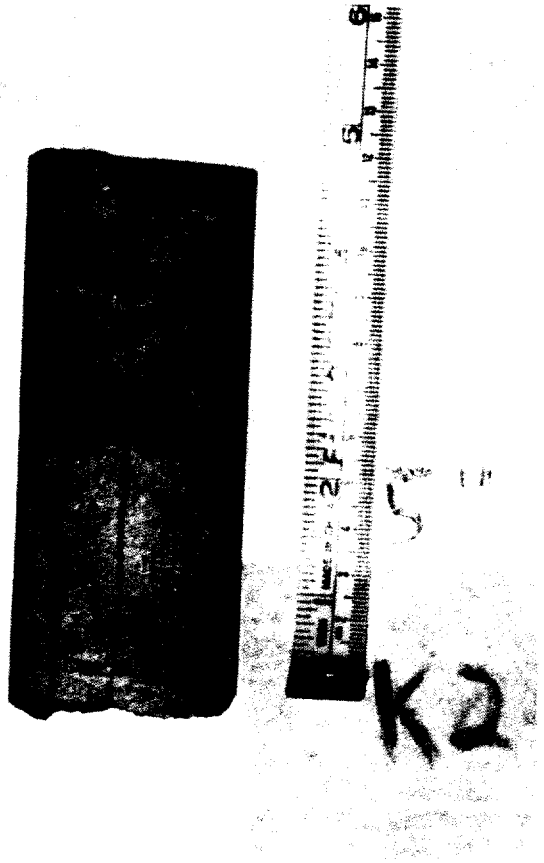

Figure 3.3. Dolostone core sample K2. Pyrite and marcasite occur as thin (0.5 mm), undulatory veins. (UW1950/4.1)

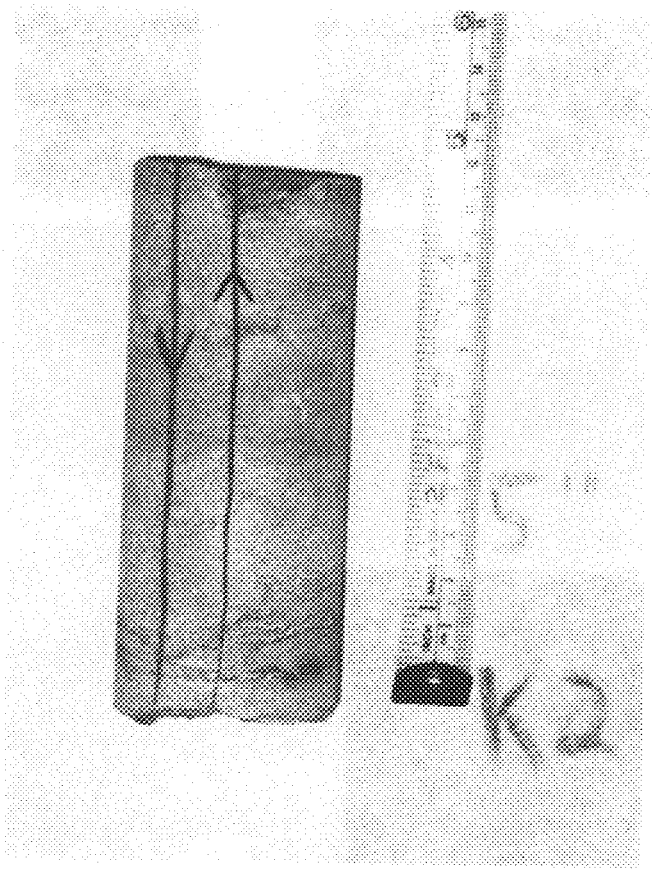

Figure 3.4. Photomicrograph of K1 in thin section. The image shows PM occurring as veining through the dolomite, compared to nodular occurrence in the St. Peter Sandstone. Field of view is 3 mm. (UW1950/4.4)

Figure 3.4. Photomicrograph of K1 in thin section. The image shows PM occurring as veining through the dolomite, compared to nodular occurrence in the St. Peter Sandstone. Field of view is 3 mm. (UW1950/4.4)

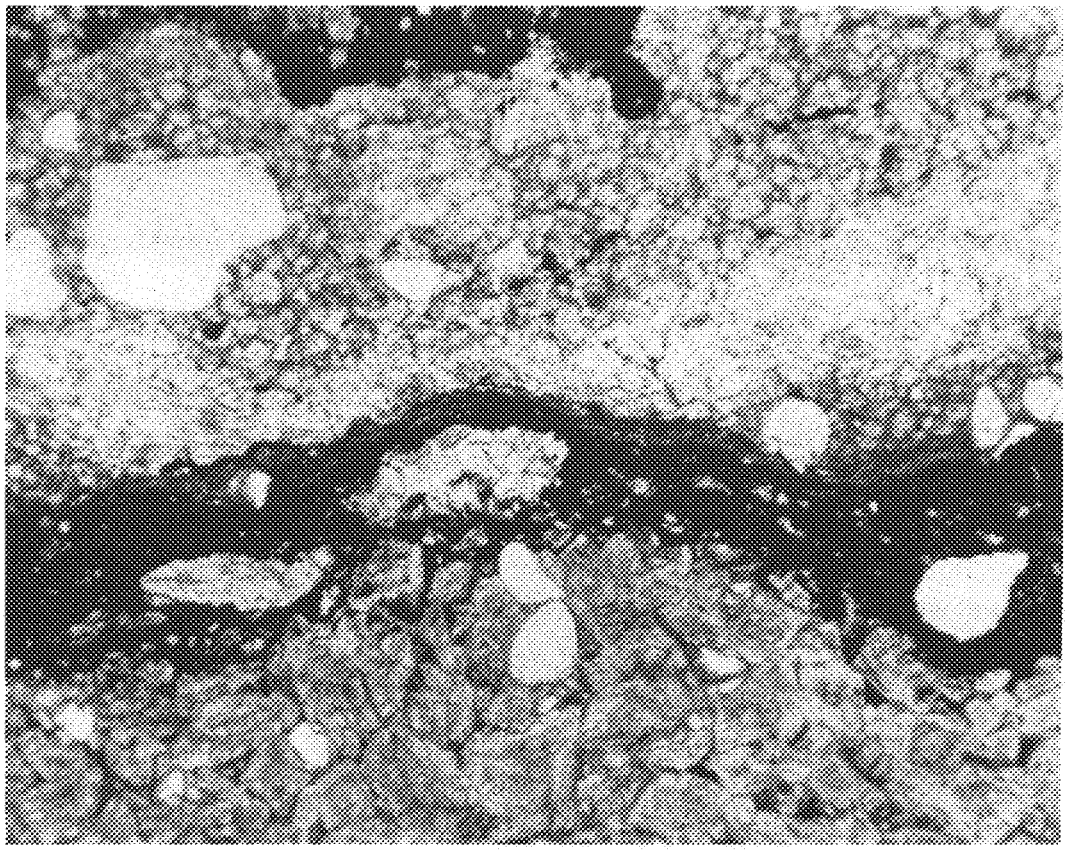

birefringence and weak to moderate anisotropy of pyrites.

BET Specific Surface Area

Brunauer Emmet Teller (BET) specific surface areas measured for K1, K2, Le7, Le25c, and AsFeS are 2.23, 1.54, 1.16, 0.83, and 0.07 m^2/g, respectively.

X-Ray Diffraction

X-Ray diffraction spectra were consistent with two iron sulfide phases (Figure 3.5), although the relative amounts of each phase in the system has not been quantified. The unreacted sandstone samples consist of quartz, pyrite, marcasite, and goethite and the unreacted dolostone sample consist of dolomite, quartz, marcasite, pyrite and minor amounts of goethite. After reaction with solution for 3 weeks, the mineralogy appeared largely unchanged (with the exception of Le25c) at the resolution afforded by XRD (Figure 3.6). Le25c was the only sample that showed significant mineralogical change; no goethite was detected before reaction, but was observed after reaction. X-Ray diffraction failed to detect discrete arsenic phases, so Electron Microprobe and Raman Spectroscopy were employed.

Electron Microprobe Analysis

Samples Le7, Le25c, K1, and K2 were probed before aqueous reaction (Figure 3.7) and Le25c was analyzed again after 21 days of reaction. Traverses were done entirely within PM grains and across grain boundaries of PM with goethite, quartz and dolomite.

Figure 3.8 shows arsenic was distributed uniformly within the PM grains. Goethite was commonly present around pyrite and marcasite grains in samples before they were reacted. In sample Le7, arsenic concentrations in the iron sulfide were lower near the boundary with goethite. In K2, the majority of the arsenic was actually associated with the

Figure 3.5. XRD scan of sandstone hand sample (a) Le7, (b) LE25c, and (c) dolostone core K2, before leaching. Analysis shows mainly the presence of quartz (Q), dolomite (D), iron sulfide phases marcasite (M) and pyrite (P), and lesser amounts of goethite (G). (UW1950/…1.1, 2.2, and 3.3)

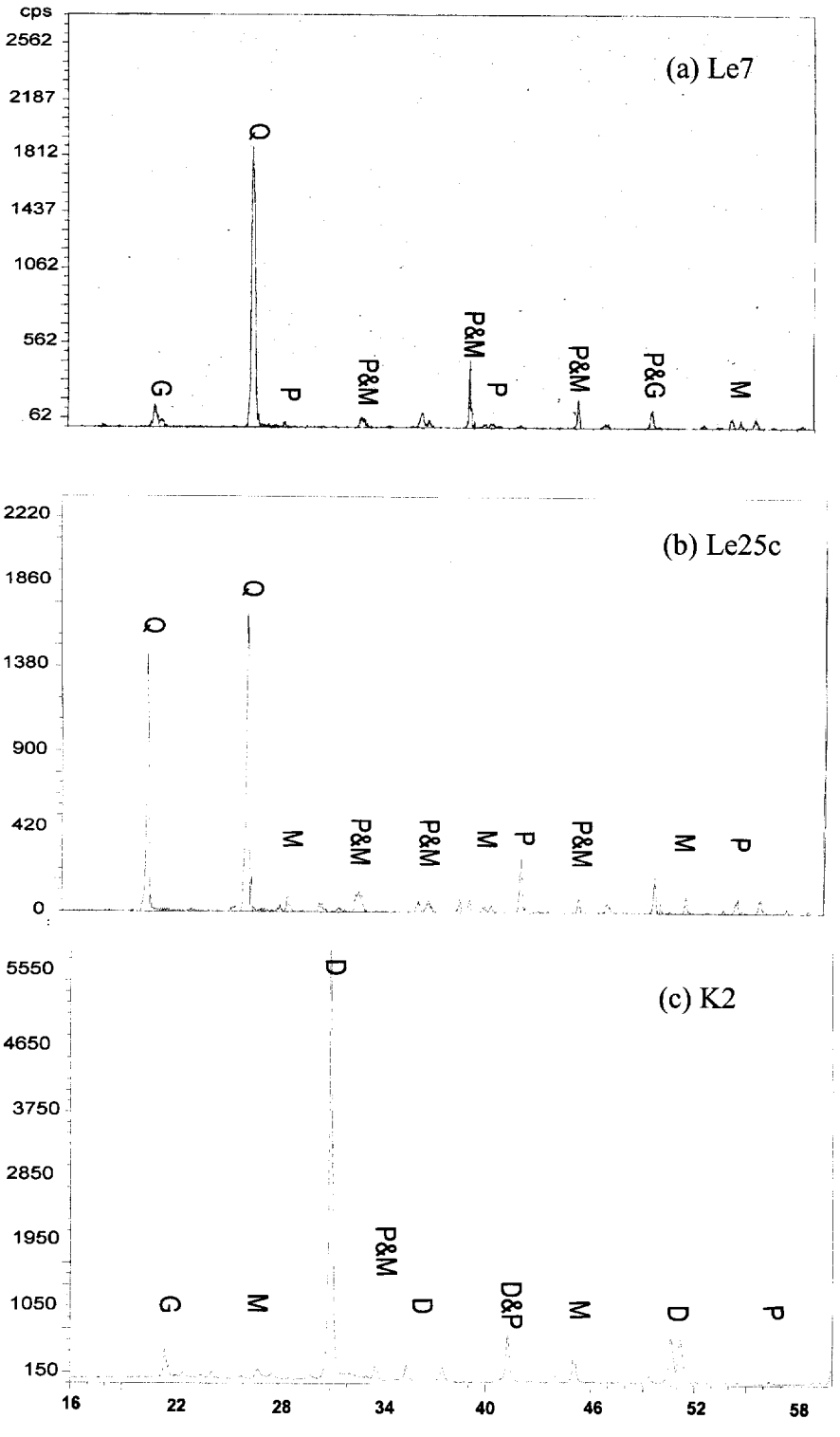

Figure 3.6. XRD scan of (a) Le25c and (b) K2 after leaching. Analysis shows the same bulk mineralogy as the initial scan, except for the appearance of goethite in Le25c. Mineral names abbreviated as in Figure 3.5. (UW1950/…2.3, 3.4)

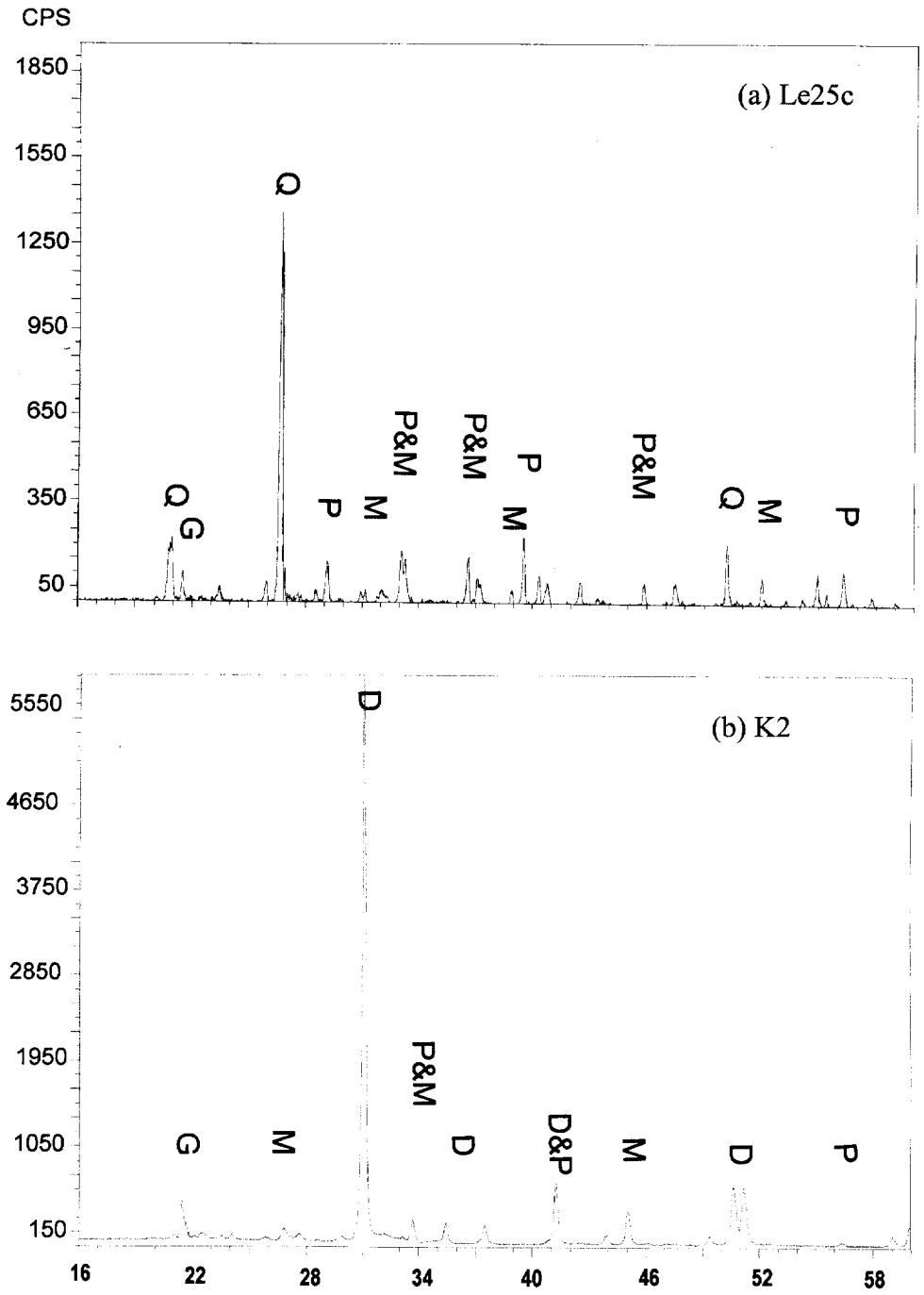

Figure 3.7 Electron Microprobe backscatter images and EDS spectra for traverses within grains before reaction (a, b) Le7, (c, d) Le25, and (e, f) K2. Lines in the photos indicate traverse positions. (UW1950/…1.2, 2.4, and 4.4).

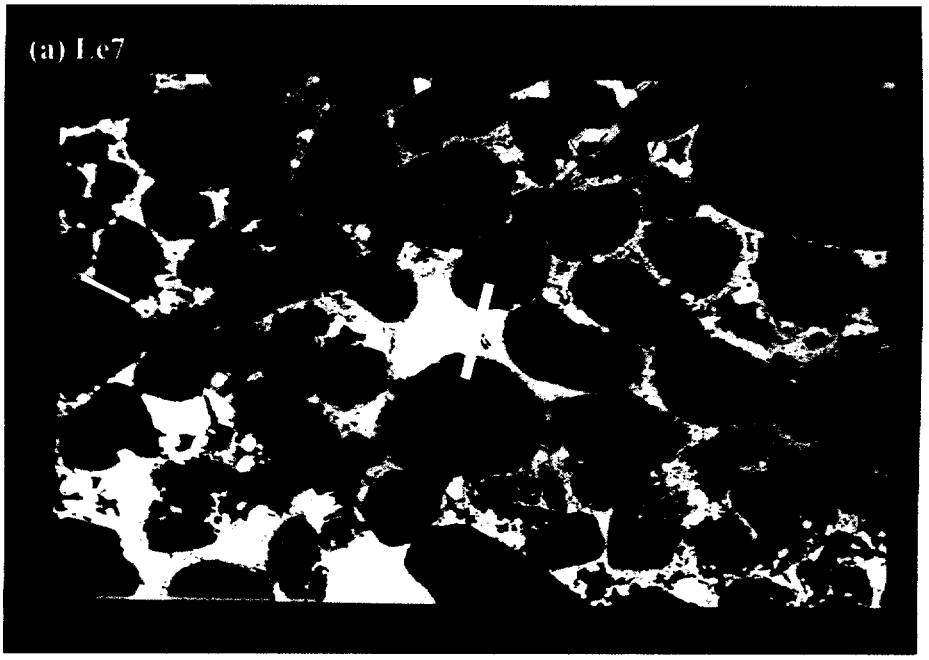

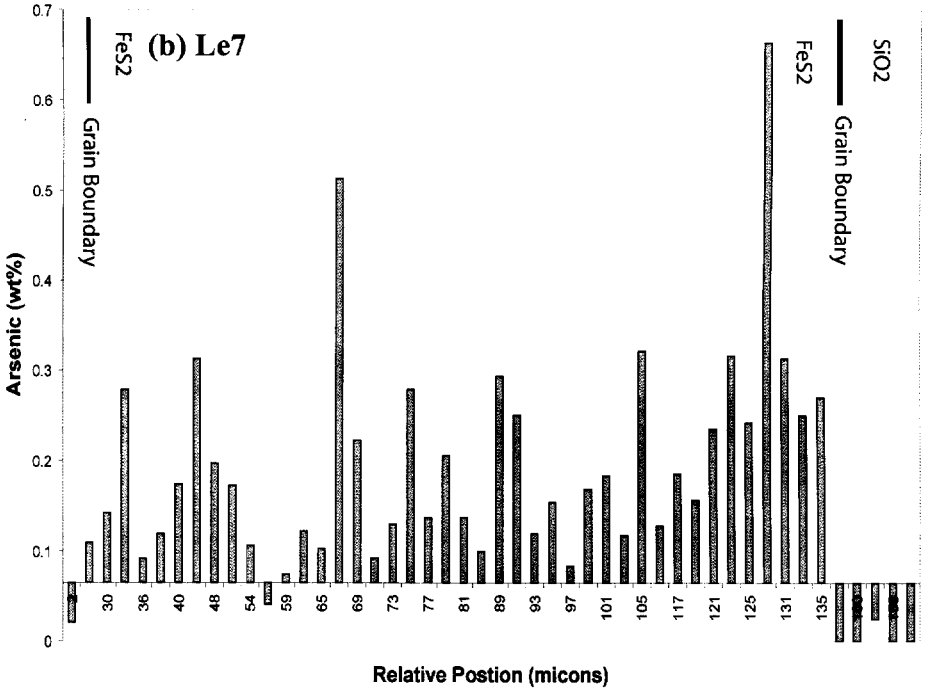

Figure 3.7 Electron Microprobe backscatter images and EDS spectra for traverses within grains before reaction (a, b) Le7, (c, d) Le25, and (e, f) K2. Lines in the photos indicate traverse positions. (UW1950/…1.2, 2.4, and 4.4).

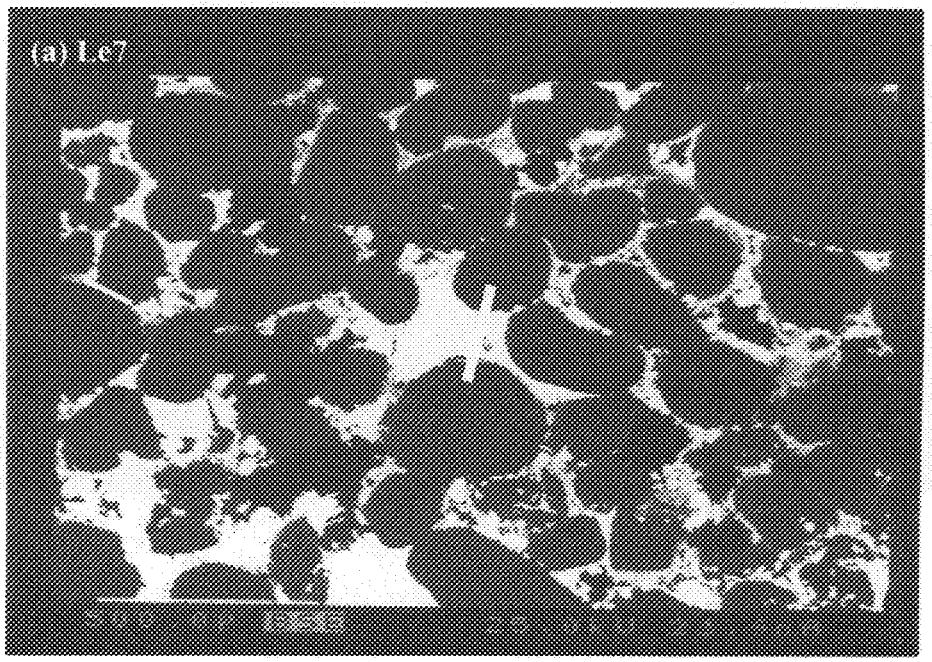

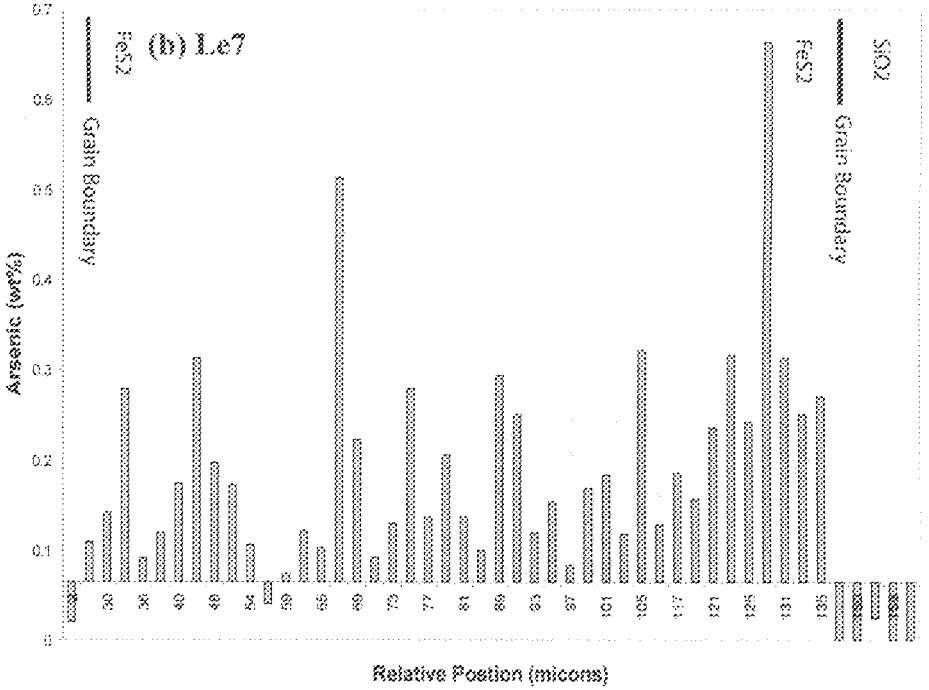

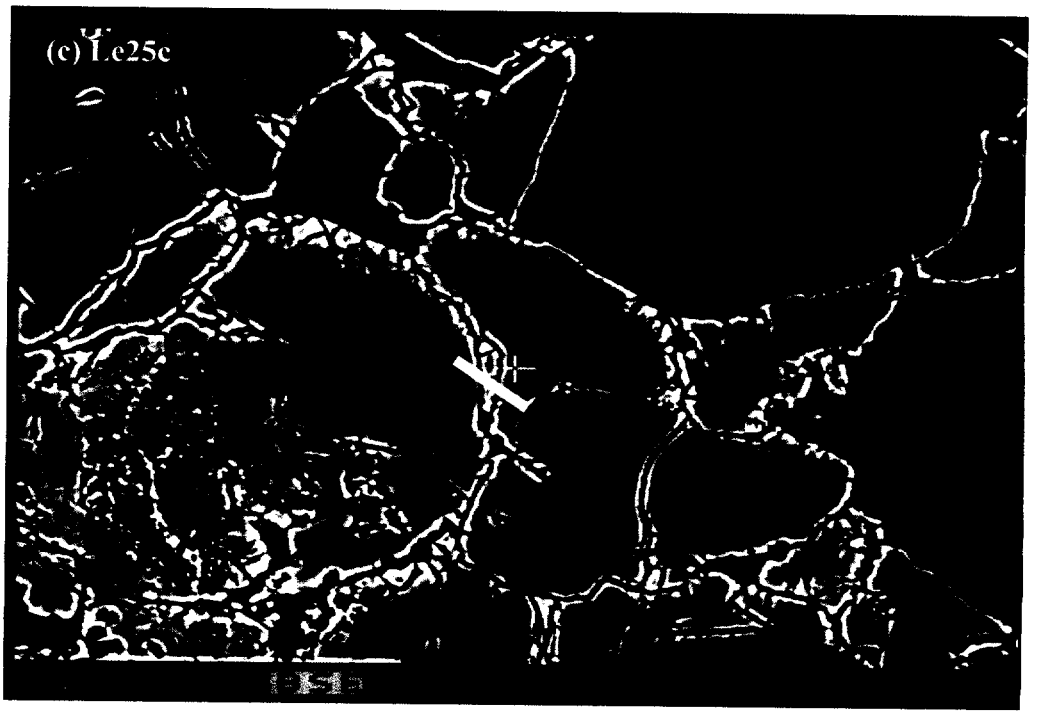
(c) Le25c

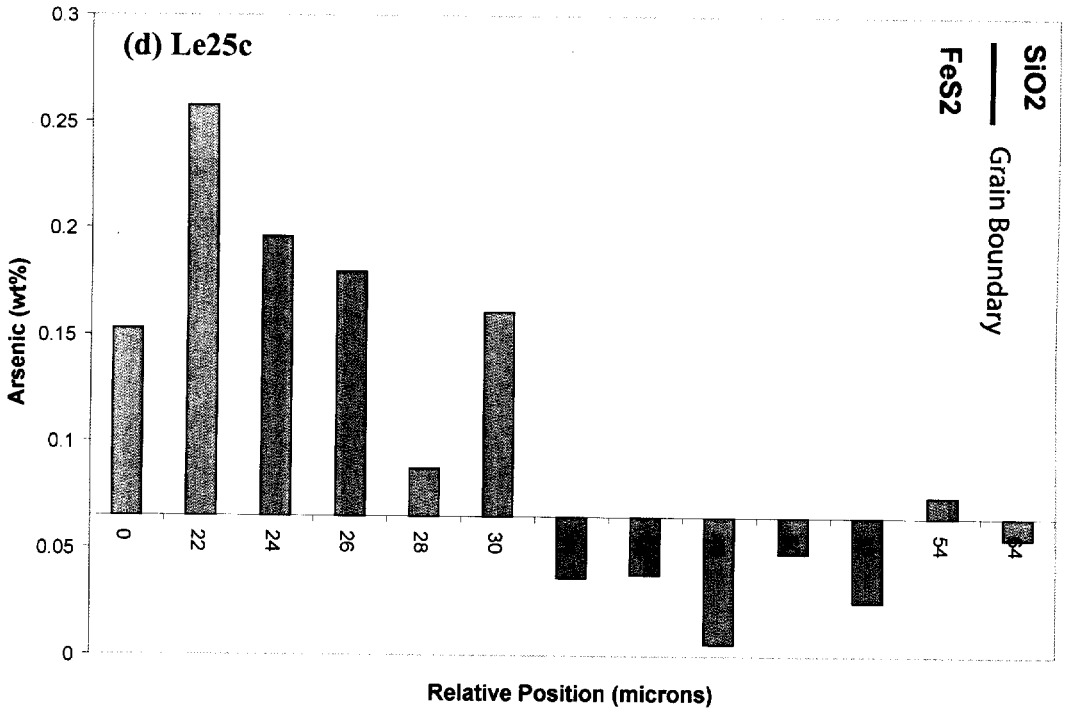
(d) Le25c
SiO2
FeS2
Grain Boundary
Arsenic (wt%)
0.3
0.25
0.2
0.15
0.1
0.05
0
0
22
24
26
28
30
54
Relative Position (microns)

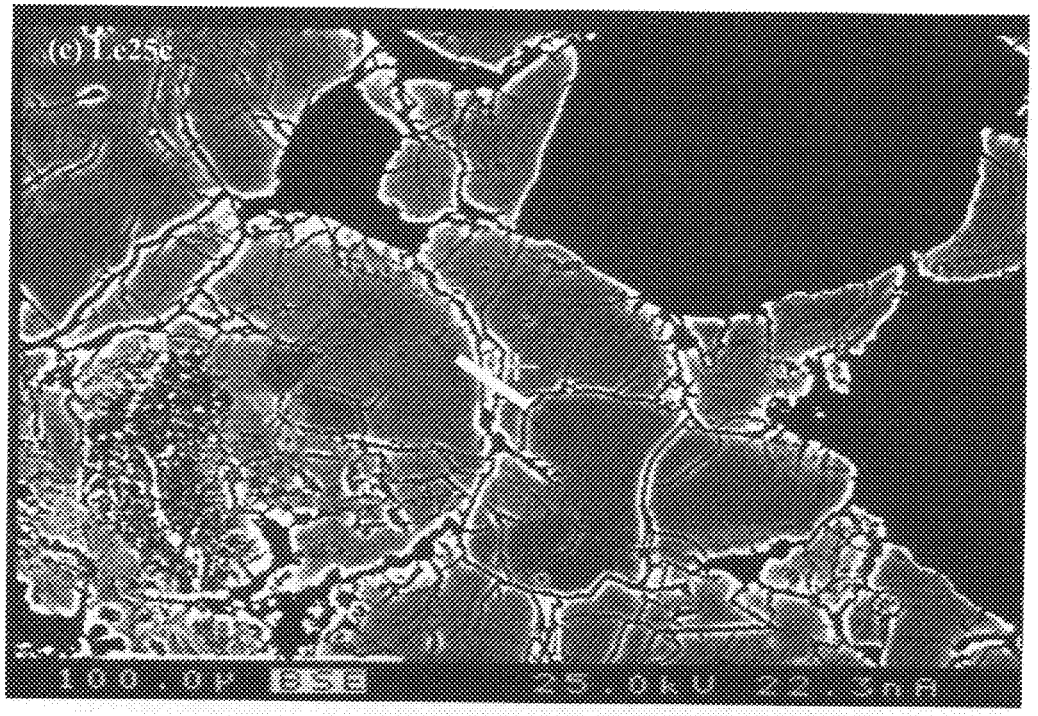
(e) Le25c

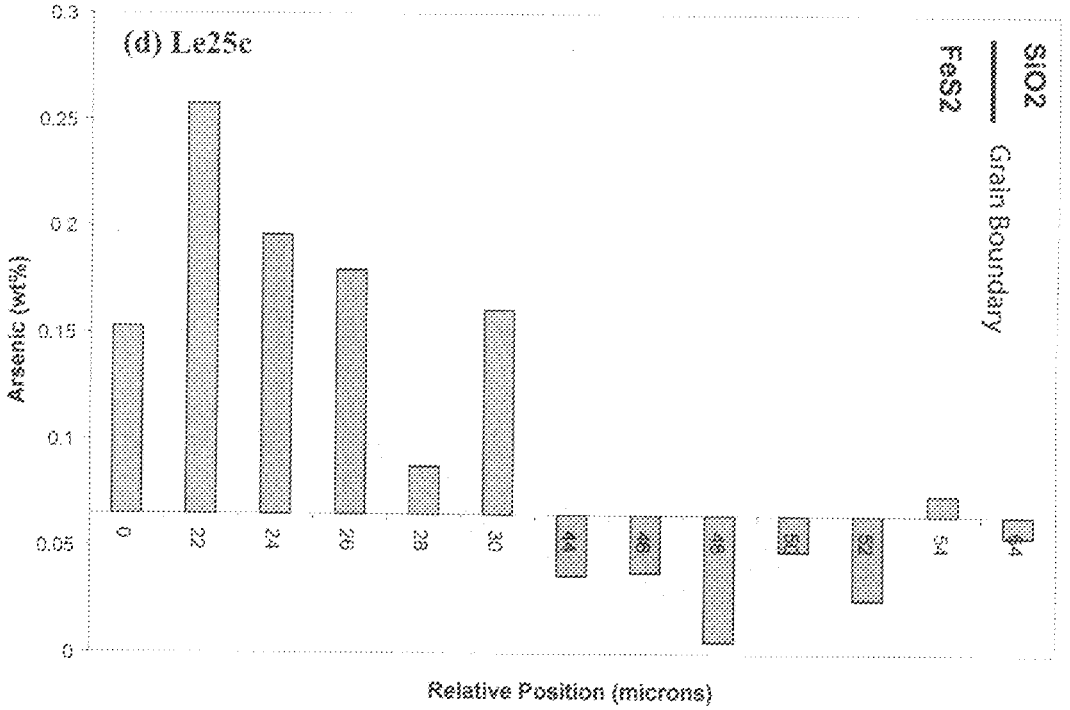
(d) Le25c
Arsenic (wt%)
0.3
0.25
0.2
0.15
0.1
0.05
0
0
22
24
26
28
30
SiO2
FeS2
Grain Boundary
Relative Position (microns)

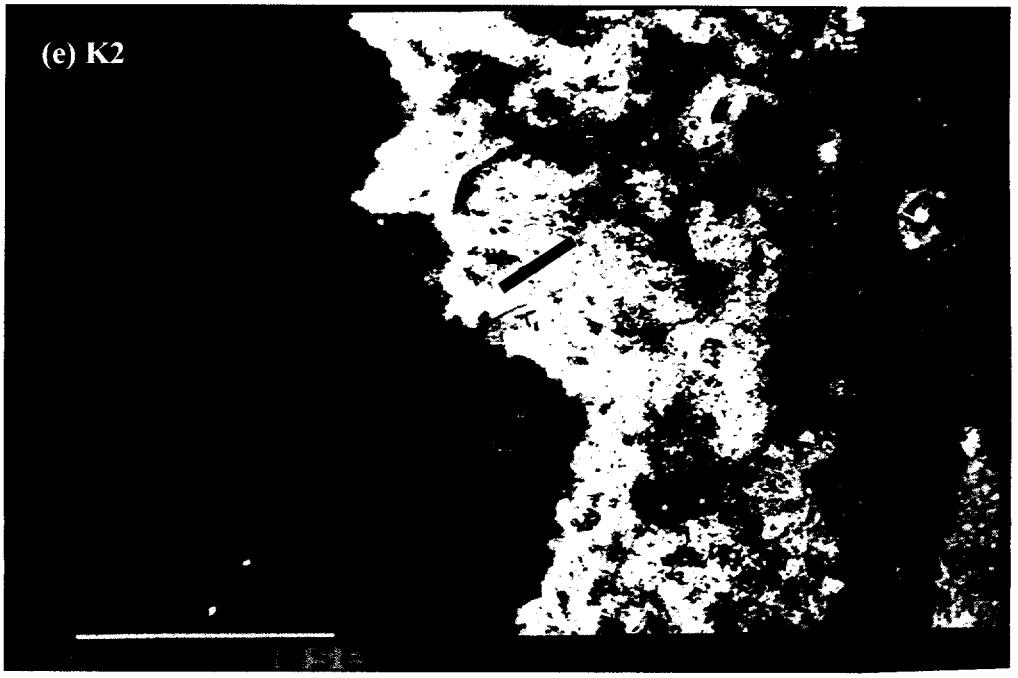
(e) K2

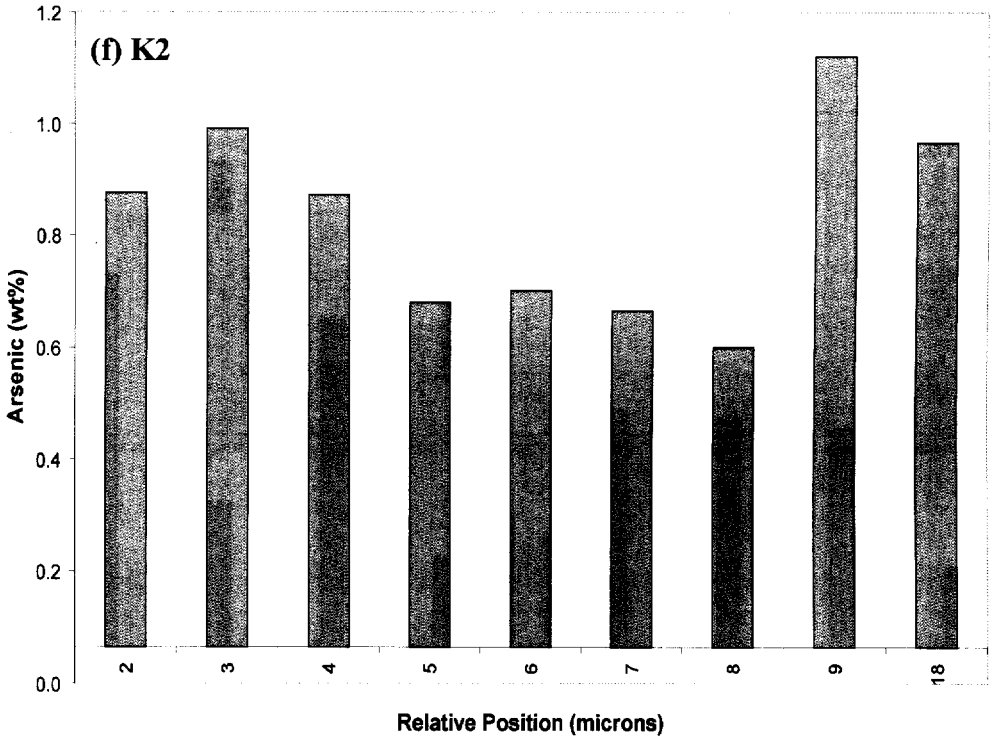
(f) K2
Arsenic (wt%)
1.2
1.0
0.8
0.6
0.4
0.2
0.0
2
3
4
5
6
7
8
9
18
Relative Position (microns)

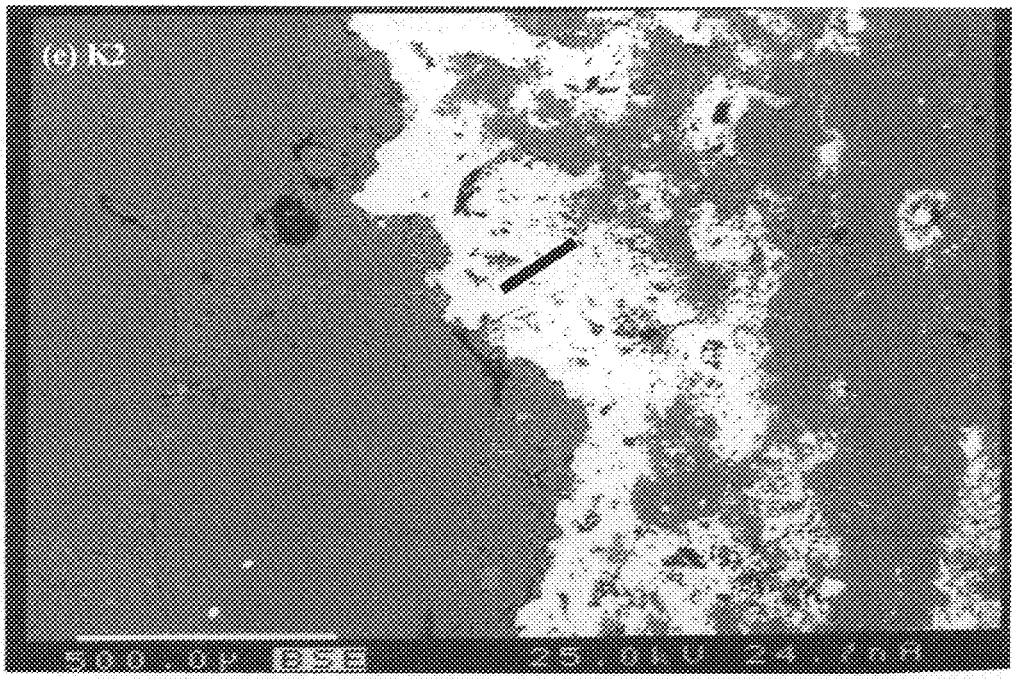
(e) K2

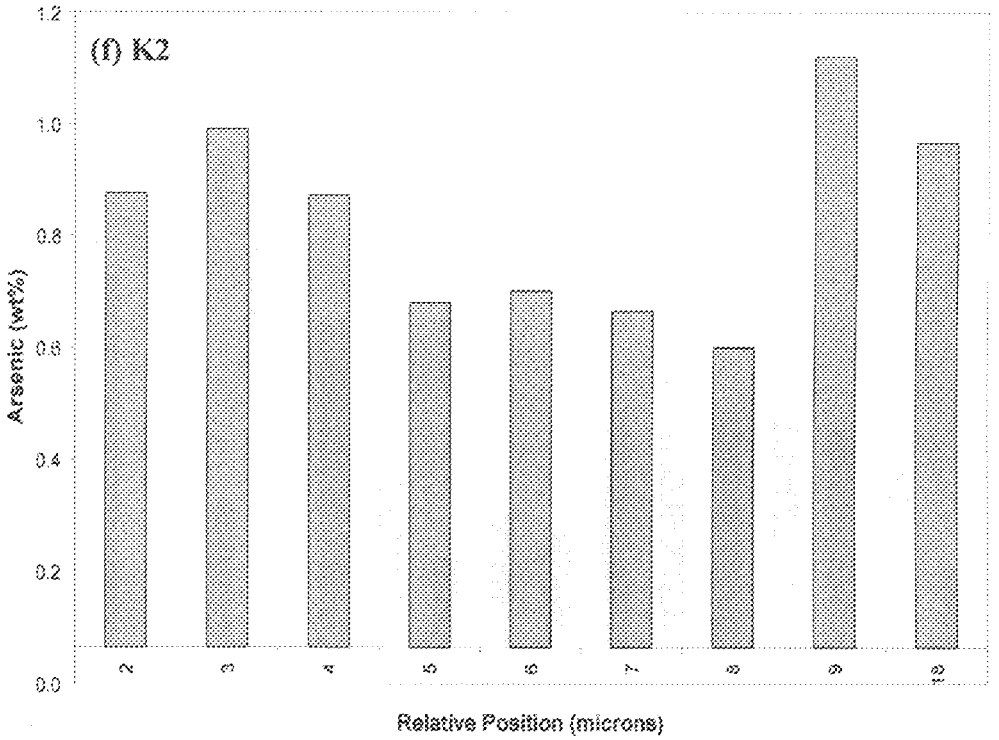
(f) K2
Arsenic (wt%)
1.2
1.0
0.8
0.6
0.4
0.2
0.0
2
3
4
5
6
7
8
9
10
Relative Position (microns)

Figure 3.8. Electron Microprobe backscatter image and EDS spectra of traverses across grain boundaries before reaction (a, b) Le7 and (c, d) K2. (UW1950/...1.2, 4.4)

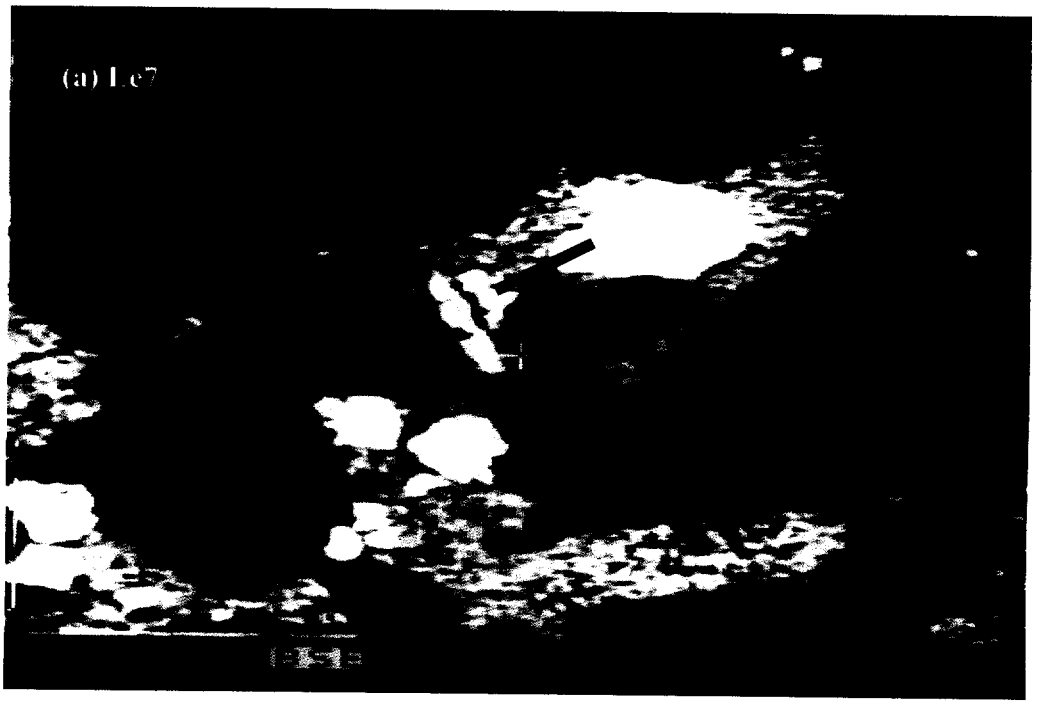

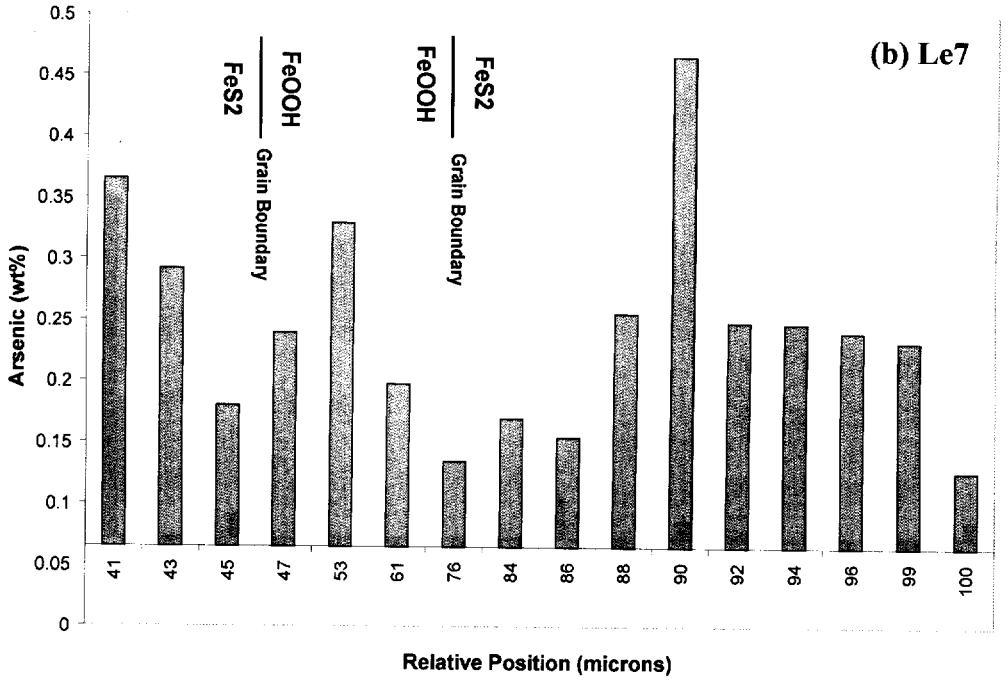

Figure 3.8. Electron Microprobe backscatter image and EDS spectra of traverses across grain boundaries before reaction (a, b) Le7 and (c, d) K2. (UW1950/…1.2, 4.4)

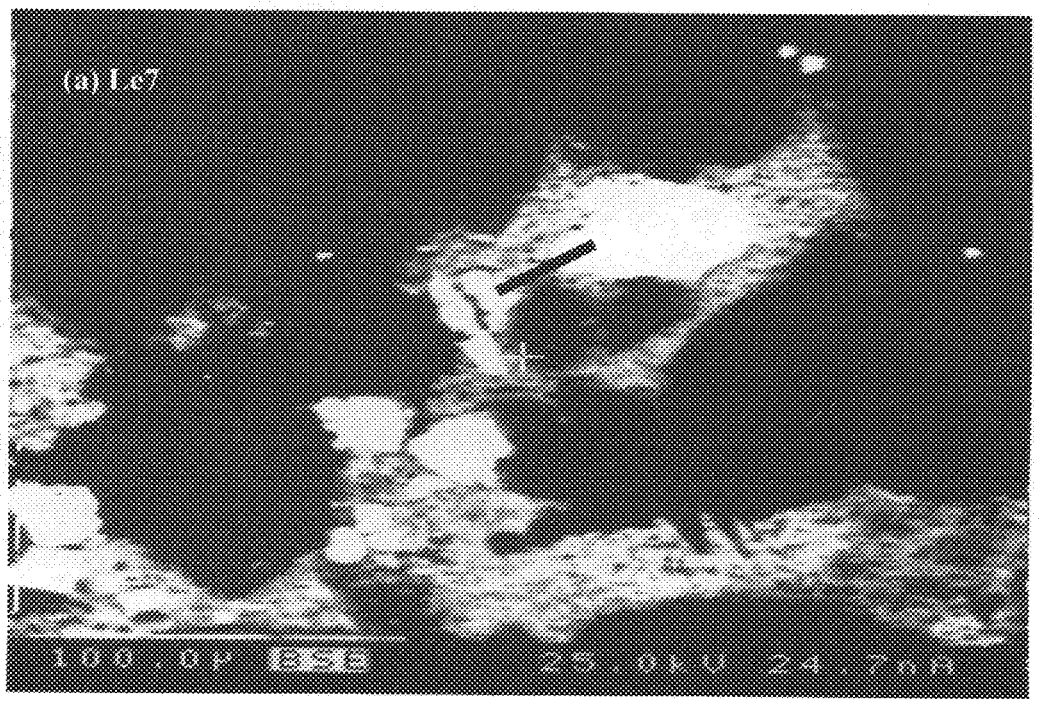

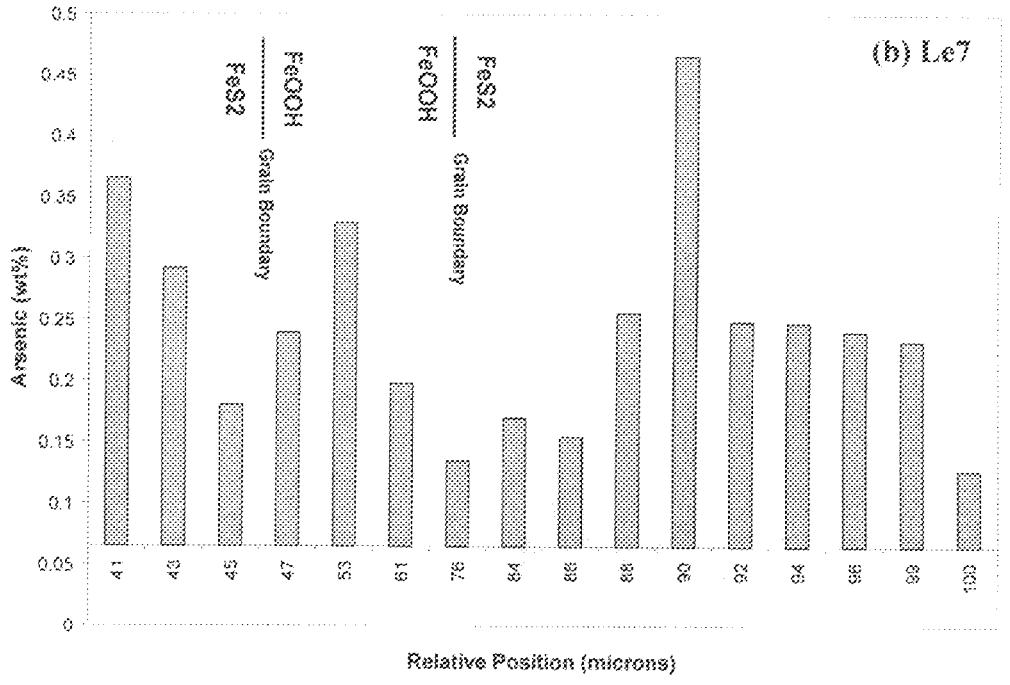

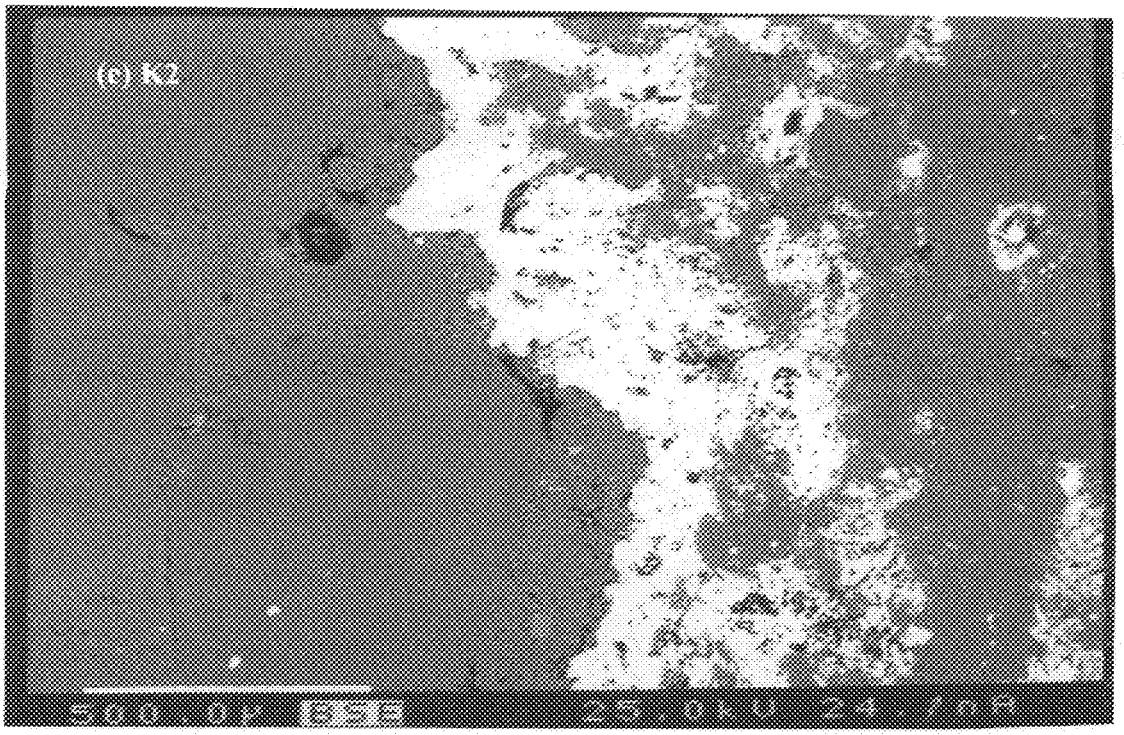
(c) K2

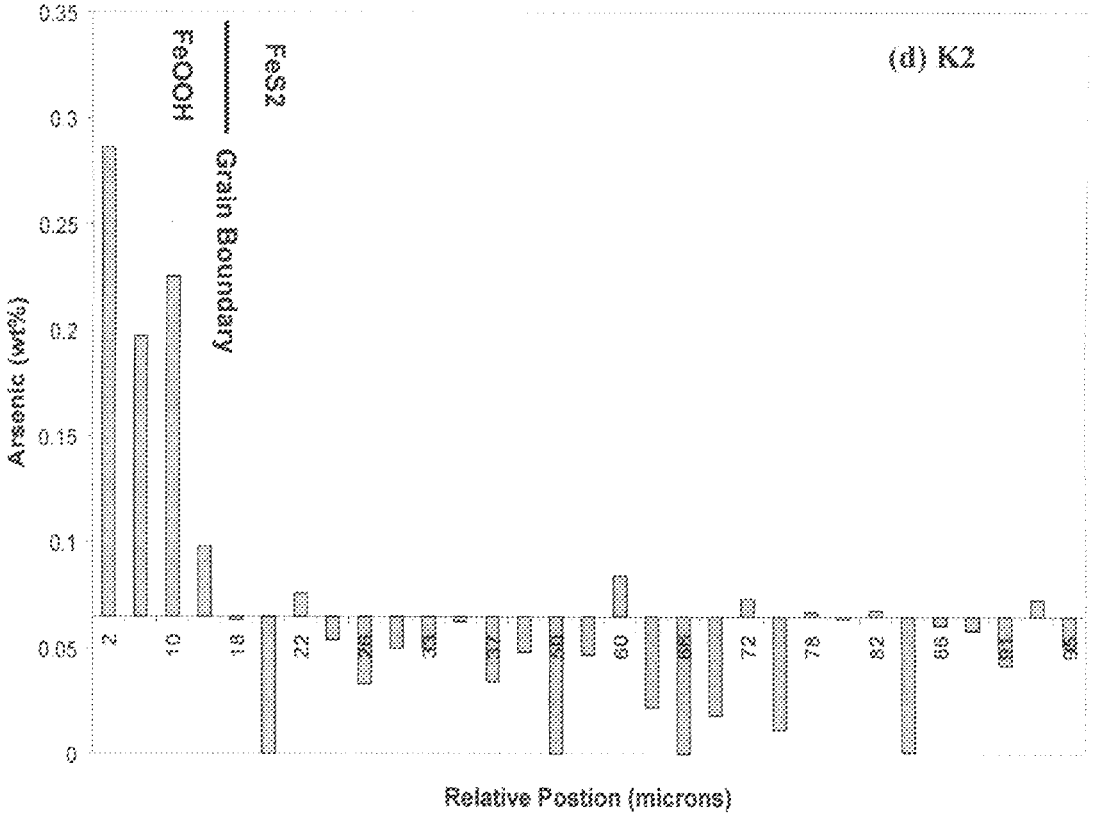
(d) K2
FeS2
FeOOH
Grain Boundary
Arsenic (wt%)
0.35
0.3
0.25
0.2
0.15
0.1
0.05
0
2
10
18
22
60
72
78
82
88
Relative Postion (microns)

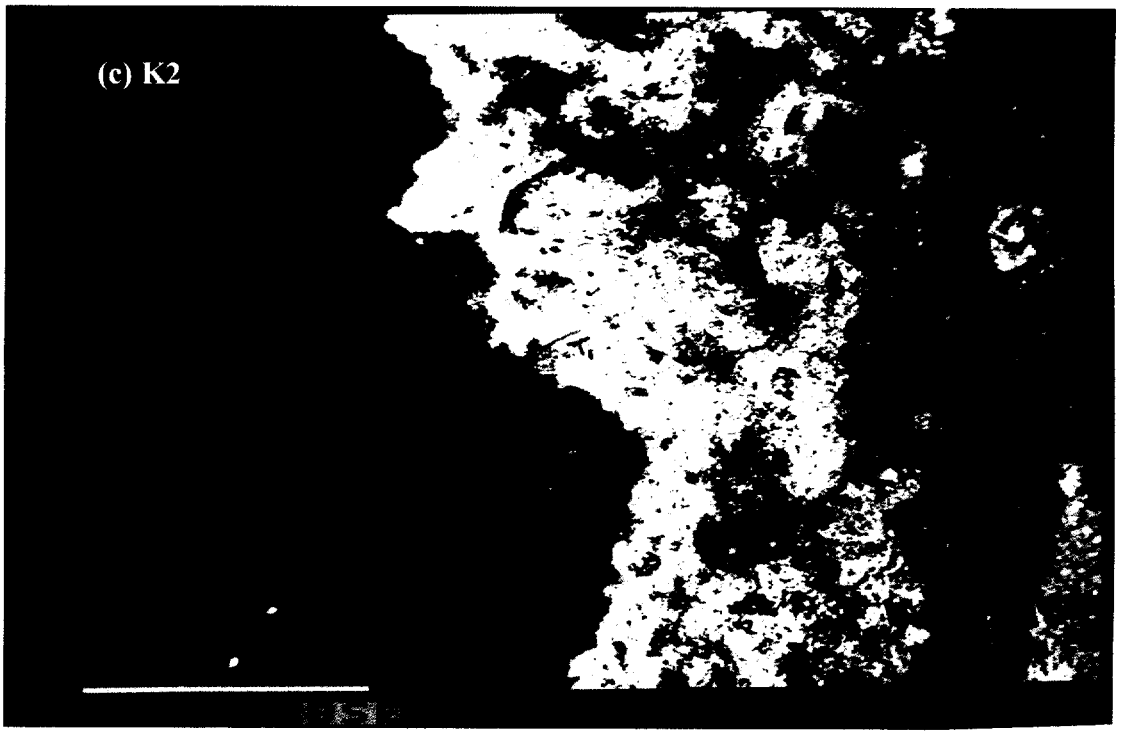
(c) K2

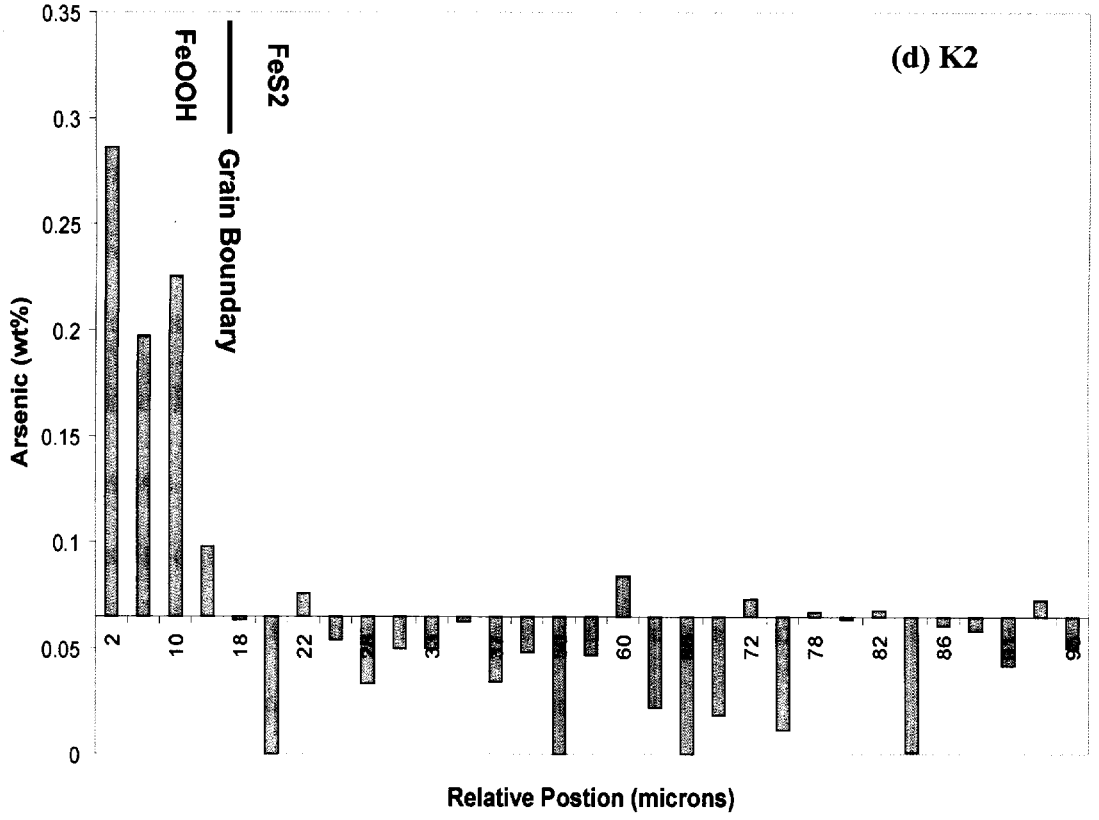
(d) K2
FeOOH
FeS2
Grain Boundary
Arsenic (wt%)
0.35
0.3
0.25
0.2
0.15
0.1
0.05
0
2
10
18
22
30
60
72
78
82
86
Relative Postion (microns)

goethite (0.25 weight %), while PM contained very little arsenic.

Reanalyzing the mineralogy of Le25c after reaction illustrates the development of an undetermined phase that formed around most PM grains during the reaction (Figure 3.9). These phases were ~1μm in scale, which was not resolvable with the Electron Microprobe EDS. Analysis shows that these undetermined phases have high oxygen content, and when iron and oxygen concentrations increase, sulfur is depleted, and arsenic concentrations become considerable, as illustrated in location 7 (Table 3.1).

Raman Spectroscopy

Raman spectroscopy shows a shift in bulk chemical composition of Le25c after reaction (Figure 3.10; Table 3.2) consistent with X-ray diffraction results and hinted at by Electron Microprobe results. Before reaction, Raman lines were identified at 388, 377, 338, 323 and 209 cm^{-1}. The peaks at 388 and 323 cm^{-1} are assigned to marcasite, 377 and 338 cm^{-1} to pyrite, and the 209 cm^{-1} corresponded to arsenic in arsenopyrite (McGuire et al., 2001; Mernagh and Trudu, 1993; Turcotte et al, 1993). Spectra of sample Le25c after solution reaction still show peaks for marcasite (323 cm^{-1}) and pyrite (400 and 338 cm^{-1}), but new lines are evident that coincide with goethite lines (397 cm^{-1}) and a peak at 446 cm^{-1} indicative of arsenic sorbed onto goethite (Courtin-Nomade et al., 2003).

3.2 Chemical Characterization

Acid Digestion of Mineral Fractions

Results of chemical digestion and ICP-AES analysis are reported in Table 3.3. Total arsenic contents of the separated PM, quartz, and dolostone fractions are 0.02 to 0.69, undetectable to 0.02, and 0.01 weight %, respectively.

Figure 3.9.Electron microprobe backscatter image of a PM grain Le25c after reaction. Data were collected as spot analysis, not line traverses. (UW1950/2.5)

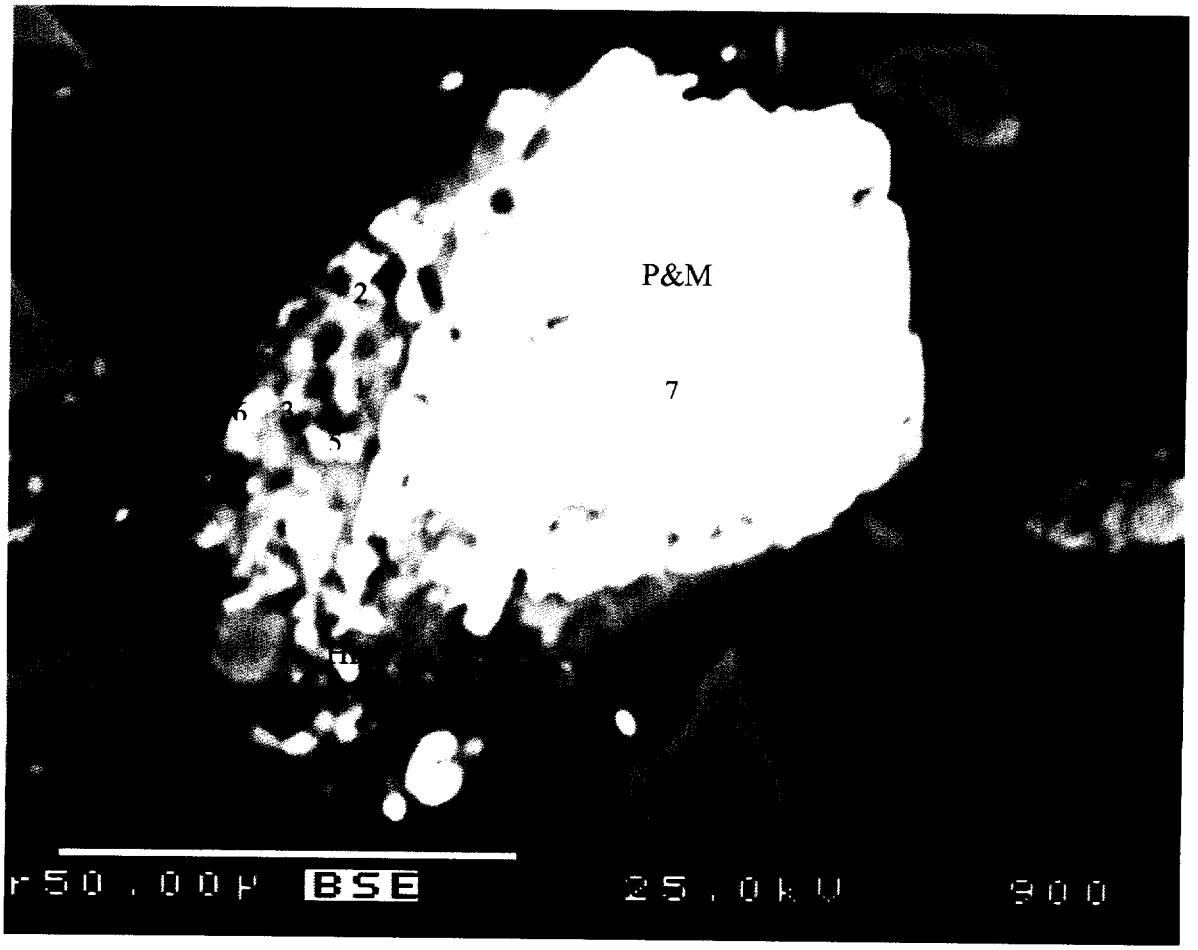

Figure 3.9.Electron microprobe backscatter image of a PM grain Le25c after reaction. Data were collected as spot analysis, not line traverses. (UW1950/2.5)

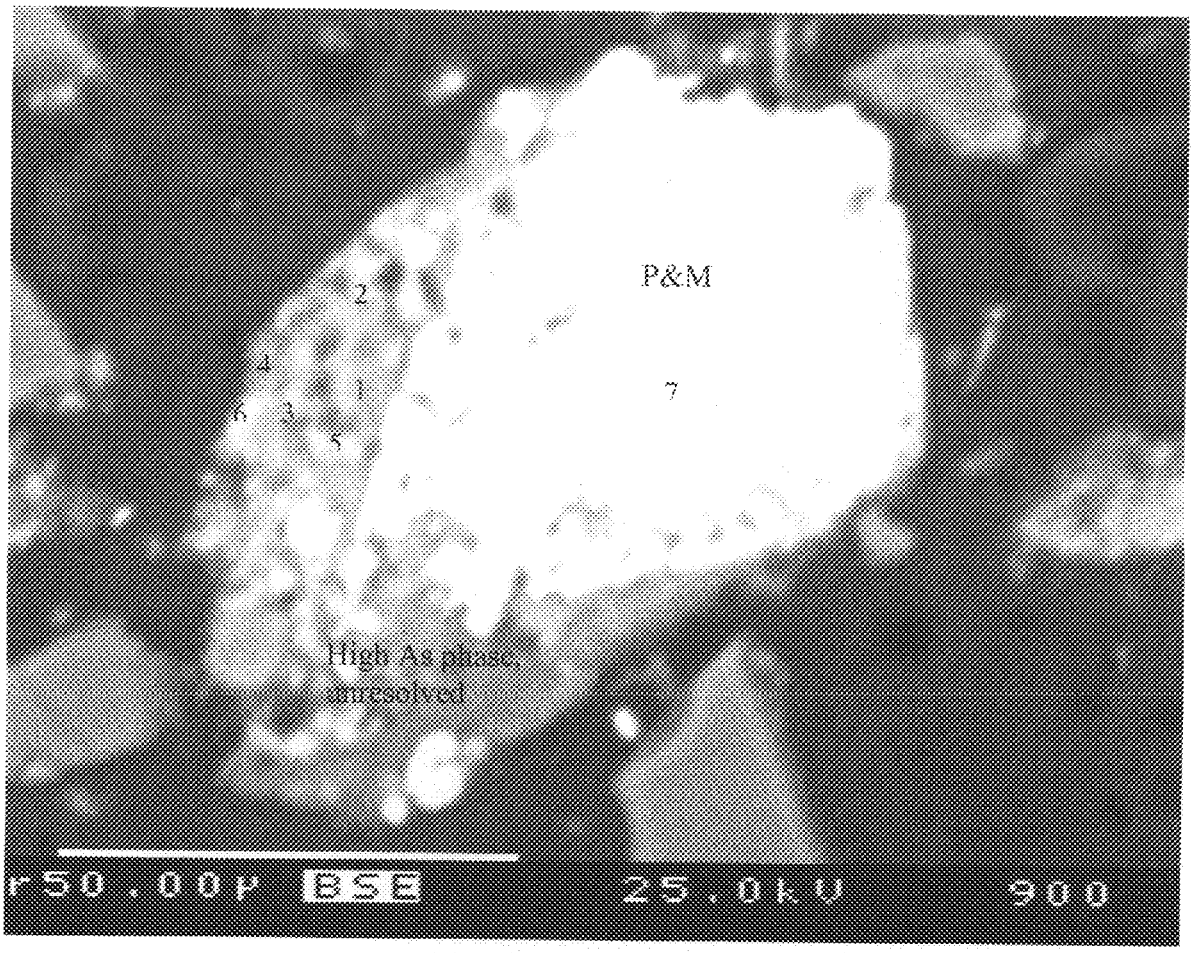

Table 3.1 Electron Microprobe Analysis for sample Le25c after reaction. Concentrations are listed in weight %. (UW1950/2.5)

Location	S	Fe	As	O	Si	Al	P	K	Ca	Totals
1	0.23	3.01	0.04	54.80	25.93	9.65	0.49	8.86	0.38	103.47
2	1.42	13.90	0.28	45.36	7.37	2.89	8.98	2.78	10.15	93.17
3	0.00	0.15	0.03	51.55	46.13	0.03	0.00	0.00	0.02	97.91
4	0.09	0.57	0.00	49.66	30.39	10.36	0.15	13.35	0.11	104.68
5	0.70	27.53	0.20	48.72	16.86	2.03	4.45	1.36	2.02	102.87
6	0.67	19.57	0.24	44.52	15.74	6.75	3.01	5.86	2.98	99.42
7	54.50	45.61	0.05	0.02	0.00	0.00	0.00	0.00	0.00	100.38

Figure 3.10. Raman spectra from pyrite nodule Le25c before and after the aqueous reaction. Vibrational peaks were identified at 388, 377, 338, 323, and 209 cm^{-1} in the pre-reacted sample (solid curve) and at 446, 440, 397, 338, and 323 cm^{-1} in the reacted (dashed curve) sample. (UW1950/...2.6, 2.7)

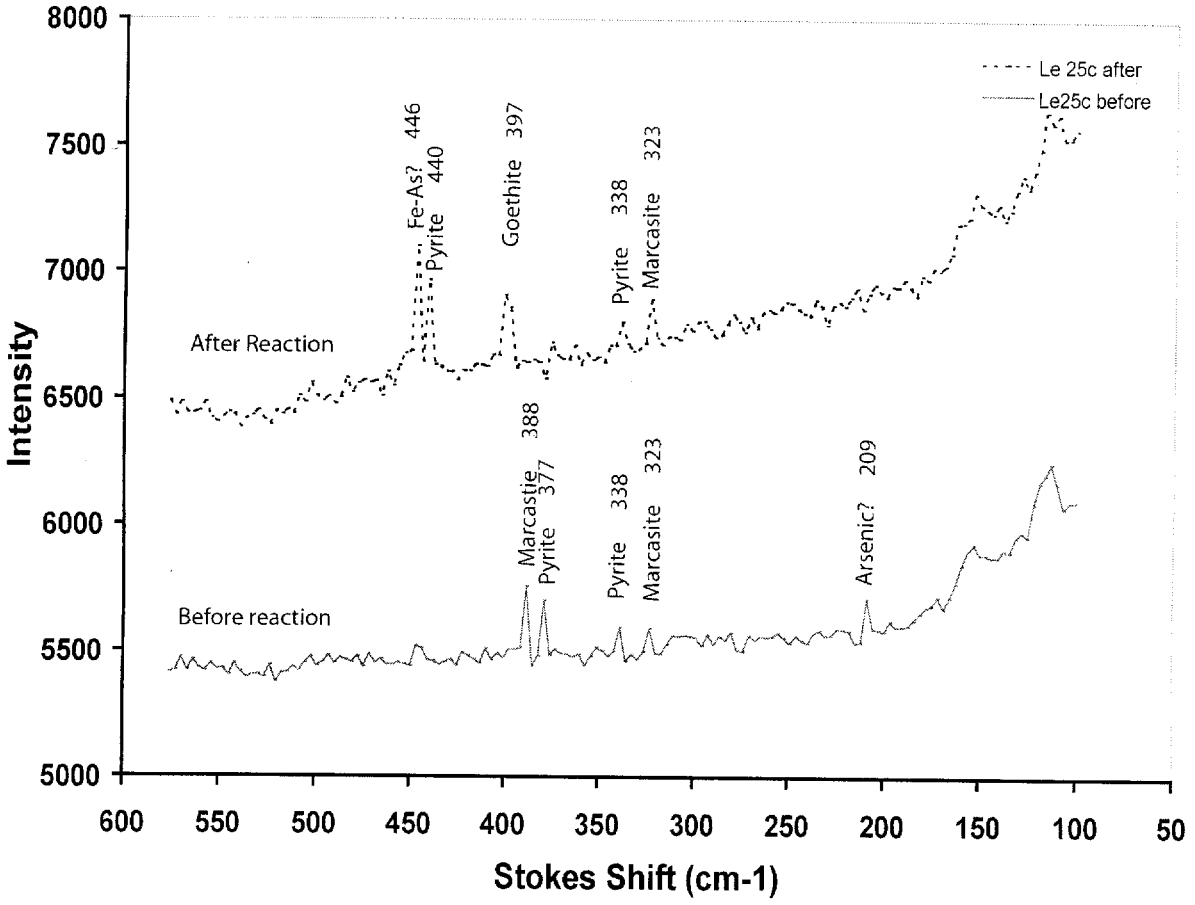

Table 3.2 Raman peaks (cm^{-1}) for iron and arsenic sulfides and goethite, which were used as standards and compared to sample Le25c before and after reaction. (UW1950/...2.6, 2.7)

Pyrite[1]	Marcasite[2]	Arsenopyrite[3]	Goethite[4]	As sorbed on[5] Goethite	Le25c[6] before	Le25c[7] after
---	---	---	675	---	---	---
---	532	582	550	---	---	---
---	---	527	---	---	---	---
428	---	481	---	450	---	446
415	---	425	400	---	---	440
377	387	388	---	---	388	397
---	---	---	---	---	377	---
342	---	---	---	---	338	338
---	324	---	---	---	323	323
---	---	274	---	290	209	---
---	---	211	---	215	---	---

1: Mernagh and Trudu, 1993; Turcotte et al., 1993; Vogt et al., 1983.

2: Mernagh and Trudu, 1993; Lutz and Muller, 1991

3: McGuire et al., 2001; Mernagh and Trudu, 1993; Turcotte et al, 1993

4: Courtin-Nomade et al., 2003

5: Courtin-Nomade et al., 2003

6: This study

7: This study

Table 3.3. Results of whole rock acid digestion and ICP-AES analysis in weight %. Sulfide, sulfide/goethite, quartz, and dolomite fractions are indicated by PM, PMG, Q, and D, respectively. (UW1950/...2.1,3.2, 4.2, 1.2, 3.1, 4.1, and 1.1)

Element	Le25c(PM)	K1(PMG)	K2(PM)	Le7(PM)	K1(Q)	K2(D)	Le7(Q)
Al	0.42	0.3	0.59	0.24	0.47	0.55	0.36
As	0.35	0.11	0.02	0.69	--	0.01	0.02
Ca	3	0.07	15.5	0.02	0.02	16.5	0.03
Co	0.1	0.05	0.02	0.04	--	0.01	--
Cu	0.2	0.1	0.11	0.2	0.03	0.01	0.03
Fe	14.6	17.9	1.23	22.4	0.54	0.76	0.61
K	0.24	0.09	0.59	0.17	0.33	0.58	0.18
Mg	0.04	0.09	9.35	0.02	0.03	10.1	0.01
Mn	0.91	0.02	0.74	0.09	--	0.78	0.02
Mo	0.02	0.02	--	0.02	--	--	--
Ni	0.17	0.2	0.02	0.13	--	--	--
P	>10	0.25	0.08	0.1	0.08	0.08	0.03
Pb	0.7	0.03	--	0.4	--	--	--
S	>10	3.85	0.95	>10	0.04	0.35	0.67
SiO2	--	--	---	--	97.9	10.9	95.9
Zn	0.03	0.21	0.01	0.04	0.02	--	0.01

3.3 Solution Analysis

Arsenic was detected in solutions reacting with the denser PM/PMG fraction, but not with the lighter quartz fraction. The following results therefore refer only to the PM/PMG fraction of each sample. Samples were run under air and nitrogen atmospheres. The dissolved oxygen content of solutions run under nitrogen was determined to be $< 1 \times 10^{-6}$ atmospheres, which corresponds to the $< 1.5 \times 10^{-6}$ atmospheres measured in the Fox River Valley aquifer (Schreiber et al, 2000). These conditions are less oxidizing than for samples left open to the atmosphere, but are still within the hematite and As (V) stability fields (Figure 3.11).

Figure 3.12 shows that total dissolved arsenic concentrations initially increase for the first hour, and then decline until no longer detected at ~120 hours. Arsenic concentrations from the iron sulfide phases were greater in the O_2 environment, although arsenic is also released in experiments run under N_2. Maximum concentrations were 0.107 (K1), 0.116 (K2), and 0.222 (Le25c) μmol L^{-1} in air, peaking at 30 minutes to 1 hour. Arsenic concentrations peak in nitrogen atmosphere ~20 minutes later than in air, with maximum arsenic concentrations at 0.048 (K1), 0.075 (K2), and 0.135 (Le25c) μmol L^{-1}. Decrease in arsenic concentrations is approximately simultaneous in both atmospheres. Monitoring of solutions over a 6 month period showed that arsenic concentrations do not increase again.

Based on thermodynamic stability, As (V) is the expected ion, but As (III) is the major oxidation state observed in solution under both air and nitrogen atmospheres. In the experiments run in oxygen, As (III) appears to be slowly converting to As (V) after ~2 hours in sample K1 and after ~ 8 hours in samples Le25c and K2 (Figure 3.13). The As (V) concentration declines again after ~6 hours in the case of K1. Under the nitrogen atmosphere,

there is no appreciable development of As (V) in solution over the time period of the experiment (Figure 3.14).

Figure 3.15 show that aqueous iron concentrations increase initially then decreased over time in the oxygen atmosphere while sulfur species concentrations increase, then plateaus. The maxima for iron and arsenic coincide at 60 minutes. The same trends are observed under N_2, but are less distinct. No distinguishable trends with other major ions were observed. Comparison of the solution reactions with the arsenopyrite sample from Mexico to the results of the Fox River Valley show, while with much higher arsenic concentrations, the same increase in arsenic concentrations along the same time scale and are followed by a marked decline in solution.

3.4 Extraction Results

The following results pertain to sample Le25c, which was analyzed because it has a high arsenic concentration, and to sample K1, which was analyzed because it contains a significant amount of goethite. Arsenic concentrations released from Le25c and K1, respectively, are 2.0 μmol $L^{-1}$and 0.667 μmol L^{-1} More arsenic was released from Le25c, even though Le25c contained less iron oxide (14.62 wt %) than K1 (17.87 wt%).

Figure 3.11. Eh-pH diagrams for (a) arsenic and (b) iron with experimental conditions under oxygen (*) and nitrogen (•) atmospheres, as indicated by symbols.

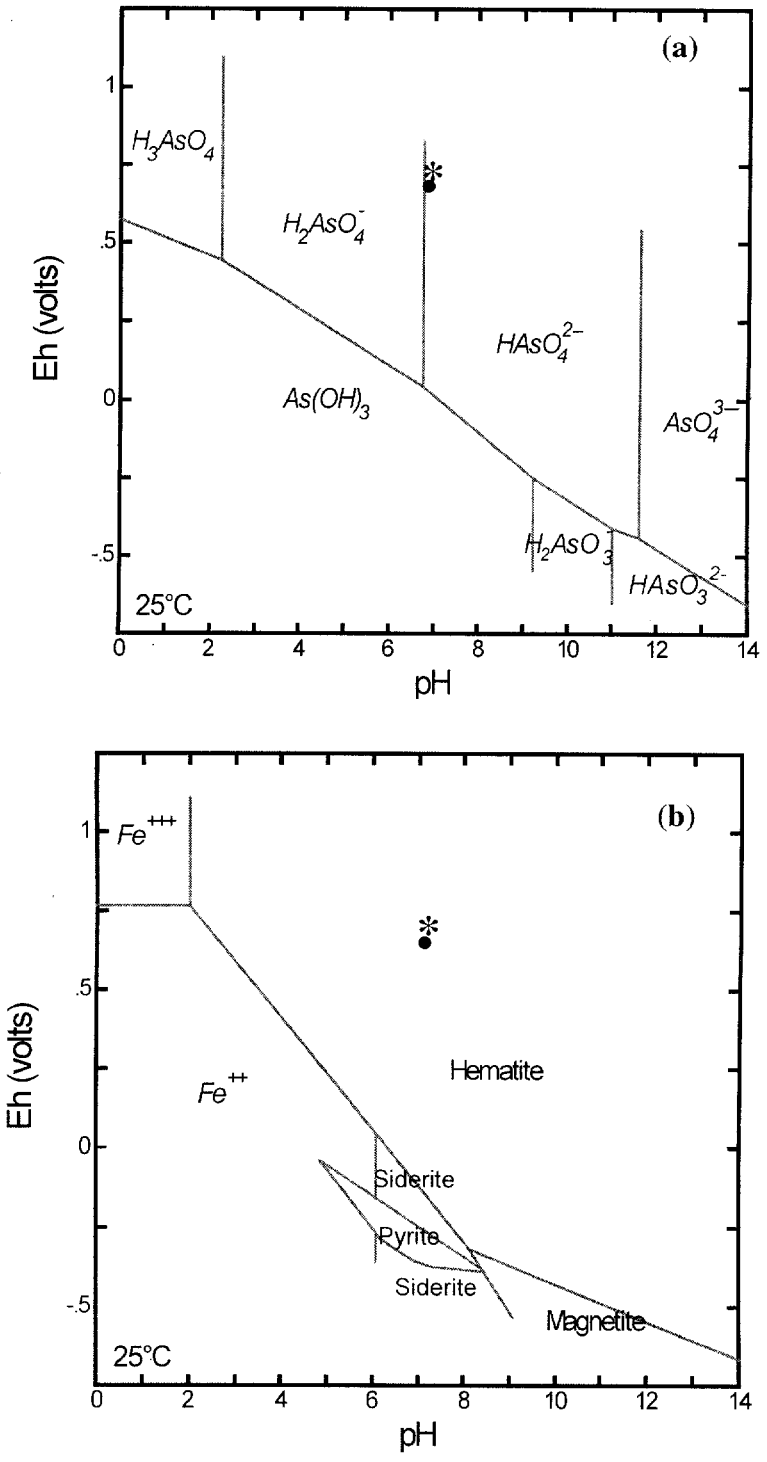

Figure 3.12. Aqueous arsenic concentrations during the first twelve hours of reaction. Experiments were conducted on sulfide/goethite fractions for samples Le25c (circles), K1 (diamonds), and K2 (squares). Open symbols represent solutions open to air and solid symbols represent solutions run under nitrogen. In all cases maximum arsenic release is higher in samples open to air. (UW1950/...2.1, 3.2, 4.2)

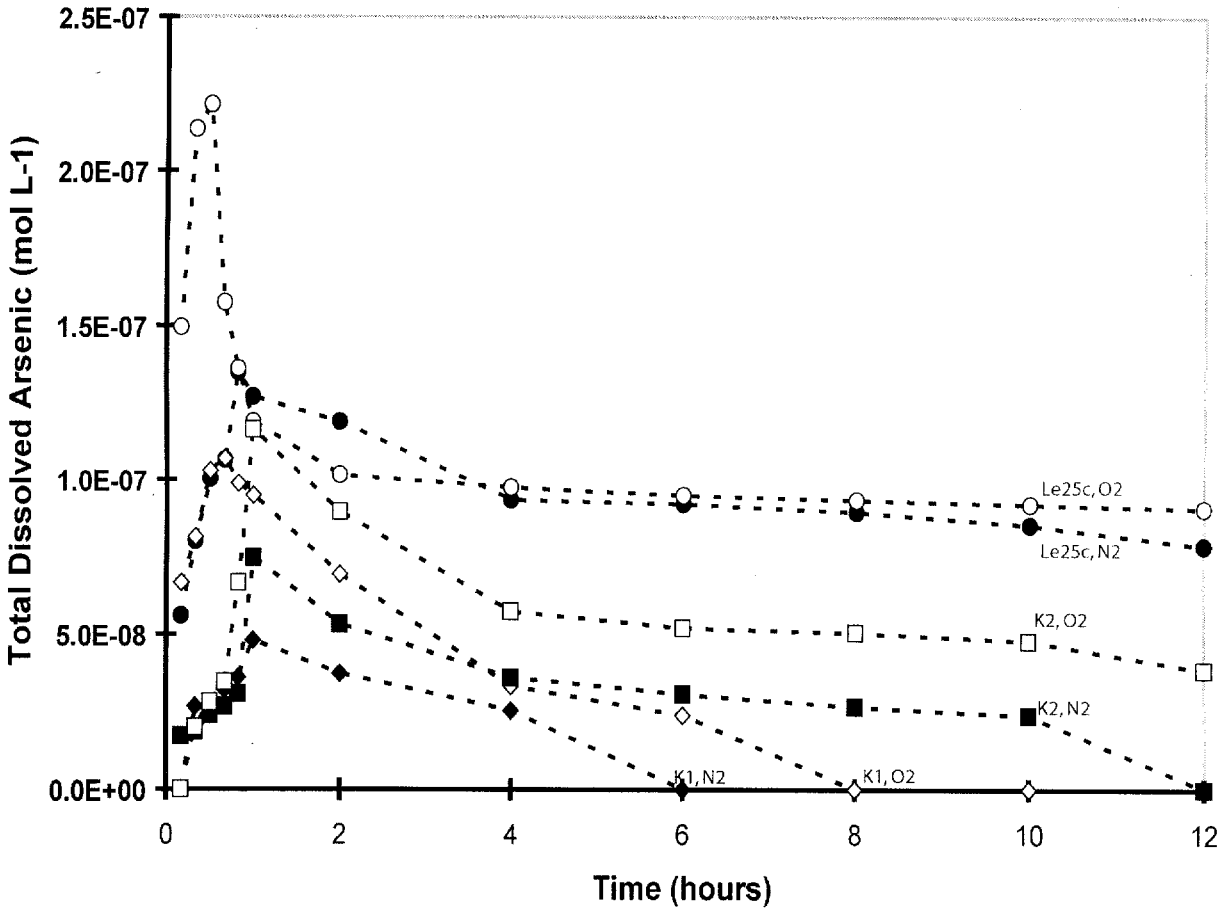

Figure 3.13. Dissolved arsenic (III) (squares) and arsenic (V) (diamonds) and total arsenic (circles) concentrations in the heavy density fraction of (a) Le25c, (b) K1, and (c) K2. Results are shown for the first twelve hours of reaction, for experiments done open to oxygen atmosphere. Vertical bars indicate magnitude of error. (UW1950/...2.1, 3.2, and 4.2)

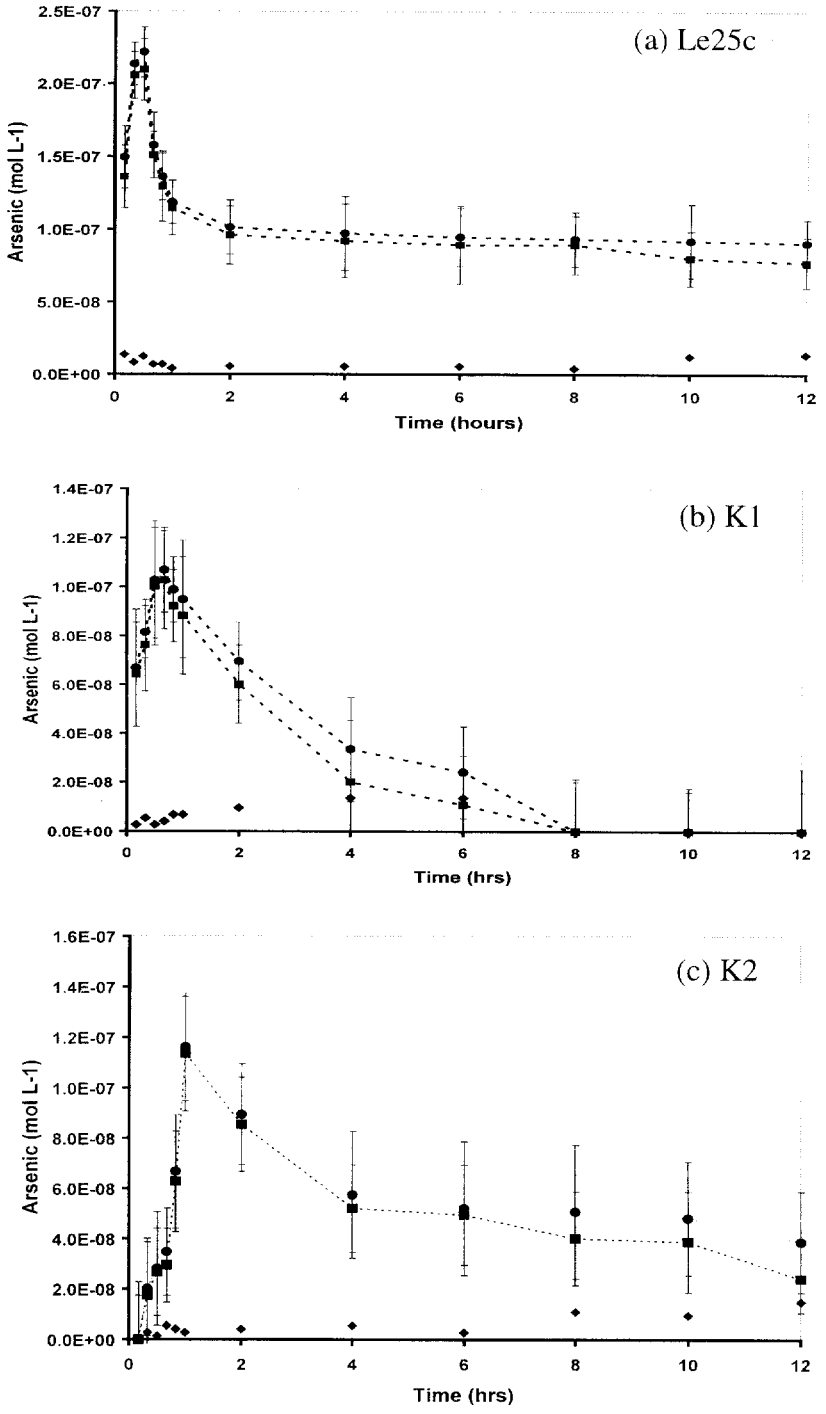

Figure 3.14. Dissolved arsenic (III) (squares) and arsenic (V) (diamonds) and total arsenic (circles) concentrations in the heavy density fraction of (a) Le25c, (b) K1, and (c) K2. Results are shown for the first twelve hours of reaction, for experiments done in nitrogen atmosphere. Vertical bars indicate magnitude of error. (UW1950/...2.1, 3.2, and 4.2)

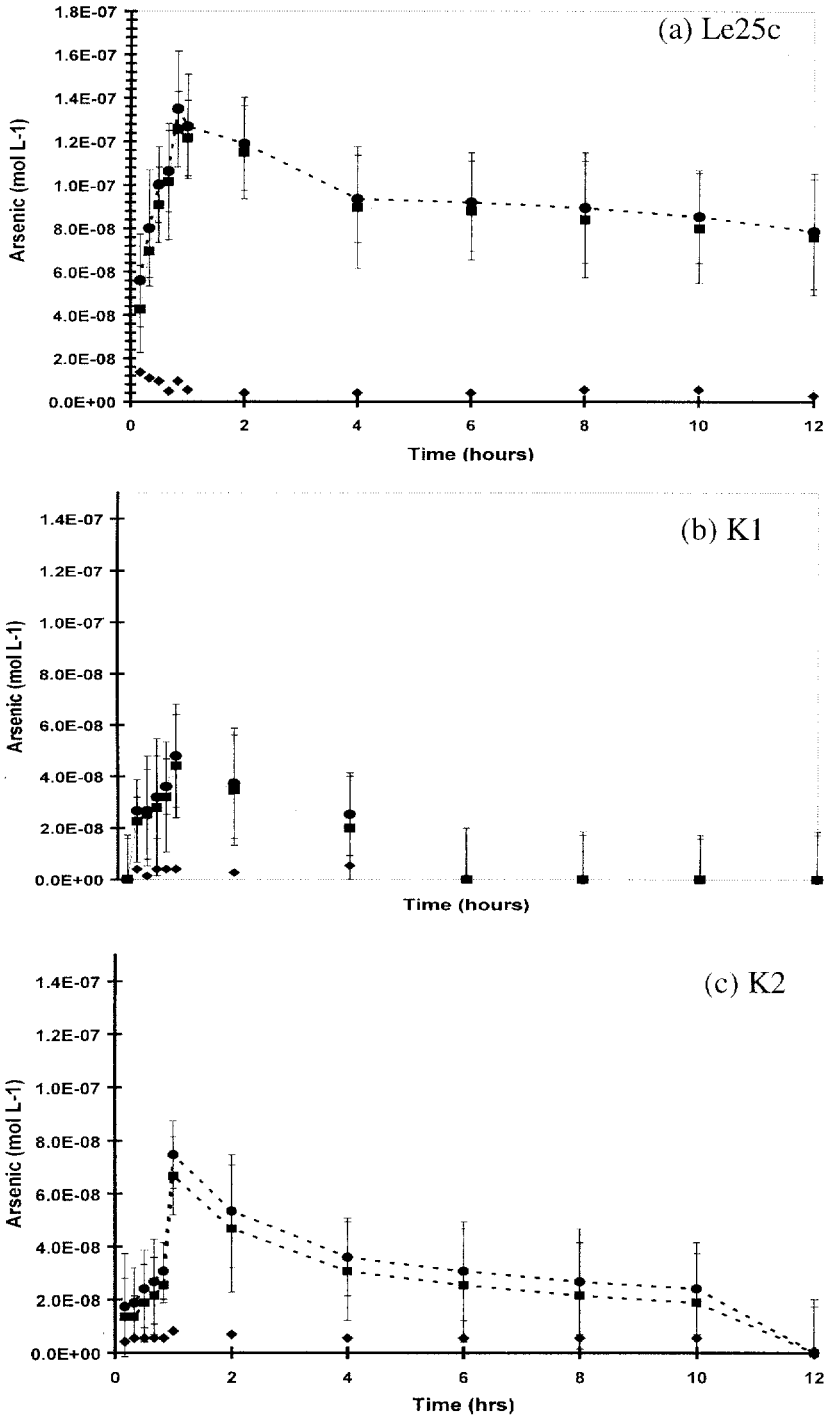

Figure 3.15. Total arsenic (circles), iron (squares) and sulfur (diamonds) concentrations in (a) Le25c for the first twelve hours of leaching and (b) for the entire experiment, open to air. (UW1950/2.1)

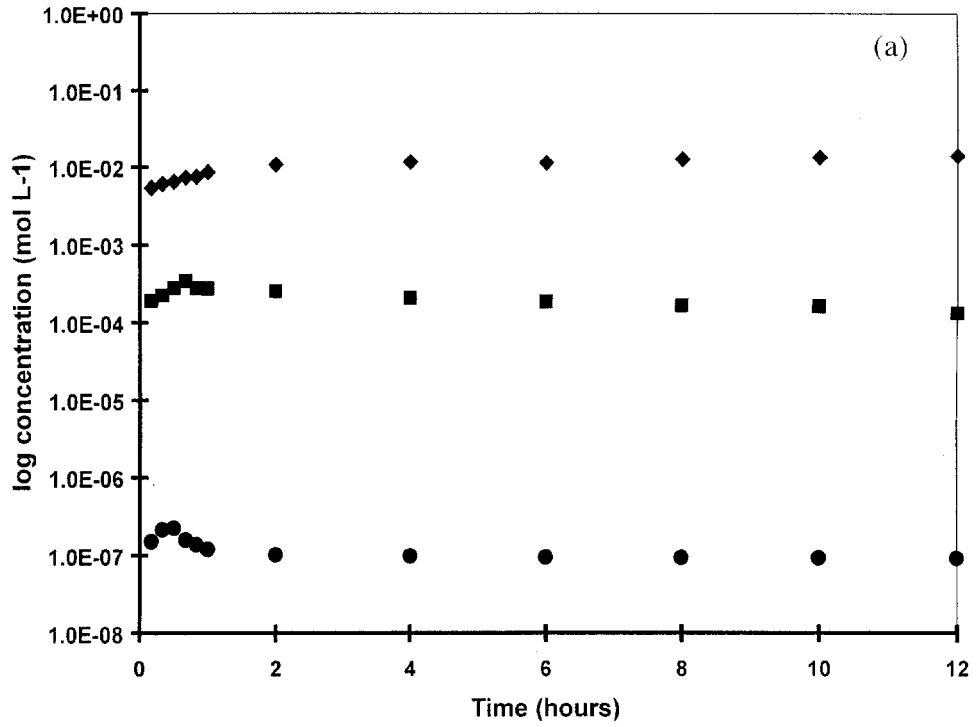

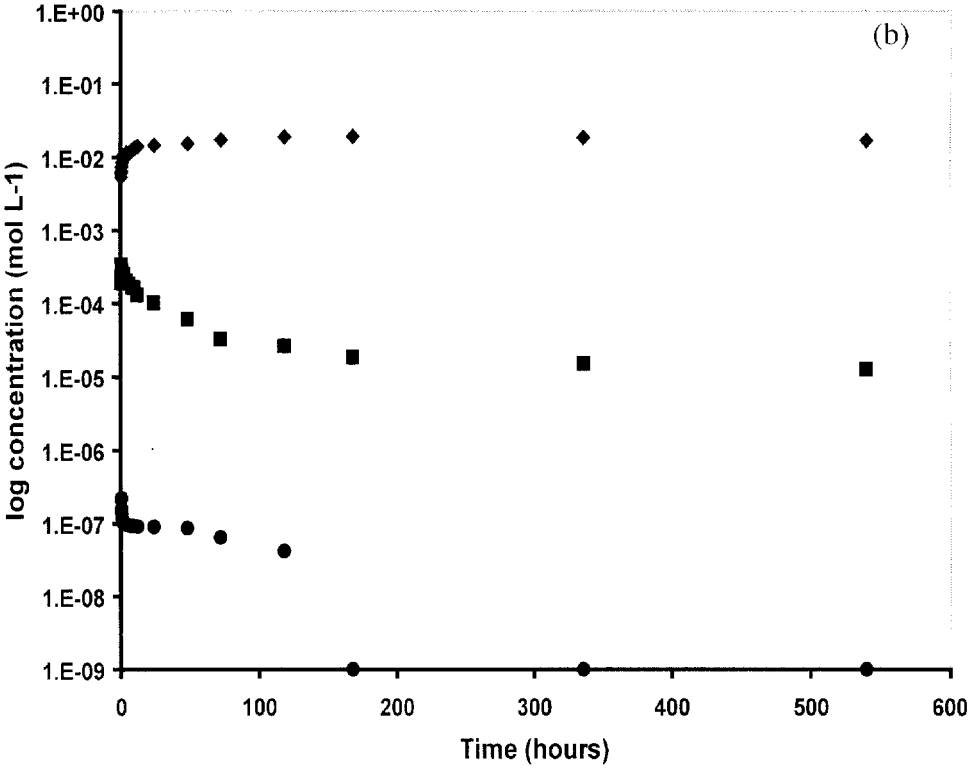

CHAPTER 4-DISCUSSION

4.1 Arsenic Occurrence

One of the objectives of this study was to identify the phase with which arsenic is associated in the Sinnipee Group Dolostone and in the St. Peter Sandstone. Arsenic could occur as a discrete arsenopyrite phase, be associated with other phases in solid solution, or occur as an adsorbate. Previous work suggested that arsenic was likely incorporated through solid solution (Schreiber et al., 2001), but this inference was not previously supported by a spectroscopic study.

In the present work Raman spectroscopy showed an arsenic line appearing at 209 cm^{-1}, which is close to a characteristic arsenic line in arsenopyrite (McGuire et al., 2001; Mernagh and Trudu, 1993; Turcotte et al., 1993), suggesting a similar bonding environment in the sample. However, the lack of other lines characteristic of arsenopyrite indicates that arsenic is not incorporated into a discrete arsenopyrite nanophase, consistent with previous work (Bostick and Fendorf, 2003). This inference is supported by XRD data which showed pyrite, marcasite, quartz, dolomite, and variable amounts of goethite were present prior to reaction, but a discrete arsenic phase was not, at least at the micron scale resolution of XRD. Electron Microprobe traverses through PM grains found arsenic relatively evenly distributed through the grains when present (Figure 3.5), suggesting that a discrete nanocrystalline arsenic phase is unlikely. The corroboration of micron and molecular scale work done by Raman Spectroscopy, XRD, and Electron Microscopy shows definitively that arsenic is incorporated into the iron sulfide structure through solid solution.

4.2 Arsenic Release and Uptake

At least two modes of arsenic release from PM are possible. One is simple desorption of arsenic from surface layers without changes to the bulk PM phase. The alternative mechanism is oxidative dissolution of PM and formation of iron oxides.

Electron Microprobe analysis showed PM grains altered by reaction up to ~25μm depth, suggesting that simple desorption from surface layers was unlikely. Aqueous concentrations of S_T, Fe_T and As_T increased for 1 hour, suggesting that dissolution of PM was occurring. This inference is supported by the detection of goethite in Le25c after reaction, by Electron Microprobe and X-Ray Diffraction, because goethite is a product of the oxidative dissolution of sulfides as indicated by reaction (1.2) in Chapter 1.

Dissolved arsenic concentrations from the oxidative dissolution of pyrite, arsenopyrite, and marcasite were calculated using rate constants from McGuire and others (2001). Values were calculated by multiplying the arsenic in the bulk, 1.5 grams of bulk sediment in 20 ml solution, the BET Specific Surface Area, the dissolution rate, and the time. Comparisons with measured As_T concentrations showed that theoretical and observed concentrations are on the same order of magnitude at times less than one hour (Figure 4.1). Assuming that the rates used in the calculations are accurate and BET surface areas are constant over time, similarities in the theoretical and observed arsenic kinetics suggest that oxidative dissolution of pyrite with simple release of arsenic into solution is the predominant arsenic release reaction. This is corroborated by maximum aqueous arsenic concentrations being lower under the slightly less oxidizing conditions of the nitrogen atmosphere (Figure 3.12) and the presence of reaction zones around PM grains (Figure 3.9).

Figure 4.1. Theoretical (hollow symbols, dashed lines) and experimental (filled symbols, solid lines) values of aqueous arsenic concentrations in the first hour of reaction. Values refer to total arsenic concentrations released by oxidative dissolution of pyrite and marcasite. Calculations show Le25c (circles), K1 (diamonds), and K2 (triangles) using their respective BET surface areas, arsenic concentrations in the bulk solid phase and using dissolution rates of McGuire et al. (2001). The inset boxes show theoretical concentrations for 504 hours (21 days). (UW1950/...2.1, 3.2, and 4.2)

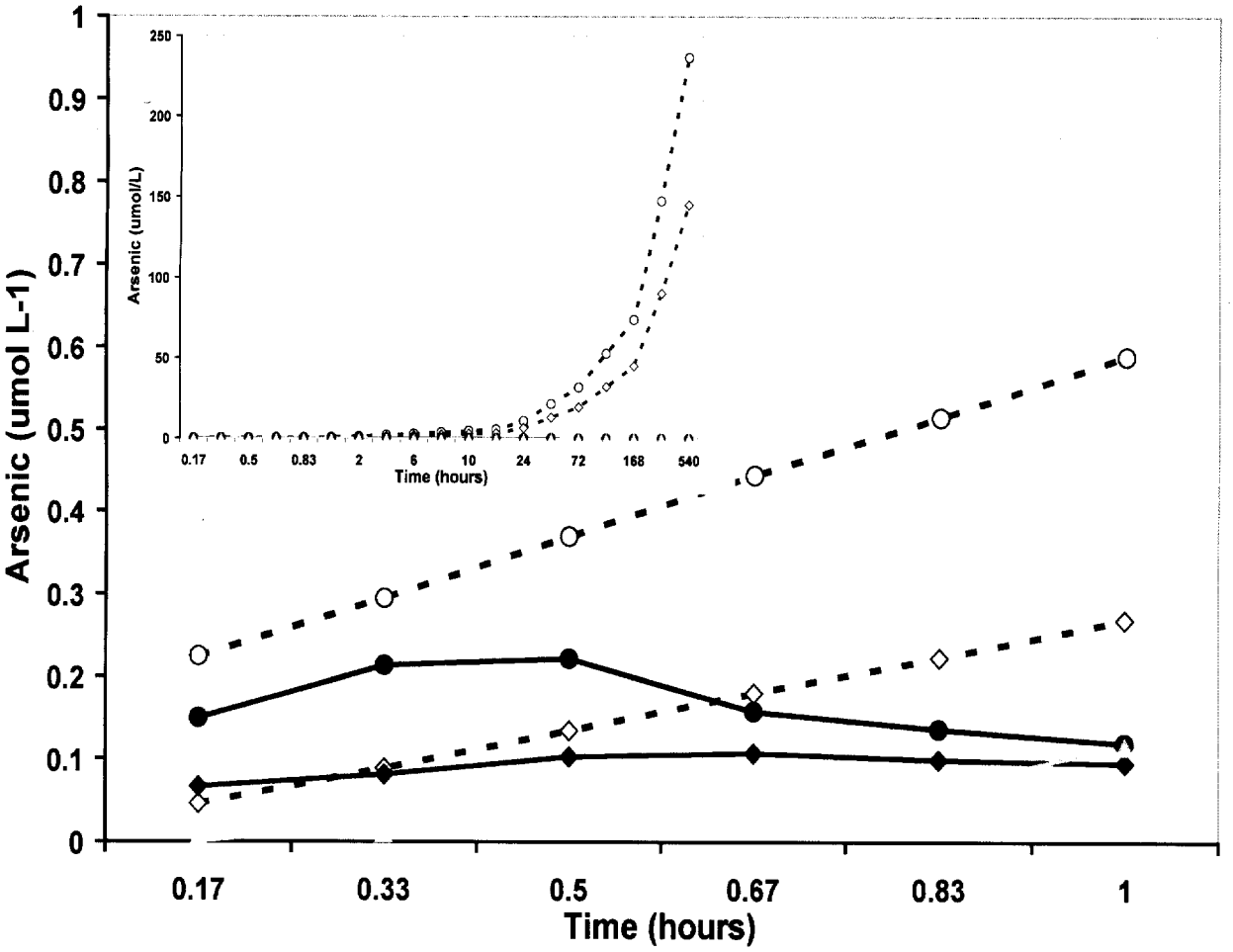

Figure 4.1. Theoretical (hollow symbols, dashed lines) and experimental (filled symbols, solid lines) values of aqueous arsenic concentrations in the first hour of reaction. Values refer to total arsenic concentrations released by oxidative dissolution of pyrite and marcasite. Calculations show Le25c (circles), K1 (diamonds), and K2 (triangles) using their respective BET surface areas, arsenic concentrations in the bulk solid phase and using dissolution rates of McGuire et al. (2001). The inset boxes show theoretical concentrations for 504 hours (21 days). (UW1950/…2.1, 3.2, and 4.2)

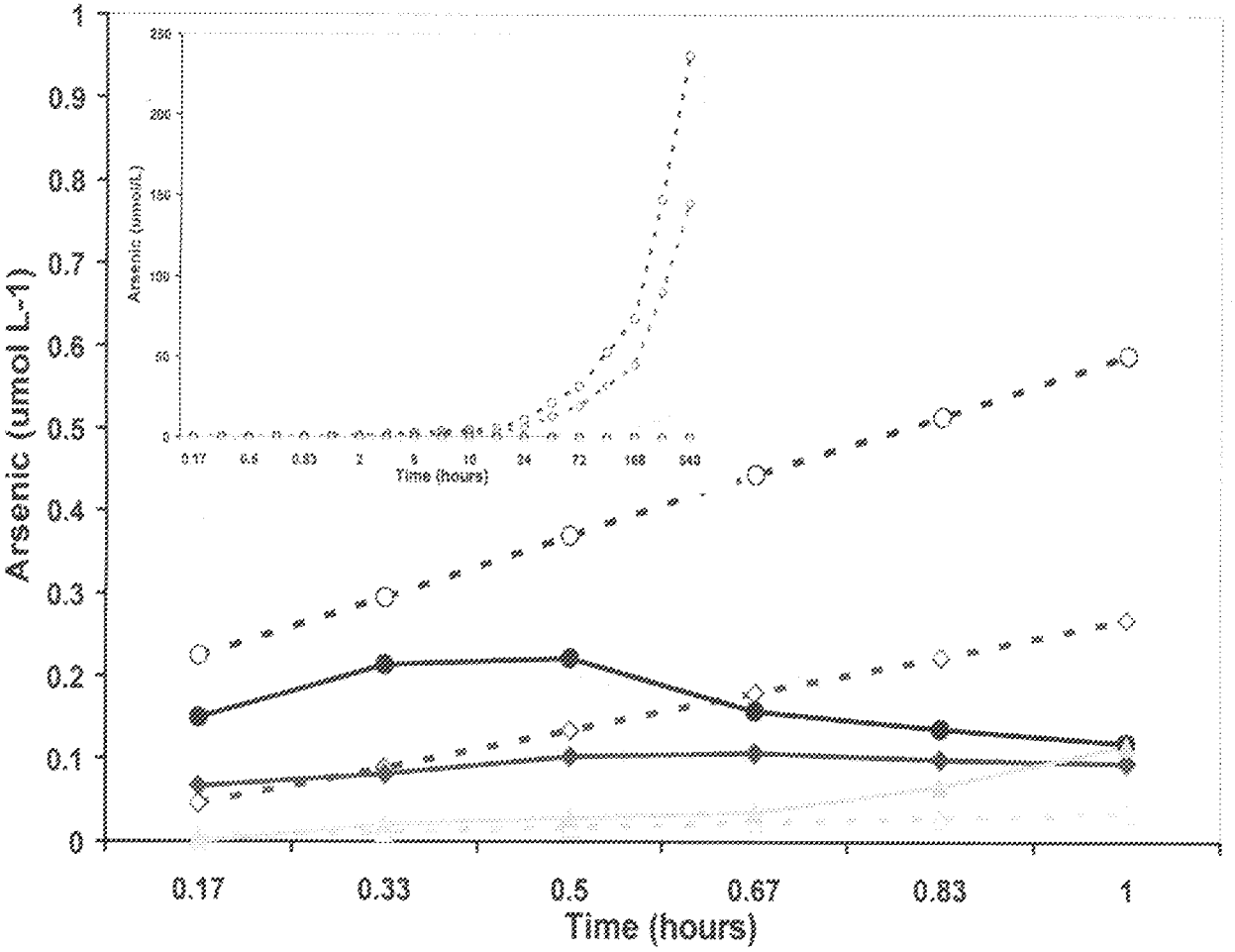

Aqueous arsenic concentrations peak in solution at ~1 hour. The initial increase in aqueous arsenic, iron and sulfur concentrations followed by declines in arsenic and iron are consistent with oxidative dissolution of PM and sorption of arsenic on the newly formed iron oxides. This inference is supported by Raman spectroscopy on Le25c after reaction showed the characteristic line at 446 cm^{-1} suggesting arsenic sorption on goethite. Also, goethite appeared in the X-Ray Diffraction spectra of reacted sample Le25c. Similar results have been reported previously for a XAS surface oxidation study of pyrite (Todd et al., 2003). Extraction results also showed significant arsenic released as iron oxides are reduced and forming aqueous complexes. Taken together, these results suggest that arsenic released by oxidative dissolution of the sulfide is taken up by the iron oxide formed as a product of the oxidation reaction.

Aqueous sulfur concentrations reach a plateau without going through a maximum, suggesting that there is no sink for removing initially released sulfate. Previous pyrite oxidation studies have shown development of surface polysulfide clusters, which would indicate a sink for sulfur ions, but those studies were done under acidic, pH = 2, conditions (Holmes and Crundewell, 2000; Sasaki et al., 1995). Further $[S]_T$ and $[Fe]_T$ does not continue to increase because the depleted oxidized reaction rims around the sulfide grain protects it from further dissolution. It is therefore reasonable that $[S]_T$ plateaus in solution and $[Fe]_T$ decreases as ferric oxides form. Development of polysulfides was not looked for through the course of this study.

Table 4.1 Arsenate (AsO_4^{3-}) adsorption equilibrium constants and arsenite (AsO_3^{3-}) on hydrous ferric oxide (Carrillo and Drever, 1997; Dzombak and Morel, 1990).

Reaction	log K
Arsenate	
$>FeOH + AsO_4^{3-} + 3H^+ = >FeH_2AsO_4^0 + H_2O$	29.31
$>FeOH + AsO_4^{3-} + 2H^+ = >FeHAsO_4^- + H_2O$	23.51
$>FeOH + AsO_4^{3-} + H^+ = >FeAsO_4^{2-} + H_2O$	------
$>FeOH + AsO_4^{3-} = > FeOHAsO_4^{3-}$	10.58
Arsenite	
$>FeOH + H_3AsO_3 = >FeH_2AsO_3^0 + H_2O$	5.41

Under the experimental solution conditions, As (V) is the stable species. In both the oxygen and nitrogen atmospheres, however, the dominant aqueous arsenic species observed is As (III). One interpretation of this result is that As (V) is removed more efficiently from solution, which would be consistent with the higher adsorption constants of As (V) versus As (III) on hydrous ferric oxides (Table 4.1; Dzombak and Morel, 1990). Alternatively, oxidation of As (III) to As (V) may be slow compared to the oxidative dissolution of PM (Ryu et al., 2002; Yan et al., 2000; Cherry et al., 1979) so that As (III) is initially released into solution. The latter explanation is more likely based on the persistence of total arsenic in solution up to 120 hours, which is consistent with previous work (Jain et al., 2000, Raven et al., 1998, Manning and Goldberg, 1997).

4.3 Implications for the Fox River Valley Groundwater

Preliminary dissolution experiments for this work showed that in unbuffered solutions, pH dropped to 2.5 and arsenic bearing PM grains released an order of magnitude more arsenic than solutions buffered at pH 7.2. Aqueous reaction experiments done in solution buffered at pH=7.2 showed release of arsenic in very low concentrations. It is therefore likely that oxidative dissolution under neutral pH conditions is responsible for the low and moderately elevated arsenic concentrations ($< 1.3 \times 10^{-6}$ mol L^{-1}) observed in many of the Fox River Valley wells. The extremely high arsenic values observed in the region probably can not occur solely from arsenic concentrations released from nodules and veins in groundwater buffered at near-neutral pH. The extremely high arsenic levels measured in the Fox River valley wells must be explained by oxidative dissolution being able to overwhelm the buffering capacity of the aquifer.

In the Fox River valley, pumping in the wells reduces water levels in the borehole and exposes the sulfide minerals to dissolved oxygen. Static water in the borehole is in direct contact with the atmosphere and forms a surface layer of dissolved oxygen. When the water is pumped, this diffused oxygen layer is drawn down the borehole until the dissolved oxygen comes in contact with a large sulfide concentration, such as in the sulfide horizon, causing oxidative dissolution of the sulfide. The oxidation reaction acidifies the groundwater immediately surrounding the well and allows further sulfide dissolution, resulting in the extreme arsenic concentrations ($>1.3 \times 10^{-6}$ mol L^{-1}) observed. The initially released aqueous arsenic is either removed through pumping or resorbed by natural aquifer materials. As the dissolved oxygen in the surface layer of water is consumed the oxidation rate decreases. Subsequently, the natural buffering of the groundwater returns the pH to neutral conditions, slowing the arsenic release rate. This process explains why the highest concentrations of arsenic released into drinking water occurs within the first hour of pumping and concentrations decline after that (Schreiber et al., 2003).

Regardless of whether the host rocks are clastic or carbonate, the reactions associated with dissolution of PM grains, arsenic release, goethite formation, and arsenic adsorption to goethite appear to be universal, based on the presence of goethite in the dolomite sample K2. One significant difference between the two sedimentary hosts is that carbonate rocks should be able to help buffer the waters, thus keeping the pH from dropping low enough to significantly enhance sulfide dissolution.

Persistence of drinking water contamination by arsenic in the Fox River Valley is related to continuous introduction of dissolved oxygen into the aquifer through continued pumping. These pulses of dissolved oxygen into the aquifer serve to temporarily shift the

equilibrium of the system towards oxidative dissolution of the sulfides. With time the equilibrium shifts back and much of the arsenic is taken up by iron oxides in the aquifer. The large sulfide cement horizon present throughout the Fox River Valley will continue to supply arsenic to drinking water as long as dissolve oxygen is supplied and oxidative dissolution can occur.

In summary, results of this work indicate that arsenic releases quickly into the groundwater by oxidative dissolution of sulfides, but concentrations decline if additional dissolved oxygen is not introduced. This study did not focus on the fate of arsenic once adsorbed to the iron oxides. If strong reducing conditions exist in the well after pumping ceases it is highly likely that arsenic could be re-released due to iron reduction (Eqn. 1.3). Another potentially complicated factor, that has thus far been poorly characterized, is the role of bacteria in contributing to the arsenic problem. If iron-reducing bacteria are present in the groundwater they could also play a significant role in remobilizing arsenic that has been taken up by the iron oxides prevalent in the Fox River Valley aquifer.

CHAPTER 5 – CONCLUSIONS

Hand and core samples were analyzed to determine the mineralogy and chemistry of arsenic bearing minerals responsible for arsenic contamination in the Fox River Valley, WI. Mineralogy of the St. Peter Sandstone and Sinnipee Group Dolostone stratigraphic units was determined using X-ray diffraction, Electron Microprobe analysis and Raman spectroscopy. A distinct arsenic phase was not detected. Rather, this work at the micron and molecular scale definitively shows that arsenic is incorporated into the pyrite and marcasite structures, rather than existing as a sorbed phase or a discrete arsenic nanophase.

Results of mineral separates reacted in solutions buffered at near neutral pH showed no detectable arsenic release from the quartz and dolomite fractions, but was released from the PM/PMG fractions.

Comparison of arsenic concentrations in experiments run under oxygen and nitrogen atmosphere, observation of iron and sulfur depletion around reacted PM/PMG grains and oxidative dissolution rate calculations indicated that arsenic is released through oxidative dissolution of the iron sulfide minerals. Arsenic is released predominately from PM & PMG grains as the As (III) species, which converts slowly to As (V) in solution.

This work shows for the first time that iron oxides form from oxidative dissolution in natural samples of the Fox River Valley and that arsenic released into solution is ultimately sorbed onto these newly forming goethites. The disappearance of arsenic from solution is attributed to the formation of iron oxides, namely goethite, observed by X-ray diffraction, Electron Microprobe analysis and Raman spectroscopy. The oxides formed during the 3 weeks of reaction with solution. Raman Spectroscopy and extraction results shows arsenic

sorption onto goethite, which is interpreted to be responsible for arsenic decline in solution experiments run under oxygen and nitrogen atmospheres.

This work indicates it is likely that oxidative dissolution, due to the introduction of dissolved oxygen into the well, is responsible for the low and moderate arsenic concentrations of arsenic in the groundwater of the Fox River valley. However, it is unlikely that these near neutral pH conditions are responsible for the extremely elevated arsenic concentrations observed during sampling of the well water. These higher concentrations are likely associated with oxidative dissolution in conjunction with large quantities of arsenic bearing PM grains overwhelming groundwater buffering capacity and lowering the pH, which drives further oxidative dissolution.

Previous field observations match current laboratory results of arsenic concentrations declining with time. Therefore, it appears that the shift in equilibrium due to initial pumping and introduction of dissolved oxygen is temporary. While perhaps not practical, this implies that the best way to keep arsenic concentrations low in potable water is to discard water from early pumping times. It may not drop arsenic concentrations below the E.P.A. drinking water standards, but coupled with a filtration unit, this practice could remediate arsenic contamination to a level safe for human usage. The alternative is to re-drill wells into a deeper confined aquifer, although this too may not be economically feasible.

List of References

Appelo, C., Van der Weiden, J., Tournassat, C., and Charlet, L. (2002) Surface Complexation of Ferrous Iron and Carbonate on Ferrihydrite and the Mobilization of Arsenic, *Environ. Sci. Technol.* **36**(14): 3096-3103.

Armienta M., Rodriques, R., Aguayo, A., Ceniceros, N., Villasenor, G., and Cruz, O. (1997) Arsenic contamination of groundwater in Zimapan, Mexico. *Hydrogeol.* J **5**(2): 39-46.

Azcue, J., Nriagu, J. (1995) Impact of abandoned mine tailings on the arsenic concentrations in Moira Lake, *J. Geochemical Exploration* **52**: 81-89.

Bethke, C. M. (1998) *The Geochemist's Workbench Release 3.0*, Hydrogeology Program, University of Illinois.

Bostick, B., Fendorf, S. (2003) Arsenite sorption on triolite (FeS) and pyrite (FeS2). *Geochim. Cosmochim. Acta* **67**(5): 909-921.

Bowell, R. (1994) Sorption of arsenic by iron oxides and oxyhydroxides in soils, *Applied Geochemistry* **9**: 279-286.

Burkel, R. S., Stoll, R. C. (1993) Arsenic as a naturally elevated parameter in water wells in Winnebago and Outagamie Counties, Wisconsin. MS Thesis, University of Wisconsin-Green Bay, Green Bay, Wisconsin.

Carrillo, A., and Drever, J. (1998) Adsorption of arsenic by natural aquifer material in the San Antonio-El Triunfo mining area, Baja California, *Environmental Geology* **35**(4): 251-257.

Chao, T., and Zhou, L. (1983) Extraction techniques for selective dissolution of amorphous iron oxides from soils and sediments. *Soil Sci. Soc. of Am. J.* **47**:225-232.

Chen, K., Dzeng, S., Yang, M., Chiu, K., Shien, G., and Wai, C. (1994) Arsenic Species in Groundwaters of the Blackfoot Disease Area, *Environ. Sci. Technol.* **28**(5): 877-881.

Cherry, J., Shaikh, A., Tallman, D., Nicholson, R. (1979) Arsenic Species as an Indicator of Redox Conditions in Groundwater. *J. of Hydrology* **43**: 373-392.

Chiu, V., Hering, J. (2000) Arsenic Adsorption and Oxidation at Manganite Surface. 1. Method for Simultaneous Determination of Adsorbed and Dissolved Arsenic Species. *Environ. Sci. Technol.* **34**(10): 2029-2034.

Cornell, R., and Giovanoli, R. (1985) Effect of Solution Conditions on the Proportion and Morphology of Goethite formed from Ferrihydrite. *Clays and Clay Minerals* **33**(5): 424-432.

Courtin-Nomade, A., Bril, H., Neel, C., and Lenain, J. (2003) Arsenic in iron cements developed within tailings of a former metalliferous mine-Enguiales, Aveyron, France. *Applied Geochemistry* **18**(3): 395-408.

Cullen, W., R., and Reimer, K. J. (1989) Arsenic speciation in the environment. *Chem. Rev.* **89**, 713-764.

Davis, J., A. (2001) Surface Complexation Modeling of Uranium (VI) Adsorption on Natural Mineral Assemblages, Melno Park, California, Office of Nuclear Regulatory Research/United States Geological Survey. NUREG/CR-6708.

Delany, J.M., and Lundeen, S.R. (1990) The LLNL thermochemical database. Lawerence Livermore National Laboratory Report UCRL-21658, 150p.

Deuel, L., and Swoboda, A. (1972) Arsenic solubility in a reduced environment. *Soil. Sci. Soc. Am. J.* **36**, 276-278.

De Vitre, R., Belzile, N., Tessier, A. (1991) Speciation and Adsorption of Arsenic on Diagenetic Iron Oxyhydroxides. *Limnology and Oceanography* **36**(7): 1480-1485.

Dzombak, D., and Morel, F. Surface Complexation Modeling, Hydrous Ferric Oxide: New York, Wiley, p. 393.

Edwards, M., Patel, S., McNeill, L., Chen, H., Frey, M., Eaton, A., Antweiler, R., Taylor, H. (1998) Considerations in As analysis and speciation. Regulatory Update. March 1998.

Farquhar, M., Charnock, J., Livens, F., Vaughan, D. (2002) Mechanisms of Arsenic Uptake from Aqueous Solution by Interaction of Goethite, Lepidocrocite, Mackinawite, and Pyrite: An X-ray Adsorption Spectroscopy Study. *Environ. Sci. Technol.* **36**(8): 1757-1762.

Fendorf, S., Eick, M., Grossl, P., and Sparks, D. (1997) Arsenate and Chromate Retention Mechanism on Goethite. Surface Structure. *Environ. Sci. Technol.* **33**(2): 315-320.

Goldberg, S. (2002) Competitive Adsorption of Arsenate and Arsenite on Oxides and Clay Minerals. *Soil Sci.Soc. Am. J.* **66**: 413-421.

Han, J., and Fyfe, W. S., (2000) Arsenic removal from water by iron-sulphide minerals. *Chinese Science Bulletin* **45**(15): 1430-1434.

Helgeson, H.C., Delany, J.M., Nesbitt, H.W., and Biidi, D.K. (1978) Summary and critique of the thermodynamic properties of rock-forming minerals. *Am. J. of Science* 278-A, 1-229.

Hemond, H. (1995) Movement and Distribution of Arsenic in the Aberjona Watershed. Environmental Health Perspectives 103, Supplement 1, February 1995. p.9.

Heinrichs, G., and Udluft, P. (1999) Natural arsenic in Triassic rocks: A source of drinking-water contamination in Bavaruam Germany. *Hydrogeology J* .17: 468-476.

Holmes, P., and Crundwell, F. (2000) The kinetics of the oxidation of pyrite by ferric ions and dissolved oxygen: An electrochemical study. *Geochim. Cosmochim. Acta* **64**(2): 263-274.

Huerta-Diaz, M., Tessier, A., and Carignan, R. (1998) Geochemistry of trace metals associated with reduced sulfur in freshwater sediments. *Applied Geochemistry* **13**: 213-233.

Jackson, B., and Miller, W. (2000) Effectiveness of Phosphate and Hydroxide for Desorption of Arsenic and Selenium Species from Iron Oxides. *Soil Sci. Soc. of Am. J.*: **64**:1616-1622.

Jain, C., and Ali, I. (2000) Arsenic: Occurrence, Toxicity and Speciation Techniques. *Water Resources* **34**(17): 4304-4312.

Jain, A., Raven, K., and Loeppert, R. (1999) Arsenite and Arsenate Adsoprtion on Ferrihydrite: Surface Charge Reduction and Net OH- Release Stoichiometry. *Environ. Sci. Technol.* **33**(8): 1179-1184.

Jain, A., Raven, K., and Loeppert, R. (2000) Effect of competing anions on the adsorption of arenate and arsenite by ferrihydrite. *J. Environ. Qual.* **29**: 1422-1430.

Jingtai, H., and Fyfe W. (2000) Arsenic removal from water by iron-sulphide. *Chinese Science Bulletin* **45**(12): 1430-1434.

Johnson, J.W., Oelkers, E.H., and Helgeson, H.C. (1991) SUPCRT92: A software package for calculating the standard molal thermodynamic properties of minerals, gases, aqueous species and reactions from 1 to 5000 bars and 0° to 1000° C. Earth Science Department, Lawrence Livermore Laboratory, 101p.

Juillot, F., Ildefonse, P., Morin, G., Calas, G., de Kersabiec, A., and Benedetti, M. (1999) Remobilization of arsenic from buried waste at an industrial site: mineralogical and geochemical control, *Applied Geochemistry* **14:** 1031-1048.

Keon, N., Swartz, C., Brabander, D., Harvey, C., and Hemond, H. (2001) Validation of an arsenic sequential extraction method for evaluating mobility in sediments. *Environ. Sci. and Technol.* **35**(13): 2778-2784.

Kim, M., Nriagu, J, and Haack, S. (2000) Carbonate Ions and Arsenic Dissolution by Groundwater, *Environ. Sci. Technol.* **34** (15): 3094-3100.

La Force, M., Hansel, C., and Fendorf, S. (2002) Seasonal transformations of manganese in a palustrine emergent wetland, *Soil Science Society of America J* .**66**(4): 1377-1389.

Langner, H., and Inskeep, W. (2000) Microbial Reduction of Arsenate in the Presence of Ferrihydrite, *Environ. Sci. Technol.* **34**(15): 3131-3136.

Lengke, M., and Tempel, R. (2003) Natural realgar and amorphous AsS oxidation kinetics. *Geochim. Cosmochim. Acta* **67**(5): 859-871.

Lin, Z., Puls, R. (2001) Studies of interfacial reactions between arsenic and minerals and its significance to site characterization. *Environ. Geol.* **4**:1433-1439.

Lombi, E., Wenzel, W., Sletten, R. (1999) Arsenic adsorption by soils and iron-oxide-coated sand: kinetics and reversibility, *J. Plant Nutr. Soil Sci.* **162:** 451-456.

Lutz, H. and Müller, B. (1991) Lattice Vibration Spectra. LXVIII. Single-Crystal Raman Spectra of Marcasite-type Iron Chalcogenide and Pnictides, FeX_2 (X=S, Se, Te; P, As, Sb), *Phy.s Chem. Mineral.* **18**: 265-268.

Manning, B., and Goldberg, S. (1997) Adsorption and Stability of Arsenic (III) at the Clay Mineral-Water Interface, *Environ. Sci. Technol.* **31**(7): 2005-2011.

McCreadie, H., Blowes, D., Ptacek, C., and Jambor, J. (2000) Influence of Reduction Reactions and Solid-Phase Composition on Porewater Concentrations of Arsenic, *Environ. Sci. Technol.* **34**: 3159-3166.

McGuire, M., and Hamers, R. (2000) Extraction and Quantitative Analysis of Elemental Sulfur from Sulfide Mineral Surfaces by High-Performance Liquid Chromatography, *Environ. Sci. Technol.* **34** (21): 4651-4655.

McGuire, M., Edwards, K., Banfield, J., and Hamers, R. (2001) Kinetics, surface chemistry, and structural evolution of microbially mediated sulfide mineral dissolution. *Geochim. Cosmochim. Acta* **65**(8): 1243-1258.

Meng, X., Korfiatis, G., Band, S., and Bang, K., (2002) Combined effects of anions on arsenic removal by iron hydroxides, *Toxicology Letters* **133**: 103-111.

Mernagh, T., Truda, A. (1993) A laser Raman microprobe study of some geologically important sulphide minerals. *Chemical Geology* **103**: 133-127.

Nickson, R., McArthur, J., Ravenscroft, P., Burgess, W., and Ahmed, K. (2000) Mechanism of arsenic release to groundwater, Bangladesh and West Bengal, *Applied Geochemistry* **15**: 403-413.

Panstar-Kallio, M., and Manninen, P. (1997) Speciation of mobile arsenic in soil samples as a function of pH, *The Science of the Total Environment* **204**: 193-200.

Raven, K., Jain, A., Loeppert, R. (1998) Arsenite and Arsenate Adsoprtion on Ferrihydrite: Kinetics, Equilibrium, and Adsorption Envelopes, *Environ. Sci. Technol.* **32**(2): 344-349.

Rawls, R., L. (2002) Tackling Arsenic in Bangladesh, *Chemical and Engineering News*, October 21st, 40-45.

Rochette, E., Bostick, B., Li, G., and Fendorf, S. (2000) Kinetics of Arsenate Reduction by Dissolved Sulfide, *Environ. Sci. Technol.* **34**(22): 4714-4720.

Ryu, J., Gao, S. Dahlgren, R., and Zierenberg, R. (2002) Arsenic distribution, speciation and solubility in shallow groundwater of Owens Dry Lake, *Geochim. Cosmochim. Acta* **66**(17): 2981-2994.

Sadiq, M., Zaida, T., Mian, A. (1983) Environmental Behavior of Arsenic in Soils-Theoretical, *Water Air Soil Pollut.* **20**: 369-377.

Sasaki, K., Tsunekawa, M., Ohtsuka, T., and Konno, H. (1995) Confirmation of a sulfur-rich layer on pyrite after oxidative dissolution by Fe(III) ions around pH 2. *Geochim. Cosmochim. Acta* **59**(15): 3155-3158.

Schreiber, M., Gotkowitz, M., Simo, J., Freiberg, P. (2003) Mechanisms of Arsenic Release ton Ground Water from Naturally Occurring Sources, Eastern Wisconsin: *in* Welch, A., and Stollenwerk, K., eds., Arsenic in Ground Water, Geochemistry and Occurrence: New York, Kluwer, p. 475.

Schreiber, M., Gotkowitz, M., Simo, J., Freiberg, P. (2000) Stratigraphic and geochemical controls on naturally occurring arsenic in groundwater, eastern Wisconsin, USA, *Hydrogeology Journal* **8**(1): 161-176.

Schwertmann, U., and Murad, E. (1983) Effect of pH on the Formation of Goethite and Hematite from Ferrihydrite, *Clays and Clay Minerals* **31**(4): 277-284.

Simo, J, Freiberg, P., and Freiberg, K. (1996) Geologic constraints on arsenic in groundwater with applications to groundwater modeling. WRC GRR 96-01. Water Resources Center, University of Wisconsin-Madison. 57p.

Simo, J., Freiberg, P., and Schreiber, M. (1997) Stratigraphic and Geochemical Controls on the Mobilization and Transportation of Naturally Occurring Arsenic in Groundwater: Implications for Water Supply Protection in Northeastern Wisconsin. WRC-GRR 97-05. Water Resources Center, University of Wisconsin-Madison. 56p.

Sohrin, Y., Matsui, M., Kawashima, M., Hojo, M., and Hasegawa, H. (1997) Arsenic Biogeochemistry Affected by Eutrophication in Lake Biwa, Japan, *Environ. Sci. Technol.* **31**(10): 2712-2720.

Stone, A., Torrents, A., Smolen, J., Vasudevan, D., Hadley, J. (1993) Adsorption of Organic Compounds Possessing Ligand Donor Groups at the Oxide/Water Interface, *Environ. Sci. Technol.* **27**(5): 895-909.

Sun X., and Doner, H., (1996) An investigation of arsenate and arsenite bonding structures on goethite by FTIR, *Soil Science* **161**(12): 865-872.

Sun, X., and Doner, H. (1998) Adsorption and Oxidation of Arsenite on Goethite. *Soil Science* **163**(4): 278-287.

Tempel, R., Shevenell, L., Lechler, P., Price, J. (2000) Geochemical modeling approach to prediction arsenic concentrations in a mine pit lake, *Applied Geochemistry* **15**: 475-492.

Tessier, A.; Campbell, P., and Bisson, M. (1979) Sequential extraction procedure for the speciation of particulate trace metals. *Analytical Chemistry* **51**(7): 844-851.

Todd, E., Sherman, D., and Purton, J. (2003) Surface oxidation of pyrite under ambient atmospheric and aqueous (pH=2 to 10) conditions; Electronic structure and mineralogy from X-ray adsorption spectroscopy. *Geochim. Cosmochim. Acta* **67**(5): 881-893.

Turcotte, S., Benner, R., Riley, A., Li, J., Wadsworth, M., and Bodily, D. (1993) Application of Raman spectroscopy to metal-sulfide surface analysis. *Applied Optics* **32**(6): 935-938.

USEPA, 2001. EPA to implement 10 ppb standard for arsenic in drinking water-EPA 815-F-01-010. 31 Oct. 2001. U.S. Gov. Print Office, Washington DC.

Vogt, H., Chattopadhyay, T., and Stolz, H. (1983) Complete First-order Raman Spectra of the Pyrite Structure Compounds FeS2, MnS2, and SiP2. *J. Phys. Chem. Solids* **44**(9); 869-873.

Wagman D. D., Evans H. H., Parker V. B., Schumm R. H., Harlow I., Bailey S. M., Churney K. L., and Butall R. L. (1982) The NBS tables of chemical thermodynamic properties. Selected values for inorganic and organic substances in SI units. *Journal of Physical Chemistry*. Ref. Data II, supp. 2: 392.

Yan, X., Kerrich, R., and Hendry, M., (2000) Distribution of arsenic (III) and arsenic (V) and total inorganic arsenic in porewaters from a thick till and clay-rich aquitard sequence, Saskatchewan, *Geochim. Cosmochim. Acta* **62**(15): 2637-2648.

Appendix A. List of sample numbers, sample locations and Geology and Geophysics Museum collection reference numbers.

UW Museum #	Sample #	Description	Location
1950/1.1	Le7	Quartz fraction of sandstone hand sample	Leonard Quarry, Winnebago County, WI
1950/1.2	Le7	PMG fraction of sandstone hand sample	Leonard Quarry, Winnebago County, WI
1950/2.1	Le25c	Hand sample of PM nodule	Leonard Quarry, Winnebago County, WI
1950/2.2	Le25c	XRD slide of powered PM fraction of Le25c, before aqueous reaction	Leonard Quarry, Winnebago County, WI
1950/2.3	Le25c	XRD slide of powered PM fraction of Le25c, after aqueous reaction	Leonard Quarry, Winnebago County, WI
1950/2.4	Le25c	Electron Microprobe Slide of hand sample, before aqueous reaction	Leonard Quarry, Winnebago County, WI
1950/2.5	Le25c	Electron Microprobe Billet of hand sample, after aqueous reaction	Leonard Quarry, Winnebago County, WI
1950/2.6	Le25c	Powdered grains used for Raman Spectroscopy, before aqueous reaction	Leonard Quarry, Winnebago County, WI
1950/2.7	Le25c	Powdered grains used for Raman Spectroscopy, after aqueous reaction	Leonard Quarry, Winnebago County, WI
1950/2.8	Le25c	Powdered grains used for Sequential Extraction, after aqueous reaction	Leonard Quarry, Winnebago County, WI
1950/3.1	K1	Quartz fraction of sandstone core sample	Algoma Township, Winnebago County, WI
1950/3.2	K1	PMG fraction of sandstone core sample	Algoma Township, Winnebago County, WI
1950/3.3	K1	XRD slide of powered PMG fraction of K1, before aqueous reaction	Algoma Township, Winnebago County, WI
1950/3.4	K1	XRD slide of powered PMG fraction of K1, after aqueous reaction	Algoma Township, Winnebago County, WI
1950/3.5	K1	Electron Microprobe Slide of core sample, before aqueous reaction	Algoma Township, Winnebago County, WI
1950/3.6	K1	150 micron grains used for Sequential Extraction, after aqueous reaction	Algoma Township, Winnebago County, WI
1950/4.1	K2	Dolomite fraction of core sample	Algoma Township, Winnebago County, WI
1950/4.2	K2	PM fraction of dolomite core sample	Algoma Township, Winnebago County, WI
1950/4.3	K2	XRD slide of powdered PM fraction of K2, before aqueous reaction	Algoma Township, Winnebago County, WI
1950/4.4	K2	XRD slide of powered PM fraction of K2, after aqueous reaction	Algoma Township, Winnebago County, WI
1950/4.5	K2	Electron Microprobe Slide of dolomite core sample, before aqueous reaction	Algoma Township, Winnebago County, WI
1950/5.1	AsFeS	Hand sample of Arsenopyrite, before aqueous reaction	Mexico

Appendix B. ICP-OES parameters.

Parameter	Value
RF power, W	1450
Nebulizer flow rate, L/ min	0.5
Argon flow rate, L/min,	15
Pump flow rate, ml/min	1.45
Auxiliary flow rate, L/min	0.3

Appendix C. Wavelengths used for ICP OES analysis.

Parameter	Wavelength	Parameter	Wavelength
As	188.979	S	181.975
As	193.696	S	180.669
As	197.197	S	182.563
As	228.812	Mg	285.213
Al	394.401	Mg	279.077
Fe	259.939	K	766.490
Fe	238.204	Na	589.592
Mn	257.610	Ca	317.933
Mn	259.372	Ca	315.887

Approved By: Nita Sahai

Prof. Nita Sahai

Date: Aug. 11, '03